USE OF INTERFACIAL TRACERS FOR CHARACTERIZATION OF NONAQUEOUS PHASE LIQUID (NAPL) DISTRIBUTION IN POROUS MEDIA

By

KANAKA PRASAD SARIPALLI

A DISSERTATION PRESENTED TO THE GRADUATE SCHOOL
OF THE UNIVERSITY OF FLORIDA IN PARTIAL FULFILLMENT
OF THE REQUIREMENTS FOR THE DEGREE OF
DOCTOR OF PHILOSOPHY

UNIVERSITY OF FLORIDA

DECEMBER 1996

This dissertation is dedicated to

Dr. Thomas M. Keinath,

with much affection and profound respect.

ACKNOWLEDGMENTS

I am thankful beyond words to Dr. Mike Annable and Dr. Suresh Rao for giving me an opportunity to work with them, which turned out to be an exciting and rewarding learning experience. Mike supported me throughout the doctoral studies with an indomitable attitude and a rare understanding. He introduced to me experiments and theory of immiscible fluids and instilled in me an aptitude for field work, for which I am very thankful. Dr. Rao recruited me to the 'Florida Group' and made my education here possible. I have been very fortunate to have worked closely with him in his laboratory and receive from him teaching in subsurface hydrology, which is a priceless education. He took a genuine interest in my professional and personal development and ensured my growth by constant demands, advice and encouragement. Both Dr. Annable and Dr. Rao supported this research with their unlimited enthusiasm, spent countless hours in discussions of research progress and provided the best of opportunities, which I deeply appreciate.

I would like to thank Dr. Joe Delfino, Dr. Wendy Graham and Dr. Kirk Hatfield for serving on my advisory committee and for their advice on several occasions. I received helpful counsel on research and career planning from Dr. Delfino, and training in surface hydrology from Dr. Graham. My special thanks are due to Dr. Hatfield, for the seed idea that tracers could be used to characterize immiscible fluid interfaces. I am very thankful to Dr. Dinesh Shah for his advice, encouragement and permission to use the research facilities. I

heartily acknowledge the advice of Dr. Dean Rhue and Dr. Bill Wade during this research, which was very helpful. I thankfully acknowledge the education I received from the Environmental Systems Engineering Department at Clemson University prior to my transfer to Florida.

I am thankful to Ms. Dong Ping Dai for her help and support in the laboratory and to Balaji, Candace, Dale, George, Gwyn, Jim, Kim, Randy, Sanjay, Shih-Hsien, Xavier and Yan for their friendship. Finally, I would like to thank my parents and Ratna, whose love is a benediction.

TABLE OF CONTENTS

ACKNOWLEDGMENTS iii

LIST OF FIGURES vii

ABSTRACT viii

CHAPTERS

1 INTRODUCTION

Immiscible Fluids in Porous Media 1
Specific Interfacial Area of Immiscible Fluids in Porous Media 13
Characterization of NAPL Contaminated Porous Media 17
Mass Transfer Across NAPL-Water Interfaces 20
Tracer Adsorption Techniques to Measure Surface Areas 22
Research Objectives and Organization 26

2 MEASUREMENT OF SPECIFIC NAPL-WATER INTERFACIAL AREAS IN POROUS MEDIA USING INTERFACIAL TRACERS: METHOD DEVELOPMENT AND HYDROLOGIC APPLICATION 30

Introduction 30
Experimental Methods 38
Results and Discussion 42
Error Analysis 67
Summary and Conclusions 73

3 SPECIFIC INTERFACIAL AREA OF CONTINUOUSLY DISTRIBUTED IMMISCIBLE FLUID INTERFACES IN POROUS MEDIA 74

Introduction 74
Experimental Methods 76
Modeling of a_{nw} - S_w Relationship 86

Summary and Conclusions 115

4 MEASUREMENT OF INTERFACIAL AREA CHANGES DURING REMEDIATION BY CHEMICAL FLOODING 116

Introduction 116
Characterization During Remediation 118
Experimental 131
Modelling the a_{nw} - N_T Relationship 148
Summary and Conclusions 156

5 USE OF INTERFACIAL TRACERS TO CHARACTERIZE NAPL MORPHOLOGY IN POROUS MEDIA 157

Introduction 157
Morphology of Irregular Source Zones 159
Experimental Methods 163
Results and Discussion 166
Summary and Conclusions 175

6 SUMMARY AND CONCLUSIONS 176

Conclusions 176
Recommendations 178

APPENDIX 180

GLOSSARY 184

LIST OF REFERENCES 189

BIOGRAPHICAL SKETCH 197

LIST OF FIGURES

Figure		Page
1-1	Growth of a NAPL ganglion trapped in a pore with increasing capillary pressure at the NAPL-water interface	4
1-2	Formation of trapped (residual) and continuous NAPL saturation regions	7
2-1	Column experimental apparatus	39
2-2.	Breakthrough curves for PFBA and SDBS in (A) IFT-Gϕ, (B) IFT-S1ϕ and (C) IFT-S2ϕ soil sorption experiments, conducted in the absence of NAPL	43
2-3.	Interfacial tension at decane-SDBS solution interface measured as a function of SDBS concentration (A) γ-*C* data (B) γ^*-Ω data fit with Eqn. 2-13	45
2-4	Breakthrough curves from (A) IFT-B and (B) IFT-PCE column experiments	46
2-5	Breakthrough curves from (A) IFT-JP1 and (B) IFT-JP2 experiments	47
2-6	Breakthrough curves from (A) IFT-F and (B) IFT-T column experiments	48
2-7	Breakthrough curves from (A) IFT-D and (B) IFT-FC40 column experiments	49
2-8	Breakthrough curves from IFT-D column experiment	50
2-9	Breakthrough curves from (A) IFT-S2-1 and (B)IFT-S2-2 column experiments	51

2-10 Isotherms for SDBS at decane-water interface measured in experiments IFT-T and IFT-D & Gibbs equation fits.....61

2-11 Isotherm for AOT-100 at decane-water interface, measured in IFT-S2 column flow experiments.....62

2-12 Isotherms obtained from column experiments IFT-T and IFT-D: Freundlich model fits to the measured data.....63

2-13 Breakthrough curves from IFT-S2-P pulse experiments in IFT-S2 column 64

2-14 Linear ranges of isotherms for (A) SDBS and (B) AOT-100.....66

3-1 Breakthrough curves for PFBA and SDBS in ISH-D column at (A) stage 1 (S_n=43%) and (B) stage 2 (S_n=50%).....77

3-2 Change in specific interfacial area a_{nw} at decane-water interface in ISH-A column as a function of water saturation.....79

3-3 Modified capillary cell used in IHS-C tracer experiments..... 80

3-4 Breakthrough curves for PFBA and SDBS in ISH-B capillary cell at various stages of decane saturation.....82

3-5 Results from capillary cell experiment ISH-C..... 85

3-6 Hypothetical Brooks-Corey curves to illustrate the linear range approximation in P_c-S_e relationship..... 92

3-7 Linearized Leverette model prediction and measured data for ISH-C capillary cell experiment.....101

3-8 Measured data and model predictions using Rose and Bruce function for ISH-C capillary cell experiment.....102

3-9 Geometric approaches to model a_{nw}-S_w relationship (A) Pore Singlet Model (B) Gvirtzman and Roberts (1991).....105

3-10 Measured data and model predictions using Cary (1990) model for ISH-C capillary cell experiment.....111

3-11 Original and modified Skopp (1984) model predictions..... 112

3-12 Transformed Sherwood number (Sh*) as a function of water saturation data from Miller *et al* (1990).....114

4-1 Schematic pictures of NAPL singlets for developing (A) equation 4-10 and (B) equation 4-16 (Pennell *et al*, 1995).....121

4-2 Ultra-low interfacial tensions at a hydrocarbon-surfactant solution interface (Noronha, 1980).....130

4-3 Breakthrough curves in IFT-S2 column experiments (A) before and (B) after emulsification of residual decane..... 133

4-4 Breakthrough curves in IFT-CS1 column experiments (A) before and (B) after cosolvent flooding of residual decane..... 134

4-5 Breakthrough curves for PFBA and SDBS during decane mobilization experiments IFT-SN1..... 138

4-6 Breakthrough curves for PFBA and SDBS during decane mobilization experiments IFT-SN2..... 141

4-7 Changes in decane saturation and decane-water a_{nw} with N_T in experiments (A) IFT-SN1 and (B) IFT-SN2..... 145

4-8 A shematic representation of the a_{nw} - N_T model (Eqn. 4-28)..... 153

4-9 Illustration of (A) an S_n-N_T curve and the corresponding (B) a_{nw} - N_T curve.....154

5-1 Morphology of a NAPL ganglion trapped in a pore (A) before and (B) after emulsification.....162

5-2 Breakthrough curves for PFBA and SDBS in IFT-S2 column (A) before and (B) after contact with 1% Igepal-70 solution..... 169

5-3 Variation of morphology index, *I*, measured in ISH-C capillary cell experiments as a function of decane saturation..... 173

A-1 Schematic of pore singlet model..... 181

Abstract of Dissertation Presented to the Graduate School
of the University of Florida in Partial Fulfillment of the
Requirements for the Degree of Doctor of Philosophy

USE OF INTERFACIAL TRACERS FOR CHARACTERIZATION OF NONAQUEOUS PHASE LIQUID (NAPL) DISTRIBUTION IN POROUS MEDIA

By

Kanaka Prasad Saripalli

December 1996

Chairman: Michael D. Annable
Cochairman: P. S. C. Rao
Major Department: Environmental Engineering Sciences

Behavior of immiscible fluids in porous media is of interest in several sciences and engineering applications. Fluid saturations S_i (volume of fluid i per unit volume of pore space, %) and specific fluid-fluid interfacial area a_{ij} (area of interface between immiscible fluids i and j per unit volume of porous medium, cm^{-1}) are important characteristics necessary to understand the behavior of immiscible fluids, as well as the heat, mass and momentum transfer processes across their interfaces. Several methods are available to measure S_i; however, no methods are available to measure a_{ij}. Measurement of a_{ij} is useful in the characterization of NAPL waste sites, petroleum fields and the vadose zone.

In the case of NAPL contaminated aquifers, NAPL and water (denoted respectively by subscript n and w) are the immiscible fluids of interest. The central goal of this study

was to develop an experimental technique to measure a_{nw} and use the technique to:

(i) measure the a_{nw} of two immiscible fluids continuously distributed in porous media,

(ii) measure the a_{nw} formed by a discontinuously trapped, residual NAPL, and characterize changes in a_{nw} during chemical flooding,

(iii) study the morphology of NAPL in different distribution settings.

Accordingly, a new tracer technique, called the 'Interfacial Tracers Technique (IFT)', was proposed to measure a_{nw}, using interfacial adsorption as the basis. Theory supporting the method, assumptions and hydrologic application were presented. The a_{nw} values measured (60 - 90 cm^2/cm^3 for water-wet systems and 200 - 330 cm^2/cm^3 for partially NAPL-wet systems) using several NAPL trapped in sands are in agreement with the current understanding of immiscible fluid behavior in porous media. Further, measured trends in the the interfacial area-saturation (a_{nw} - S_w) relationship agreed with the thermodynamic prediction of Leverette (1941) and a simple geometric prediction (pore singlet model). In addition, earlier theoretical approaches to predict a_{nw} - S_w function were reviewed.

Further, measurement of changes in a_{nw} as a function of total trapping number (N_T) during mobilization of NAPL by surfactant flushing was investigated. A functional relationship derived between a_{nw} and N_T predicted the measured trends reasonably. Further, interfacial area a_{nw} and the NAPL area-to-volume ratio I, termed the morphology index, were proposed as two useful indices to adequately describe the NAPL morphology. The findings have potential applications in the characterization at waste sites and petroleum reservoirs, as well as in research on immiscible fluid behavior in porous media.

CHAPTER 1
INTRODUCTION

Immiscible fluids (e.g. air, water and oil) co-exist in porous media, such as soils, aquifers, petroleum reservoirs and packed beds. Behavior of immiscible fluids co-existing in porous media is of fundamental interest in several sciences, including environmental science, porous media physics, hydrogeology, soil science, petroleum engineering and chemical engineering. Air and water in the unsaturated soil zone, petroleum and water in an oil reservoir, and non-aqueous phase liquids (NAPLs) and water in a contaminated aquifer are some relevant examples. At many hazardous waste sites, accurate characterization of the trapped NAPL distribution in soil before, during and following remediation is necessary for assessing the level and extent of contamination, quantifying risk , designing remediation systems and technology performance assessment. Currently, there is a pressing need for innovative technologies to characterize NAPL in the sub-surface. As such, understanding the behavior of NAPL and water in porous media is of great theoretical and practical interest in environmental engineering and contaminant sub-surface hydrology. Theory of immiscible fluids forms a proper basis for such study.

Immiscible Fluids in Porous Media

In most porous media applications of interest, the nonwetting phase (NAPL, designated by subscript *n*) is static while the wetting phase, typically water (subscript *w*), is either static or flowing at a slow flow rate. When two or more immiscible fluids co-exist in

a porous medium under static (no-flow) conditions, they attain a unique, equilibrium distribution. A sharp interface separates the two fluids, across which pressure and density differences prevail. The unbalanced cohesive force acting tangentially to the interface, called interfacial force, is balanced by a difference in the two fluid pressures across the interface. This difference in pressure is known as capillary pressure, P_c:

$$P_c = P_{mw} - P_w \tag{1-1}$$

Capillary pressure between the fluid phases in a porous medium is related to gravity, saturation, pore size and shape, interfacial force, contact angle, density difference between the fluids and the radii of curvature of interfaces. The nonwetting phase pressure P_{mw} is typically higher than the wetting phase pressure. This is a consequence of the interfacial forces' tendency to compress the nonwetting phase relative to the wetting phase, causing the interfacial concavity towards the nonwetting phase. Curvature of the interface is related to capillary pressure by the Laplace equation:

$$P_c = \gamma\left[\frac{1}{R_1}+\frac{1}{R_2}\right] \tag{1-2}$$

where γ is the interfacial tension and R_1 and R_2 are the principal radii of curvature at the immiscible fluid interface. Eq. 1-2 is applicable to any immiscible fluid interface, and does not involve the solid-NAPL-water contact angle and pore size explicitly.

The only forces acting on static fluid elements are gravity and pressure forces. Because pressure is a scalar, the force due to pressure acting on a fluid particle is due to

the variation of pressure in space (dP/dx). A balance of force components in a static system on each of the two fluids per unit volume of porous medium is given by

$$-\frac{\partial P}{\partial x_i} - \rho g = 0 \qquad (1\text{-}3)$$

where ρ is fluid density and g is acceleration due to gravity. The solution to this equation, for a two phase system, is

$$P_c = P_{nw} - P_w = (\rho_{nw} - \rho_w)gh + P_{c_o} \qquad (1\text{-}4)$$

where the subscripts w and nw referring respectively to the wetting and nonwetting phases, and P_{Co} being capillary pressure measured at a datum. In porous media, capillary pressure, radii of curvature of the interface and fluid saturations are all interrelated. An increase in capillary pressure, either by increasing the P_{nw} or a decrease in the P_w leads to a reduction in the curvature and a corresponding reduction in the wetting phase saturation S_w. Fluid saturation is defined here as the volume of fluid per unit volume of pore space. Reduction of S_w with an increase in P can be explained conceptually considering a spherical NAPL ganglion trapped in a single pore (Corey, 1985), as shown in Fig.1-1. The ganglion is surrounded by the wetting fluid, water. As the capillary pressure is increased, a volume of water is removed from the pore and an equal volume of NAPL is added to the ganglion, which grows larger. This concept, which explains the variation of S_w and S_n with P_c, can be extended to porous media, which are an ensemble of pores of different sizes and geometry.

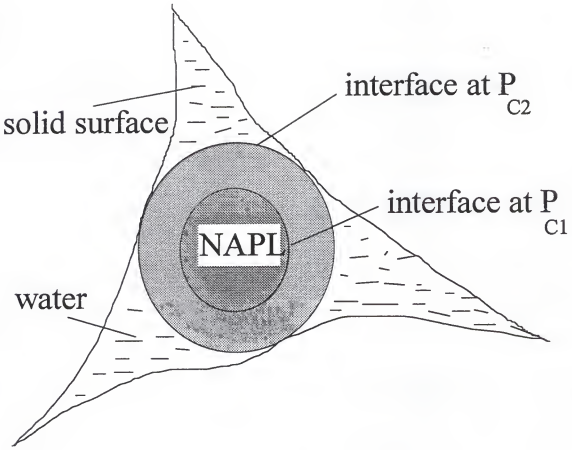

Figure 1-1. Growth of a NAPL ganglion in a soil pore
with increasing capillary pressure at the NAPL-water interface

If a reservoir of NAPL is in contact with an initially water saturated soil, the capillary pressure has to be increased to a value P_e, called the nonwetting phase entry pressure, before water in the largest pore opening will drain and allow the nonwetting phase to occupy the pore spaces. As the capillary pressure further increases, the nonwetting phase progressively invades the relatively larger pores, until, at very large capillary pressures, the nonwetting phase occupies all but the very small pores. At any capillary pressure P_c, all pores of radii larger than $2\gamma/P_c$ will contain both nonwetting and wetting phases, while the smaller pores are completely filled with the wetting phase alone. Thus, in a porous medium containing two continuous immiscible fluids in contact, the fluid saturations are strong functions of capillary pressure and pore size distribution of the medium. A plot of the experimentally measured P_c - S_w relationship, (capillary pressure-saturation curve, an example shown in Fig. 1-2) can effectively capture the dependence of fluid saturations on the capillary pressure and the pore size distribution (Corey, 1985).

Pores in a soil are of irregular shapes and sizes, and can extend over several adjacent grains. As such, each pore can represent capillaries of a range of radii. The wetting phase volume trapped in pores of very small radii and adsorbed as films to the pore walls can not be removed even at very large capillary pressures. The corresponding wetting phase saturation, which cannot easily be removed even by applying very large capillary pressures, is referred to as the residual saturation S_r. Residual saturation can vary from 0 to 15% or more, depending on the soil's pore size distribution, clay content, texture and surface characteristics. Since the water corresponding to S_r does not contribute to advective flow and does not vary with P_c, it is convenient to define an effective wetting

phase saturation S_e, as below, to use in the construction of capillary pressure-saturation relationships:

$$S_e = \frac{S_w - S_r}{1 - S_r} \tag{1-5}$$

Often, the absolute and effective water saturations (i.e., S_e and ${}_wS$) are used interchangeably (Mercer and Cohen, 1990). Implicit in such usage is the assumption that the residual saturation S_r is negligible when compared to the prevailing water saturations, which is reasonable for coarse grained soils such as sands.

Trapped and Continuous NAPL Saturations

The volume of a NAPL per unit volume of pore space in the medium is known as its saturation S_n. The area of interface between NAPL and water per unit volume of porous medium is known as the specific fluid-fluid interfacial area a_{nw}. NAPL saturations and specific interfacial areas are two important characteristics necessary to understand the distribution and morphology of NAPL in porous media, and hence their fate and transport.

In the study of immiscible fluid behavior in porous media, it is convenient to divide the total nonwetting phase saturation range (0 to 1) into 'trapped saturation' and 'continuous saturation' regions (Fig.1-2). The nonwetting phase is trapped in the pores as isolated ganglia at capillary pressures ranging from zero to P_d; the corresponding saturation is known as residual or trapped nonwetting phase (NAPL) saturation. In the residual NAPL saturation region, the nonwetting phase initially exists in the larger

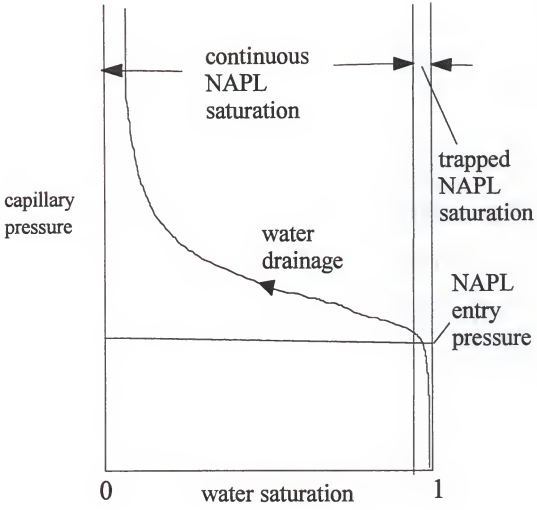

Figure 1-2 Formation of trapped and continuous NAPL saturation regions

sections of the pores as disconnected ganglia, which grow in size with increasing capillary pressure, penetrating increasingly smaller sections of the pore networks, finally to form a nonwetting phase connected across the length of the medium at P_d.

The character of porous medium itself, including pore shape and size, largely determines the trapped saturation and its morphology. Such trapping occurs in unique and statistically reproducible patterns, which are controlled by capillary, viscous and buoyancy forces (Mohanty, 1980; Stegemeier, 1977). Capillarity is due to the unbalanced force resulting from cohesion within each fluid phase and adhesion between the solid phase and each of the fluids. The capillary force is proportional to the interfacial tension at the fluid-fluid interface and the wetting character of fluid at the solid surface, and inversely proportional to the pore size. Viscous or dynamic forces are proportional to the permeability and the pressure gradient across the porous medium. Buoyancy is a gravitational force proportional to the density difference between the fluids. At typical groundwater flow rates, capillary forces often dominate over viscous and buoyancy forces.

Theoretical and experimental investigations using micromodels, pore network models and flow experiments suggest that the magnitude and morphology of the trapped nonwetting phase is a strong function of the ratio of pore body to pore neck radii, called the 'aspect ratio', interfacial tension and potential gradient. At the pore level, two trapping mechanisms have been identified. One is 'snap-off' or 'choke-off', whereby the nonwetting front displacing water in a pore neck becomes unstable and ruptures (Roof, 1970; Mohanty, 1981). High aspect ratio has been shown to cause snap-off with the resulting blob occupying single pore bodies (Morrow and Heller, 1985), the blob shape

being nearly spherical. High aspect ratios generally lead to high residual saturations of nonwetting phase, the only recovery during water flooding coming from the pore throats. At lower aspect ratios, NAPL is bypassed by water in multiple pore structures, resulting in larger oil blobs. Rose and Witherspoon (1956) and Moore and Slobod (1956) introduced the 'pore doublet' model to describe trapping by bypassing. A doublet is made of two pores, a narrow pore and a wider pore joined at both ends. During a nonwetting phase imbibition into a water filled, water wet doublet at low flow velocities, the dominant capillary forces cause the water to preferentially occupy the narrower pore and bypass the isolated nonwetting phase in the wider pore. For bypassing to occur, the down stream connection of pores has to have a high wide pore-to-narrow pore cross section ratio (Wilson *et al*, 1990). If the nonwetting phase saturation is established by drainage instead of imbibition, the residual nonwetting phase distribution is essentially similar (Chatzis *et al*, 1983). While the pore singlet and doublet models explain the formation of ganglia at a single pore level, several pores may be collectively bypassed in a porous medium, leaving blobs which extend over several pores (Wilson *et al*, 1990; Stegemeier, 1977; Larson *et al*, 1970).

In summary, aspect ratio is a key characteristic of porous media that dictates the magnitude and morphology of the nonwetting phase. Dense packings of uniform size beads and bead packs fused by sintering offer high aspect ratio pore networks, whereas heterogeneous packs have low aspect ratio pores. Since soils possess an ensemble of pores and are characterized by pore size distributions, the nonwetting phase morphology also is marked by blob size distributions (Chatzis *et al*, 1983; Mayer and Miller, 1992).

Continuous NAPL Saturation

As mentioned previously, immiscible fluids can coexist in porous media under static equilibrium conditions, or with one or both of the fluids flowing, termed here as 'dynamic (flow) condition.' Typically, water flows past the nonaqueous phase liquid in the porous formations of interest. In either case, it is the capillary pressure (P_c) distribution along the length (h) of the porous medium that governs the distribution of immiscible fluids. Both S_n and a_{nw} are primarily influenced by the capillary pressure distribution. Presence of fluid fluxes in the 'dynamic' case influences the capillary pressure. In this case, where water is flowing steadily past a static, nonaqueous phase at a flow rate of Q_w, the governing one-dimensional flux equation is given as

$$Q_w = \frac{k_w}{\mu_i}\left[\frac{\partial P_c}{\partial x} - (\Delta\rho)g\frac{\partial h}{\partial x}\right] \qquad (1\text{-}6)$$

where P_c is capillary pressure at any location at a distance h from an arbitrary datum (where $P_c = 0$), k_w is the relative permeability, μ is viscosity of water, $\Delta\rho$ is the density difference between the two fluids and g is acceleration due to gravity. In the case of static equilibrium, $Q_w = 0$, simplifying Eqn. 1-6 to $P_c = \Delta\rho g h$.

The above equation enables one to define the P_c distribution along the flow direction (x) of the column. With increases in capillary pressure (above the P_d value), the nonwetting phase saturation further increases. Earlier theoretical and experimental investigations confirmed that S_n increases with increase in capillary pressure in the pressure region above

P_d, which can be called the 'continuous saturation' region (Fig. 1-2). In this context, continuous nonwetting phase saturation can be defined as the saturation S_n corresponding to all P_c values above P_d, in which region the nonwetting phase becomes well connected and is increasingly larger in volume. For any porous medium containing immiscible fluids, the relationships S_n - P_c, a_{nw} - S_n and a_{nw} - P_c represent a complete knowledge of the static fluid behavior in the medium, at least at a macroscopic (Darcy) scale. Several functional relationships are available in the literature to describe the P_c - S_w relationship, notable among them the Brooks-Corey and Van Genuchten functions. Brooks and Corey suggested the empirical relationship

$$S_e = [P_d / P_c]^{\lambda} \tag{1-7}$$

where $P_c > P_d$ and $S_e < S$, where P_d is the capillary pressure where desaturation first occurs on a drainage cycle and λ is a parameter representing the pore size distribution, typically equal to about 2 (Corey, 1985). For media having a uniform pore-size, the index λ would be a large number. In contrast, media with a wide range of pore sizes would have a small value of λ that could theoretically approach zero. This relationship is sensitive to the value of S_r. The parameter λ has important implications on not only the P_c-S_w relationship, but also on the nonwetting fluid morphology, its specific interfacial area and its removal by mobilization.

Measurement of NAPL Saturation, S_n

Several methods are available for the characterization of fluid saturations. Gamma ray attenuation techniques can be used to estimate the fluid saturations in porous media (Dane *et al*, 1992). Recently, partitioning tracer techniques were developed to measure NAPL saturations in porous media *in-situ* (Jin *et al*, 1994; Wilson and Mackay, 1995). Several mathematical models are also available to model and predict the fluid saturations in porous media as a function of capillary pressure (Leverett, 1941; Corey, 1985; Van Genuchten,1980). At the field scale, core sampling, cone penetrometer testing, geophysical logging and tracer test methods are the techniques available for characterization. Among these methods, the partitioning tracer technique may be more effective at both laboratory and field scales, in terms of larger sample volumes represented, accuracy, relative convenience and replicate data sets obtained by using a suite of tracers in a single experiment (Jin *et al*, 1994). Partitioning tracers are chemicals such as alcohols, which, when contacted with the residual NAPL phase in a tracer test, partition into the NAPL phase from the aqueous phase and elute out of the soil later than a nonpartitioning (conservative) tracer. The extent of chromatographic separation of the tracer pulses, which is represented by a retardation factor, depends on the fraction of time the tracer spends in the NAPL phase compared to that in the water, which is a function of the tracer-NAPL partitioning coefficient K and NAPL saturation S_n. Partitioning tracers have been successfully used to measure the fluid saturations in both laboratory (Jin *et al*, 1995; Wilson and Mackay, 1995) and contaminated aquifer (Annable *et al*, 1996) settings.

Specific Interfacial Area of Immiscible Fluid Interfaces in Porous Media

Physicochemical processes in bulk phases as well as at the phase boundaries (interfaces) are driven by energy gradients. Interfacial phenomena, such as adsorption, and mass, heat and momentum transport processes across the interface are dependent on interfacial energy. The extent of such processes in a system is directly proportional to the interfacial area. Thus, interfacial phenomena are prevalent in systems where a large expanse of interface is available. Area is a measure of the extent of an interface, just as volume is a measure of the extent of a bulk phase. The specific surface area between phases (such as NAPL and water) must be determined if any physico-chemical interpretation of their behavior is to be possible (Adamson, 1982).

Quantification of a_{nw} in porous media containing NAPL and water is important for several reasons. Measurement of a_{nw}, along with S_n, is necessary for a complete description of the immiscible fluid morphology. Understanding of transport processes at NAPL-water interfaces, such as heat, mass and momentum transfer, require the knowledge of a_{nw}. In the recent past, researchers have begun to recognize a_{nw} as a fundamental variable necessary to describe the status of immiscible fluids in porous media (Gray and Hassanizadeh, 1990; Morrow, 1970). Equilibrium distribution of immiscible fluids in porous media corresponds to an energy status at which the total free energy is a minimum (Morrow, 1970). Surface free energy, an important component of total free energy, is directly proportional to the fluid interfacial area a_{nw}, just as the bulk phase free energies are proportional to the phase volumes or S_n. Once the measurement of a_{nw} becomes available, constitutive relationships such as the soil water characteristic curves, can be

available, constitutive relationships such as the soil water characteristic curves, can be described in terms of three fundamental variables: P_c, S_n and a_{nw} (Gray and Hassanizadeh, 1991a; Hassanizadeh and Gray, 1993). The relative permeabilities of immiscible fluids may be functions of a_{nw} also, as the interfacial friction offers resistance to flow (Gvirtzman and Roberts, 1991). Microorganisms are believed to thrive at the fluid interfaces, as this location offers maximum accessibility to the hydrocarbon substrate and the nutrients dissolved in water (Atlas, 1988). Thus, measurement and prediction of a_{nw} will lead to a better understanding of the immiscible fluid statics and dynamics in porous media as well as several physico-chemical and biological processes at the fluid interfaces. Measurement of a_{nw} also has several technological applications. Characterization of NAPL waste sites, which is a prerequisite for remediation, can be improved by the conjunctive measurement of S_n and q_w. Measurement and modeling of NAPL dissolution will benefit from a knowledge of a_{nw} (Powers *et al*, 1991; Miller *et al*,1990). Similar applications can be found concerning petroleum reservoirs, packed beds and soil unsaturated zone.

Immiscible fluid morphology in porous media is a function of the medium's pore size distribution, its wettability and the interfacial tensions present at the various phase interfaces (*i.e.*, the fluid-fluid and solid-fluid interfaces). Even in ideal, spherical glass bead packs, pore channels are complex and nonuniform, both in shape and size (Iwata *et al*, 1980; Dullien, 1953). The geometric complexity of pores, together with the dependence of capillary forces on pore-size, results in complex fluid morphology relationships in the porous media. Because of the complex shapes and sizes the immiscible fluid interfaces assume, direct measurement of the specific interfacial area a_{nw} is difficult (Morrow, 1970; Pffankuch, 1984; Miller *et al*,

1990; Reeves and Celia, 1995; Bradford and Leij, 1996). For the same reasons, mathematical modeling of the interfacial areas in porous media is often highly idealized, based on assumptions about pore geometry which may not necessarily be true (Leverett, 1941). Over the past several years, there were many models developed to predict a_{nw} as a function of the fluid saturation and/or capillary pressure (Leverett, 1941; Miller *et al*, 1990; Skopp, 1985; Cary, 1994; Morrow, 1970; Gvirtzman and Roberts, 1991; Rose and Bruce, 1949 and Bradford and Leij, 1996).

Visual imaging techniques, such as nuclear magnetic resonance, optical microscopy and scanning probe microscopy may eventually facilitate a detailed visualization of the immiscible fluid interfaces in porous media (Gray and Montemagno, 1995). These techniques have yet to be applied to the measurement of a_{nw}. Since the resulting images typically represent a two-dimensional view of the fluid interfaces, repetitive imaging from several angles and at several locations may be necessary to accurately measure the interfacial areas. In the absence of direct measurement techniques, it is instructive to review the various theoretical models available to predict the specific interfacial areas.

Three different approaches have been reported in the literature for analysis and interpretation of static immiscible fluid distribution in porous media. One approach was to study the problem from geometric analysis; typically, ideal spherical particles and close-packed hexagonal distributions were assumed. Works by Smith (1933) and Versluys (1917) are often quoted in this regard. Alternatively, the static fluid distribution was analyzed from a capillary, thermodynamic point of view, which does not call for any assumptions about fictitious grain shapes and distributions. Leverett (1941) developed

theory and interpreted experimental results, taking this approach. Empirical modeling was the third approach, which gave rise to several different functional relationships between capillary pressure and saturation.

Theoretical models relating the fluid saturations, interfacial areas and capillary pressure can also be divided into three categories: (1) thermodynamic models, (2) geometric models and (3) mixed empirical models. Geometric models often involve assumptions about the solid and pore geometry (Smith, 1933; Gvirtzman and Roberts, 1991), but do not invoke the concept of capillary retention of fluids in pores. In contrast, thermodynamic models (Leverett, 1941; Morrow, 1970; Bradford and Leij, 1996), which are based on the fundamental relationship between the capillary pressure across an immiscible fluid interface and the interfacial curvature, (the well-known Laplace equation), do not involve any geometric assumptions. Mixed empirical models use a combination of the thermodynamic and geometric approaches (Rose and Bruce, 1949; Cary, 1994; Skopp, 1985).

In general, interfacial area of the NAPL-water interface should increase with increasing P_c as the NAPL saturation increases. Leverett (1941) proposed the following relationship based on thermodynamic principles,

$$a_{nw} = -\frac{\epsilon}{\gamma}\int_{S_w}^{1} P_c dS_w \qquad (1\text{-}8)$$

where ε is porosity. By substituting Eqn. 1-7 in 1-8 will result in an expression for a_{nw} in terms of water saturation S_w. Prediction and measurement of the a_{nw} - S_w relationship are discussed more fully in Chapter 3.

Characterization of NAPL Contaminated Porus Media

When a nonaqueous phase liquid (NAPL) is introduced into the subsurface, gravity causes it to migrate downwards towards the water table, while a portion of it is retained in the vadose zone by capillary trapping. Once the NAPL reaches water table, it either floats on the water table or sinks further into the aquifer, depending on whether it is lighter than water (an LNAPL) or denser than water (a DNAPL). In the case of a DNAPL, a part of the liquid is retained in both vadose and saturated zones, and the rest, if available in sufficient volume, migrates towards the bottom layers. The fraction of NAPL left behind by the migrating free phase is entrapped in the soil pore spaces mainly under the influence of capillary forces under ambient groundwater flow conditions. This fraction, known as the trapped saturation or residual saturation, exists in the subsurface as isolated, discontinuous ganglia of complex shapes and sizes. Residual NAPL source zones can contaminate large volumes of groundwater for long periods of time, owing to the low water solubility of their constituents, and thus create large plumes of contaminated water. Further, the drinking water standards for many NAPL constituents are orders of magnitude lower than their water solubility, which implies that dilution of the NAPL saturated plumes can not easily abate contamination. Thus, even a small NAPL source zone can pose a large and persistent risk to groundwater quality. Various technologies were developed over the years to enhance NAPL remediation.

The task of delineating contamination at these sites presents unprecedented difficulties to the scientific, engineering and regulatory communities. These difficulties are often exacerbated when the conventional characterization techniques based on drilling are used, due

to remobilization of NAPL and possible displacement of contamination, which render the samples unreliable (Feenstra and Cherry, 1995). Determination of the "nature and extent" of contamination, a regulatory requirement in the site investigations, is difficult to meet in practice, because of the complex nature of NAPL distribution.

At many hazardous waste sites, successful remediation of aquifers contaminated with trapped nonaqueous phase liquids (NAPL) requires accurate site characterization, of which characterization of NAPL source zones is the most important requirement. The properties that can adequately describe the morphology of any irregular object, such as the NAPL source zone, are its location, volume, specific interfacial area and the area-to-volume ratio. A complete NAPL source zone characterization requires knowledge of the physico-chemical character, location and volume of the NAPL ganglia, their shape, size and morphologic distribution. In order for any NAPL remediation method to be effective, NAPL zones must be properly characterized (Mackay and Cherry, 1989). Partitioning tracers are useful in quantifying the volume as S_n. Methods to delineate the morphologic distribution of NAPL would greatly add to the site characterization; such methods are not currently available. At the laboratory scale, researchers have used physical methods such as blob casting and visual techniques such as CAT-SCAN, to study the NAPL morphology (Chatzis *et al*, 1983; Mayer and Miller, 1992). Information gained from such techniques is semi-quantitative at best. In contrast, interfacial and phase partitioning tracers have the potential to offer a simple, nondestructive methods to delineate the NAPL morphology.

Remediation Performance Assesssment

At hazardous waste sites, removal of nonaqueous phase contaminant liquids (NAPLs) by mobilization, using surfactant and cosolvent flushing, is an attractive remediation option. Study of the changes in NAPL saturations (S_n) and specific NAPL-water interfacial areas (a_{nw}) before, during and after the remediation process is essential in the characterization of waste sites, remediation planning, design, evaluation and risk assessment. Empirical indices, such as the capillary number (N_{Ca}) and recently the total trapping number (N_T), were presented in the literature as means of describing the trapping and removal of NAPL by mobilization (Taber, 1969; Pennell *et al*, 1995). Capillary number is a generic term for the ratio of viscous to capillary forces. Several researchers have observed that mobilization of NAPL commences when the capillary number exceeds a critical value (Taber, 1979). Similarly, 'solubilization parameter,' can serve as an index of solubilization of a NAPL during enhanced dissolution processes (Wade, 1995). It is useful to investigate the relationship of such remediation indices to the NAPL characteristics, particularly the S_n and a_{nw}, to effectively describe the mobilization and solubilization processes and describe the same in a generic fashion. Earlier experimental methods available for the measurement of S_n allowed the characterization and modeling of the S_n-N_{Ca} relationship adequately. In contrast, since no methods were available to measure a_{nw}, no attempts to measure or model the a_{nw} -N_T were reported.

Mass Transfer Across NAPL-Water Interface

Mass transfer across the NAPL-water interface is a very important phenomenon that controls the dissolution of NAPL constituents into groundwater and hence the extent of contamination. Mass transfer in all three NAPL distribution scenarios, viz., trapped NAPL, static equilibrium and dynamic (flow) conditions can be described by Fick's law, the basic equation used to describe mass flux across an interface:

$$J = K_l(C_s - C) \tag{1-9}$$

where J is mass flux from the nonaqueous phase fluid to the aqueous phase, K_l is the mass transfer coefficient, C_s is the maximum or equilibrium concentration of a constituent in water and C is the actual concentration in the pore water. While the discussion here focuses on water and NAPL the theory can also apply to gas-liquid systems. Equation 1-9 can be written in terms of the rate of change of mass per unit volume of soil (V):

$$\frac{dC}{dt} = a_{nw}\, k_l(C_s - C) \tag{1-10}$$

However, since no methods were available to measure a_{nw}, a bulk mass transfer coefficient $K_l = a_{nw}\, k_l$ is often used in experimental studies and modeling of mass transfer (Miller *et al*, 1990; Powers *et al*, 1992). One-dimensional flow experiments are conducted in laboratory columns to determine the bulk mass transfer coefficients K_l. The governing equation is

$$\frac{\partial C}{\partial t} + K_l(C - C_s) = D_L\frac{\partial^2 C}{\partial z^2} - v\frac{\partial C}{\partial z} \tag{1-11a}$$

where D_l is the longitudinal dispersion coefficient and v is the water velocity. The steady state solution (Carslaw and Jaeger, 1959) for Eqn. 1-11a with boundary and initial conditions,

$$(0,\ t)=0 \quad ; \quad \frac{dC}{dz}=0 \quad at \quad z=\infty \tag{1-11b}$$

and appropriate for a laboratory column can be written as

$$\frac{C}{C_s} = 1-\exp\left[\frac{v-\sqrt{v^2+4D_L K_l}}{2D_L}z\right] \tag{1-12}$$

By measuring concentration in effluent water samples from columns at steady state constituent transport, values of K_l can be obtained. With bulk transfer coefficients K_l and the areas a_{nw} determined at different fluid saturations, the relationship between interfacial surface areas and mass transfer coefficients can be investigated, which lends a rational basis for the modeling of mass transfer across immiscible fluids in general and across the NAPL-water interface in particular. Further, measurement of a_{nw} and the intrinsic mass transfer coefficients in flow experiments also facilitates the elucidation of kinetics of mass transfer and nonequilibrium effects in NAPL dissolution. Results from such investigation will also offer insights about mass transfer across other interfaces, such as across the NAPL-vapor interface, for example, during vapor phase enhancement of volatilization by steam stripping.

Tracer Adsorption Techniques to Measure Surface Areas

Solid-Fluid Surface Areas

Surface area largely determines many physical and chemical properties of materials; it is often a controlling factor in many biological processes. Surface area of soils per unit mass is defined as its specific surface (m^2/g). Soils vary widely in their specific surface and also in the reactive nature of their surfaces. Water retention and movement, cation exchange capacity and chemical adsorption are closely related to the specific surface. Clay-size particles contribute most of the inorgainc surface area of soils. The purpose of surface-area measurements is commonly to determine the accessibility of internal surfaces to molecules or ions which can adsorb thereon. The systems of interest are mostly hydrated systems. As such, a measurement procedure which estimates surface area accessible under hydrated conditions is often preferred. Thus, techniques based on adsorption of molecules from solution, such as ethylene glycol and ethylene glycol monoethyl ether, are popular for the measurement of soil specific surface area (Carter *et al*, 1986).

Due to the fractal nature of interfaces, especially solid surfaces due to their microscopically rough nature, surface area is scale dependent. For example, the conventional surface area of a cubic stone of side 1 cm is 6 square cm. However, since its surfaces are not microscopically smooth, the 'actual' surface area, measured by adsorption of tracer molecules for instance, can be orders of magnitude larger. In this example, the measure used, a meter scale, is not fine enough to measure the contribution to surface area from the porous and rough nature of the surface, whereas the nitrogen

molecules are capable of such measurement. Thus, surface area is an operational concept, which is a function of the measurement technique and the associated theory (Sposito,1984; Adamson, 1982).

Sposito (1984) discussed two important reasons for the operational nature of specific surface area. First, the properties of the solid surfaces in a soil can often be altered during the preparation of the soil for a surface area measurement. For example it may be required to dry the soil thoroughly and maintain it under vacuum. Similarly, treatments with chemical reagents may be required for purposes of sample standardization. Both of these techniques can alter the shape and size of soil particles and void spaces. Second, if a surface reaction is involved in the measurement of specific surface area, the measured value reflects the surface functional groups that participated in that reaction only. Surfaces that are not reactive under the conditions of measurement are not taken into account. As such, the results are meaningful only if applied to molecules similar to the probe molecules reacting with surfaces similar to those in the measured sample.

Several techniques are available to measure the specific surface area of solids. These methods include physical techniques such as optical and electron microscopy, X-ray diffraction, porosimetry and permeability studies, and chemical techniques such as the methods based on heat of immersion measurement, rate of dissolution of solid powders, positive adsorption and negative adsorption methods (Sposito, 1984; Adamson, 1982). Sposito (1984) lists three basic experimental conditions for the measurement of specific surface area with an adsorption method:

1. There must be a chemical reaction between the tracer molecule and the

surface of interest, that leads to an accumulation (adsorption) of the tracer on the surfaces,

2. The mass of adsorbate per unit mass of soil corresponding to one layer of adsorbate should be determined,
3. The packing area, which is the amount of surface area allotted to each adsorbed molecular unit at monolayer coverage, must be known.

In addition to these three requirements, it is preferable that the adsorbate is retained on the soil by surface adsorption alone, and no other loss mechanism (such as precipitation or degradation) is operative. Further, there is a tacit assumption that the area of surface occupied per molecule is a constant for a given surface. A monolayer formation is preferred in such measurements, as multi-layer formation involves more assumptions while measuring the surface area.

When the above conditions are met, the specific surface area of a soil can be measured using the equation (Adamson, 1982; Gregg and Sing, 1982):

$$A = \frac{MNa}{V10^{16}} \tag{1-13}$$

where A (cm^2/cm^3) is the surface area of the porous solid of volume V (cm^3), M (moles) is the mass of a tracer adsorbed at equilibrium, a ($Å^2$) is the area per molecule of tracer adsorbed on the surface at monolayer adsorption and N is Avogadro's number.

The adsorptive molecule is chosen so as to react selectively with the particular surface functional groups whose areal distribution is of interest. Often, rather weakly interacting, nonselective adsorbates such as nitrogen gas are used, to measure as much surface area as possible. Stereochemical hindrance can be a serious limitation to the use of nitrogen as an adsorptive. The relatively large Van der Waals radius of the N_2 molecule prevents it from accessing the functional groups in very small void spaces.

Gases such as nitrogen tend to adsorb on solid surfaces in response to the force field at or very near the surface. The quantity of gas adsorbed can provide a measure of the surface area. Adsorption is the process through which there is a net accumulation of a substance at the common boundary between two contiguous phases. Adsorption data are usually described using isotherms; Langmuir isotherm and BET isotherm are two widely used models in surface area measurements. A form of Langmuir equation applicable to gas tracer adsorption is given below:

$$P/V_g = 1/k_2 V_g + P/V_m \qquad (1\text{-}14)$$

where V_g is the volume of gas adsorbed per gram of adsorbent at pressure P, k is a constant and V_m is the gas volume adsorbed per gram soil when a complete monolayer has been formed. Slope of the plot P/V vs. P at constant temperature is equal to $1/V_m$. Once this slope is known, the surface area is obtained as the product of the number of molecules in V_m and the area occupied per molecule. The Langmuir equation is based on the assumptions that only a monolayer is formed and the heat of adsorption is uniform during adsorption of the monomolecular layer.

Immiscible Fluid-Fluid Interfacial Area

In subsurface hydrology, tracer methods offer an attractive alternative or addition to the conventional methods of characterization. Use of tracers for characterization of the subsurface involves the input of a known quantity of a reactive tracer, which can be a chemical, organism or energy that reacts with the subsurface in a specific way, and comparing its output response to that of an inert, non-reactive tracer. By designing the tracer's character suitably, the necessary information of interest about the subsurface can be obtained. For example, use of dyes as tracers to locate the groundwater stream lines is a standard tracer method in subsurface hydrology. As noted earlier, partitioning tracers have been successfully used to measure the fluid saturations in both laboratory and contaminated aquifer settings.

Combining the concepts of surface area measurement *via* tracer adsorption with the hydrologic principles of tracer flow and transport in porous media can result in a new tracer technology capable of measuring the immiscible fluid-fluid interfacial areas in the subsurface. Development of such technology will require a tracer that possesses the characteristics of sorbates for surface area measurement as described earlier, and a hydrologic method to measure and interpret the tracer transport behavior through porous media. The focus of the present work was on the development and application of such a tracer technique.

Research Objectives and Organization

The central goal of this study was to develop an experimental technique to measure a_{nw} in porous media containing NAPL and water as two immiscible fluids, and use the

technique so developed to:

(i) characterize a_{nw} of two immiscible fluids continuously distributed in porous media,

(ii) measure the a_{nw} of a NAPL-water interface in porous media, and characterize changes in a_{nw} as a function of mobilization of NAPL, and

(iii) study the morphology of NAPL existing in different morphologic distribution settings.

Research findings in this dissertation are organized as six chapters. Presented in Chapter 2 is a new experimental technique, called the 'Interfacial Tracers Technique (IFT),' to measure a_{nw} of a trapped NAPL-water distribution. The principles and theory supporting the method, assumptions involved, description of the method and the a_{nw} values measured using the method are presented, supported by experimental results obtained using different NAPLs and interfacial tracers. Also in Chapter 2, the hydrologic application of the interfacial tracers technique, which is necessary for the development of field tracer technology, is discussed. Development of retardation equations and measurement of the isotherms of adsorption of interfacial tracers at the NAPL-water interface are the important features of such development.

Discussed in Chapter 3 are the elucidation and measurement of the interfacial area - saturation (a_{nw}-S_w) relationship, which is important in the study of immiscible fluid behavior in porous media. In the absence of tools to measure a_{nw}, past research focussed on the development of mathematical models to model the a_{nw} - S_w relationships. In chapter

3, the available a_{nw} - S_w models are comparatively reviewed, and the similarities, applicability and unification of the various models discussed. Using interfacial tracers, the a_{nw} - S_w relationship for decane-water interface in glass bead columns was experimentally measured. Fits of mathematical models to the measured data indicate that some of the available models can predict the a_{nw} - S_w relationship satisfactorily. This work will contribute to the development of realistic models to predict the a_{nw} - S_w relationship and an experimental method to verify the predictions.

Measurement of interfacial area changes during mobilization of NAPL by surfactant flushing is discussed in Chapter 4. Study of the changes in NAPL saturations (S_n) and specific NAPL-water interfacial areas (a_{nw}) before, during and after the remediation process is essential in the characterization of waste sites, remediation planning, design, evaluation and risk assessment. Since methods were not available to measure a_{nw}, no attempts to measure or model the a_{nw} - N_T were reported earlier. In the current work, experimentally measured a_{nw} - N_T curves are presented, using interfacial tracers, and surfactant-flushing as a means of mobilization. In addition, a simple analytical model to predict the same relationship also is presented.

Discussed in Chapter 5 is the use of interfacial tracers to characterize the morphologic distribution of NAPLs in porous media. In the current work, interfacial area a_{nw} and the NAPL area-to-volume ratio I, termed the morphology index, were proposed as two useful indices that can adequately describe the NAPL morphology. In column experiments, the NAPL morphology was deliberately changed using three different techniques: (1) emulsification; (2) capillary pressure alteration; and (3) different modes

of NAPL loading. It was found that a given NAPL at a given saturation can exist in a sand in vastly different morphologic distributions. The morphology index *I* is shown to be an effective parameter that can capture such differences in morphology. The methods and results presented in the present work have potential applications in the characterization and remediation design of NAPL sites and petroleum reservoirs, as well as in multi-disciplinary research concerning immiscible fluid behavior in porous media.

CHAPTER 2

MEASUREMENT OF SPECIFIC NAPL-WATER INTERFACIAL AREAS IN POROUS MEDIA USING INTERFACIAL TRACERS: METHOD DEVELOPMENT AND HYDROLOGIC APPLICATION

Introduction

Measurement and prediction of the specific NAPL-water interfacial area a_{nw} will lead to a better understanding of the immiscible fluid statics and dynamics in porous media as well as several physico-chemical and biological processes at the fluid interfaces. Further, these parameters are also essential in the characterization of waste sites, remediation planning, design, evaluation and risk assessment. Traditional mass/volume balance methods and recently reported partitioning tracer methods (Jin *et al*, 1994; Wilson and McKay, 1995; Annable *et al*, 1996) can be used to measure S_n. However, no methods are currently available to measure a_{nw}. Several researchers have emphasized the need for an experimental method to measure the NAPL-water interfacial area (Gvirtzman and Roberts, 1991; Powers *et al*, 1991 & 1992; Reeves *et al*, 1995; Bradford and Leij, 1995; Cary, 1994). Among the various methods conceivable to characterize porous media, tracer methods rank high due to their non-destructive nature, economy and their ability to present information integrated over large sample volumes.

Use of adsorbing tracer molecules, such as nitrogen, to measure the specific surface areas of porous solids is a well established technique. The specific surface area of a solid is

measured as the product of the area per molecule of the tracer adsorbed at the solid-vapor interface and the number of molecules covering the surface as a monolayer at saturation adsorption (Adamson, 1982; Gregg and Sing, 1982):

$$A = \frac{MNa}{V10^{16}} \tag{2-1}$$

where A (cm^2/cm^3) is the surface area of the porous solid of volume V (cm^3), M (moles) is the mass of a tracer adsorbed at equilibrium, a ($Å^2$) is the area per molecule of tracer adsorbed on the surface at monolayer adsorption and N is Avogadro's number.

Interfacial tracers are chemical species that accumulate at the NAPL-water interface by adsorption, but do not dissolve or partition into the NAPL phase. As such, interfacial tracers can be used in tracer flow experiments through a soil containing NAPL, to measure the specific NAPL-water interfacial area, based on the same principle used in nitrogen adsorption (Eqn. 2-1). Unlike nitrogen adsorption, the former is a flow-based technique, as will be shown later. In the case of solid surfaces, partitioning of the tracer into the solid phase is not a concern. However, in the case of a NAPL-water interface, the tracer should adsorb at the interface, but should not partition into the NAPL phase. In other words, the interfacial tracer should be soluble in water and not significantly soluble in the NAPL phase.

The three assumptions involved in using interfacial tracers for measuring interfacial areas are that: (1) the tracer adsorbs at the interface but does not partition into the bulk NAPL phase; (2) the adsorption culminates as a monolayer coverage; and (3) each tracer molecule occupies a constant, known molecular area at the NAPL-water interface. These

assumptions are reasonable in the case of anionic surfactants adsorbing at a NAPL-water interface. Anionic surfactants are excellent candidates for use as interfacial tracers, with their insignificant solubility in the NAPL phases, high water solubility and relatively high critical micellar concentration (CMC) values. It is reasonable to assume that anionic surfactants adsorbing at a hydrophobic oil-water interface attain monolayer, saturation adsorption coverage at the CMC (Rosen, 1978). Anionic surfactant monomers at the carbon/aqueous interface, a model hydrophobic surface, were found to exhibit a saturation monolayer coverage of the interface at the CMC (Hough and Rendall, 1983). Anionic surfactants adsorb at the hydrophobic oil-water interface with the hydrophilic head groups oriented towards the aqueous phase. A bilayer formation on the resulting negatively charged interface is not likely.

To illustrate the measurement of a_{nw} in laboratory or field experiments, consider a porous medium of volume V, containing a NAPL (or air)-water interface, through which water is flowing at a constant rate. At time zero, a nonreactive tracer (e.g. pentafluorobenzoic acid (PFBA) or bromide) or an interfacial tracer, of known molar concentration C_o, is introduced at the inlet as a step input. Travel of the interfacial tracer is retarded relative to the nonreactive tracer, due to adsorption at the NAPL-water interface, which is measured by a 'retardation factor', defined from advection-dispersion theory of reactive solute transport through porous media, as:

$$R_t = \frac{\mu_{ift}}{\mu_{nr}} = 1+\frac{a_{nw}}{\theta_w}(K_o)|_{Co,T} \qquad (2\text{-}2)$$

where $K_o = G_o/C_o$ and

$$\mu = \int_0^{\infty} (1 - C/C_o)dt \qquad (2\text{-}3)$$

Here, $C(t)$ is the effluent concentration of tracer - either interfacial tracer (subscripted *ift*) or nonreactive tracer (subscripted *nr*)- monitored at the column outlet, θ_w is the water content expressed as a fraction, G is the sorbed phase concentration of the interfacial tracer at the NAPL-water interface, K_o is slope of the isotherm for adsorption corresponding to interfacial and solution phase concentrations G_o and C_o respectively, and μ is proportional to the tracer mass retained in the porous medium due to adsorption. Eqn. 2-2 is based on the assumption of reversible, equilibrium adsorption of the interfacial tracer at NAPL-water interface, and a clean solid matrix which does not adsorb the interfacial tracer. If adsorption of the interfacial tracer on the background solid (soil) matrix is significant, then Eqn. 2-2 will can be modified to include the contribution of solid matrix to sorption, as below:

$$R_t = \frac{\mu_{ift}}{\mu_{nr}} = 1 + \frac{a_{nw}}{\theta_w}(dG/dC)|_{Co,T} + \frac{\rho}{\theta_w}(dS/dC)|_{Co,T} \qquad (2\text{-}4)$$

where dS/dC is the slope of the isotherm for adsorption of SDBS on the sand matrix. Assuming a linear isotherm, dS/dC in Eqn. 2-4 can be replaced by a constant K_s. In a real aquifer setting, the aquifer material is likely to adsorb the interfacial tracer. The term dG/dC in Eqn. 2-2 and 2-4 should be assessed at the initial concentration C_o of the tracer experiment, from a measured isotherm. In the special case of a linear isotherm, the term dG/dC can also be replaced by a constant, K_t.

Equation 2-3, and hence 2-2 and 2-4, as written, are applicable to step input tracer experiments; in the case of pulse input experiment with a pulse input duration of t_s, Eqn. 2-3 will have to be corrected for pulse width, by subtracting $t_s/2$ from the right hand side, as

$$\mu = \frac{\int_0^\infty tCdt}{\int_0^\infty Cdt} - \frac{t_s}{2} \qquad (2\text{-}5)$$

With this modification in the definition of μ, the equations 2-2 and 2-4 will be applicable as written for pulse input experiments as well.

In a tracer step input experiment with infinite pulse duration ($t_s = \infty$), the relative concentration of the tracer, $C^* = C(t)/C_o$, plotted as a function of the number of pore volumes eluted, results in a sigmoidal breakthrough curve. Pore volume P is the volume of water filling the pore spaces, and is equal to $V\theta_w$. Water content of the soil can be determined as P/V, assuming that the immobile water content is negligible. When adsorption of the tracer at available NAPL-water interfaces attains equilibrium, the breakthrough curve culminates in a plateau at a C^* value of unity and the area bounded by the breakthrough curve and the C^* = 1 horizontal line represents R_{ift} (Nkedi-Kizza *et al*, 1987). The total mass of tracer adsorbed at the interface of interest, M, can be obtained as $(R_f\text{-}1)PC_o$ which, upon substitution into Eqn. 2-1, yields:

$$a_{nw} = \frac{(R_{ift} - 1)PC_oNa}{V\ 10^{16}} \qquad (2\text{-}6)$$

In the case of pulse input experiments, which are typical of hydrologic applications, Eqn. 2-2 or 2-4 will have to be used, to calculate a_{mr}. Eqn.2-6 will be applicable to pulse experiments only when the adsorption isotherm of the interfacial tracer at the NAPL-water interface is linear. Use of Eqn. 2-2 or 2-4 in pulse input applications necessitates the evaluation of adosrption isotherms for the interfacial tracer at the NAPL-water and solid-water interfaces.

Adsorption of anionic surfactants from dilute aqueous solutions at an oil-water or air-water interface can be described using Gibbs adsorption equation, one of the fundamental equations of surface chemistry used to describe the adsorption of any chemical species at an interface (Adamson, 1982; Rosen, 1978):

$$\Gamma = -\frac{C}{2RT}\,(d\gamma/dC) \qquad (2\text{-}7)$$

where Γ (mole/cm^2) is the Gibbs surface excess of surfactant, γ (dynes/cm) is the interfacial tension at the oil-water interface and C is the aqueous phase molar concentration of surfactant, R is universal gas constant and T (°K) is temperature. Activity of surfactant monomers remains constant in the supra-CMC concentration range as micelles begin to form at the CMC, leading to adsorption saturation at and above the CMC. The factor 2 in the denominator is an addition to the original Gibbs equation, to account for the fact that oppositely charged groups of an ionic surfactant adsorb at the interface in equal measure to maintain electrical neutrality of the interface. If the adsorption from aqueous solution occurs in the presence of a swamping amount of indifferent electrolyte that has a common ion with the surfactant, then the Gibbs equation (Eqn. 2-7) will be applicable without the factor 2 in

the denominator (Adamson, 1982; Rosen, 1978). In surface science literature, the quantities G (mass adsorbed per unit interfacial area) and Γ (Gibbs surface excess), are often used interchangeably, even though there is a subtle difference between the experimentally measured G and the thermodynamic entity Γ (Novosad, 1979). In the present work, G and Γ are used interchangeably.

Gibbs adsorption equation is a thermodynamic equation that describes adsorption in a generic fashion. In surface science literature, modifications to the Gibbs equation were proposed for its application to ionic surfactant sorption at liquid-liquid interface (Pethica, 1953; Haydon and Philips, 1957; Haydon and Taylor, 1959). Further, in the case of ionic surfactant sorption at liquid interfaces in the absence of an electrolyte, researchers also have found that the measured surface excess G is only 50% of that predicted by Eqn. 2-6, indicating that the factor of 2 in the denominator was redundant (Adamson, 1982; Osipow, 1962; Pethica, 1953). A similar discrepancy was observed in this study also, as will be shown later.

Alternative isotherms are available to describe the adsorption of surfactants at the hydrocarbon-water interface. For adsorption of long-chain ions, such as sodium dodecyl sulfate, at the oil-water interface, Davies and Rideal (1961) derived from theoretical considerations a Freundlich-type isotherm, of the form

$$G = K C^q \qquad (2\text{-}8)$$

where K and q are empirical constants. Measured data using sodium long-chain sulfates of various chain lengths at an oil-water interface at 50°C agreed well with Eqn. 2-8, when used

with q=2/3 (Davies and Rideal, 1961). Such an isotherm, derived specifically for the adsorption of long-chain anionic surfactants such as SDBS at the oil-water interface, is convenient for use in retardation equations (Eqn. 2-2 and 2-4) and hence in hydrologic applications of the interfacial tracers method.

Another approach to describing the adsorption of a surfactant at the liquid-liquid interface is the 'equation of state' approach. For dilute solutions, solute-solute interactions are negligible (i. e. Henry's law is valid), and the variation of γ with C will be linear ($d\gamma/dC$ constant), thus resulting in a linear isotherm (Adamson, 1982; Tadros, 1995), of the form

$$G = K_i C \tag{2-9}$$

A linear isotherm is convenient for hydrologic applications as the slope dG/dC in Eqns. 2-2 and 2-4 becomes a constant K_i which is independent of the tracer initial concentration C_o. For a given interfacial tracer-NAPL-water system, linear isotherm also results in the same retardation factor that is independent of the input pulse width. This result simplifies the analysis of pulse tracer experiment data, especially those from field tracer tests. In this context, linearization of a non-linear isotherm, such as a Freundlich isotherm (Eqn. 2-8) is a useful approximation (Rao, 1995). Applying the 'secant method' of linearization (Rao, 1995) to the Freundlich isotherm (Eqn. 2-7) at any given C_o, a 'linearized adsorption coefficient', K_i, can be defined as below:

$$K_i = K C_o^{q-1} \tag{2-10}$$

The linearized adsorption coefficient, K_i, can then be used as a constant in the place of the

slope dG/dC in Eqns. 2-2 and 2-4, just as in the case of a linear adsorption isotherm.

Values for the area per molecule, a, for a number of surface active species are available in the literature, reported typically at the CMC value of the surfactant. If step input tracer experiments are conducted at a C_o other than the *CMC* (sub-*CMC*), the resulting R, can still be used to calculate a_{nw} using Eqn. 2-5, provided an appropriate a value (corresponding to the C_o) is used. If the isotherm for interfacial tracer is nonlinear, Freundlich type (Eqn. 2-8), then the area per molecule at any sub-*CMC* concentration can be obtained as

$$a|_{C_o} = a|_{CMC}\,(CMC/C_o)^q \qquad (2\text{-}11)$$

Isotherms for the adsorption of interfacial tracer at the NAPL-water interface are further discussed later in this chapter, *vis-a-vis* the experimental results.

Experimental

The experimental objectives of this study were to measure a_{nw} using different NAPLs, interfacial tracers and porous media to obtain isotherms for the adsorption of an interfacial tracer at the NAPL-water interface, and to illustrate the hydrologic application of the method, as described by Eqns. 2-2 and 2-4. Column experiments were conducted using sodium dodecyl benzenesulfonate (SDBS, ICN Biochemical, >90% pure), sodium dioctyl sulfosuccinate (Aerosol OT-100) and valeric acid (Fischer Scientific, >99% pure) as the interfacial tracers, to measure a_{nw} in clean sands and glass bead packs. Decane, perchloroethene (PCE), FC-40 (an inert fluorocarbon) and a complex jet fuel mixture from a contaminated site at Hill Air Force

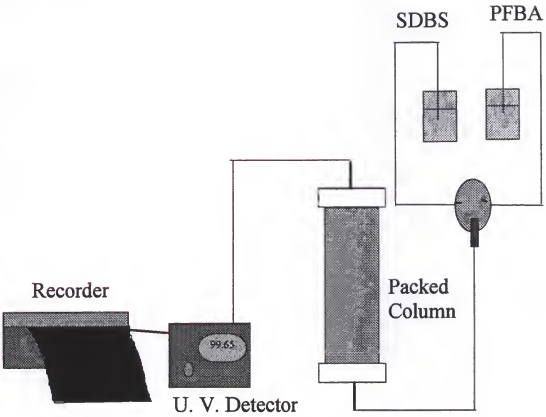

Figure 2-1. Column experimental apparatus

Base, Utah (called JP-OIL hereafter) were used as the NAPL phases. The experimental apparatus used is shown in Fig. 2-1. It was verified in batch experiments that SDBS, AOT-100 and valeric acid do not partition into the bulk NAPL phases appreciably. Pentafluorobenzoic acid (PFBA) was used as the non-reactive tracer.

Glass beads in the size range of 150 to 500 μm (Cataphote corporation), a clean sand (sand S1, washed several times with methanol/water, and hydrochloric acid/water and baked at 450 °C for several hours) and a partially clean sand (sand S2, washed several times with methanol/water and oven dried over night) were used as porous media in the experiments. The NAPLs were introduced into the porous media, using a syringe pump at a flow rate of 0.2 ml/min. A part of the NAPL was later removed by injecting water into the columns, at a flow rate of 1 ml/min. At the end of loading, pore spaces in the columns were filled partially with NAPL at a saturation S_n. Steady volumetric water flow was established using an HPLC pump (Gilson Co., Model 305) prior to injection of tracers. In separate experiments, both interfacial tracers (SDBS, AOT or valeric acid) and non-reactive tracers (PFBA) were injected continuously until the relative concentration C^* in the effluent reached unity. Effluent from the column experiments was analyzed for both tracers using spectrophotometric methods, both in-line and from discrete samples. The SDBS and PFBA concentrations in collected samples were analyzed using an UV spectrophotometer (Milton Roy Co., Spectronics 605) at 260 and 254 nm respectively. Characteristics of columns used in the experiments are summarized in Table 2-1.

Table 2-1. Characteristics of Interfacial Tracer Experiment Columns

column	length/dia cm	porous medium	pore volume, ml	NAPL	S_n %
IFT-Gϕ	5 x 2.54	glass beads	9.7	none	0
IFT-S1ϕ	5 x 2.54	sand S1	10.3	none	0
IFT-S2ϕ	5 x 2.54	sand S2	10.6	none	0
IFT-A	15 x 2.54	glass beads	22.2	decane	21.8
IFT-B	5 x 2.54	glass beads	8.1	decane	16.4
IFT-JPOIL	5 x 2.54	glass beads	7.9	JPOIL	27.5
IFT-FC40	5 x 2.54	glass beads	9.6	FC-40	7.4
IFT-PCE	5 x 2.54	glass beads	6.1	PCE	24.0
IFT-D	5 x 2.54	sand S1	8.1	decane	20.4
IFT-T	5 x 2.54	Sand S2	7.9	decane	16.0
IFT-F	5 x 2.54	Sand S2	6.8	decane	20.4
IFT-S2	5 x 2.54	sand S2	8.6	decane	19.6

Results and Discussion

Measurement of Specific Interfacial Area a_{nw}

The specific NAPL-water interfacial area a_{nw} values measured in different column experiments, along with the interfacial tracer used in each experiment, are summarized in Table 2-2. All of the column experiments were conducted with step input concentration (C_o) of the interfacial tracers less than or equal to the CMC, as the supra-CMC surfactant solutions might dissolve decane in the columns, thus changing the morphology and a_{nw} value. Reduction in interfacial tensions achieved using sub-CMC surfactant solutions was not sufficient to initiate mobilization in the experiments; significant enhancement in solubilization of decane, a sparingly soluble alkane, in the absence of micellization is equally unlikely.

Experiments in columns IFT-Gϕ, IFT-S1ϕ and IFT-S2ϕ were conducted to measure the background sorption of interfacial tracers onto the solid matrix, in the absence of any NAPL. Breakthrough curves for PFBA and SDBS in these experiments (Figs. 2-2(A) to (C)) reveal that SDBS did not adsorb significantly on the glass beads (IFT-Gϕ) and sand1 (IFT-S1ϕ), whereas it did adsorb significantly on sand S2 (IFT-S2ϕ) with R = 1.06, resulting in a linear adsorption coefficient (K_s) estimate of 0.014 ml/g . As such, a constant K_s value of 0.014 ml/g was used in Eqn. 2-4 for calculating a_{nw} in experiments using S2 sand. For all other experiments (using glass beads or S1 sand), K_s was zero.

The a_{nw} values reported for experiments using SDBS in decane-water systems were calculated using Eqn. 2-4 with an isotherm slope K_o of 2.5×10^{-4} cm at an SDBS C_o of 0.418 µg/ml (CMC), which is obtained from a measured interfacial tension- SDBS

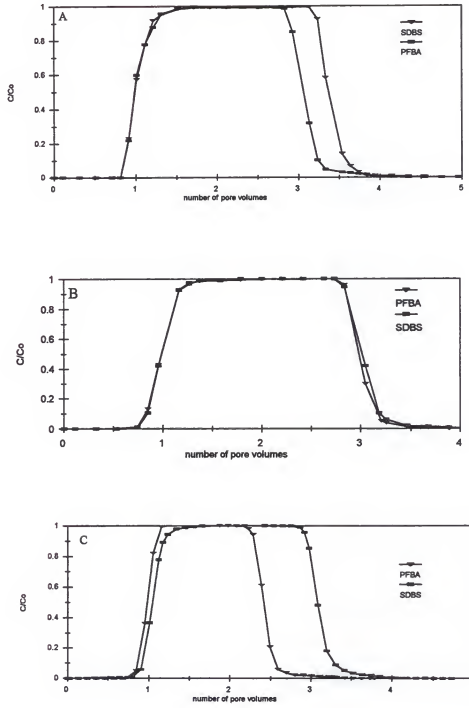

Figure 2-2. Breakthrough curves for PFBA and SDBS (different pulse durations) in (A) IFT-Gϕ, (B) IFT-S1ϕ and (C) IFT-S2ϕ soil sorption experiments, conducted in the absence of NAPL

concentration (γ-C) plot, shown in Fig. 2-3 (A). For these SDBS-decane-water experiments, the a_{mw} values were calculated using Eqn.2-5 as well, with an a value of 61 Å^2, and these areas agree well with the values calculated using Eqn. 2-4. It should be noted that Eqns. 2-4 and 2-5 represent the same principle, viz. using the mass of interfacial tracer adsorbed as a measure of a_{mw}. Eqn. 2-5, which corresponds to a step input experiment is a special case of Eqn.2-4, and can be applied to all but one (IFT-S2-P) experiments in this study, which were step input experiments by design. IFT-S2-P experiments were pulse input tracer experiments conducted in the coulmn IFT-S2. Breakthrough curves for the interfacial tracers and PFBA in various experiments listed in Table 2-1 are presented in Figures 2-4 through 2-9.

In experiments using AOT-100 and valeric acid as tracers, the reported a_{mw} values were calculated using Eqn. 2-5 alone with appropriate a values, based on earlier reported a values for these tracer compounds (Rosen, 1978; Adamson, 1982; Davis and Rideal, 1961; Oh and Shah, 1993). As can be seen from Eqn.2-5, area per molecule a is central to the measurement of a_{mw}. The area per molecule a, which is equal to $1/M^{\Gamma}$, is typically obtained as - $[C/2NRT](d\gamma/dC)$ at any given sorbate concentration C, $d\gamma/dC$ being the slope of the γ-C plot at that concentration (Rosen, 1978; Adamson, 1982). Values of a reported for a number of anionic surfactants at air-water and heptane-water interfaces range from 45 to 72 Å^2 (Adamson, 1982). Oh and Shah (1993) estimated a of sodium dodecylsulfate at hexadecane/water and air/water interfaces as 68.9 and 51.8 Å^2 respectively. Sodium dodecylbenzosulfonate (SDBS) exhibited saturation adsorption on graphon, a hydrophobic surface, at the CMC, with an a value of 60 Å^2 (Hough and Rendall, 1983). We obtained a

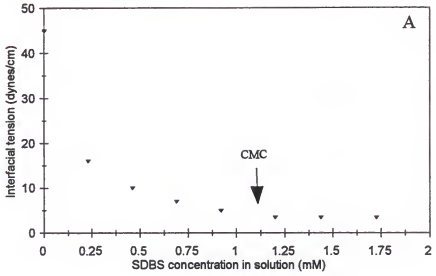

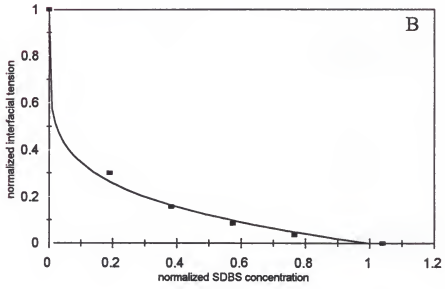

Figure 2-3. Interfacial tension at decane-SDBS solution interface measured as a function of SDBS concentration (A) γ-C data (B) γ^*-Ω data fit with Eqn. 2-13

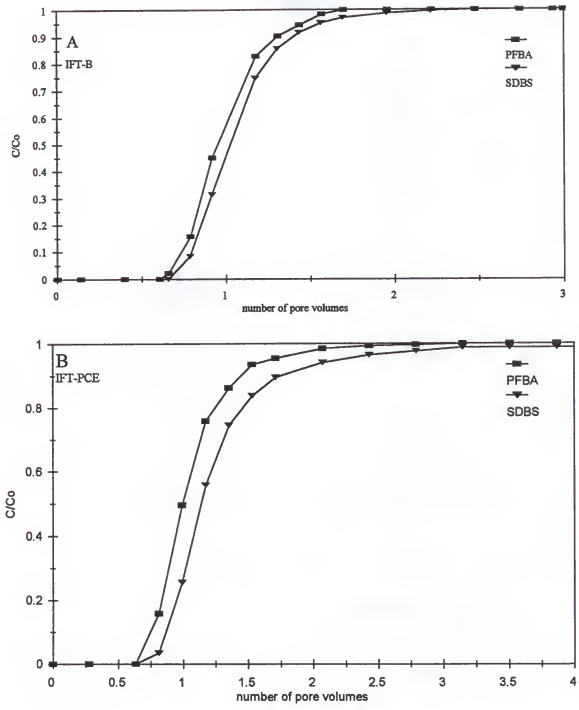

Figure 2-4 Breakthrough curves from (A) IFT-B and (B) IFT-PCE column experiments

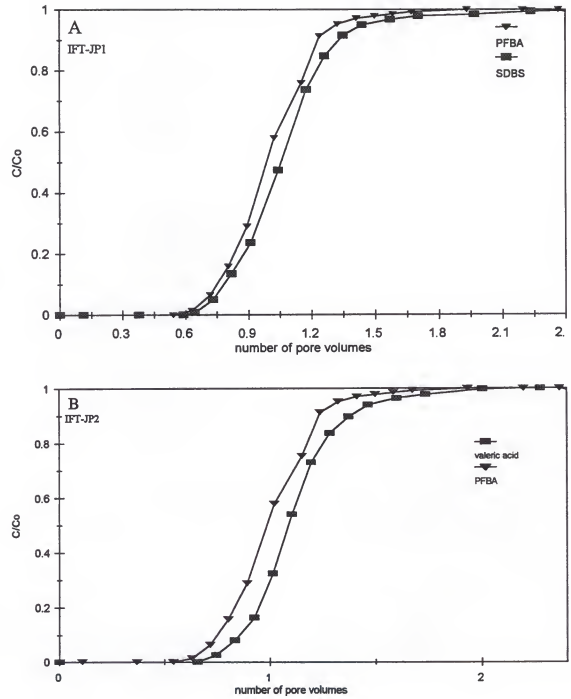

Figure 2-5 Breakthrough curves from (A) IFT-JP1 and (B) IFT-JP2 experiments

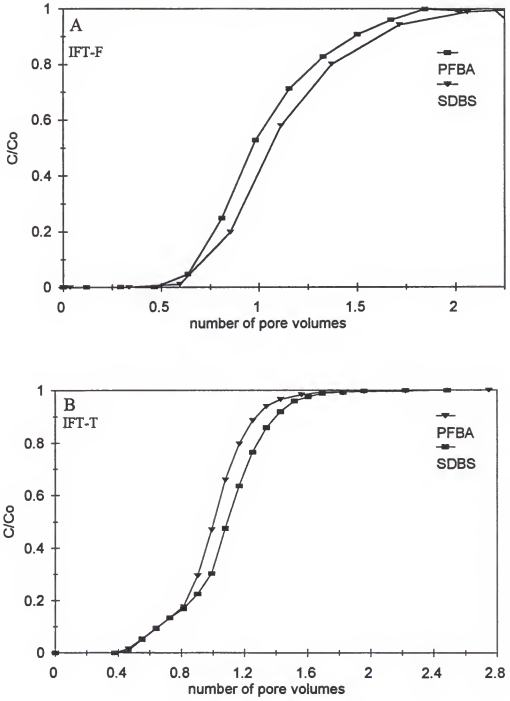

Figure 2-6. Breakthrough curves from (A) IFT-F and (B) IFT-T column experiments

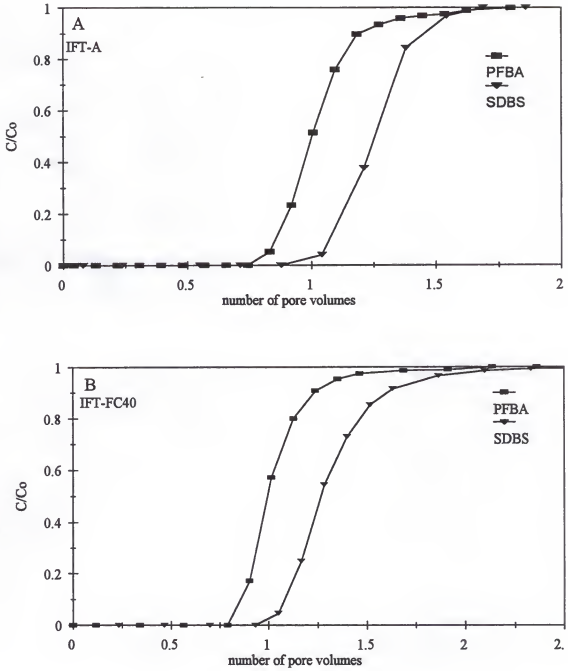

Figure 2-7 Breakthrough curves from (A) IFT-A and (B) IFT-FC40 column experiments

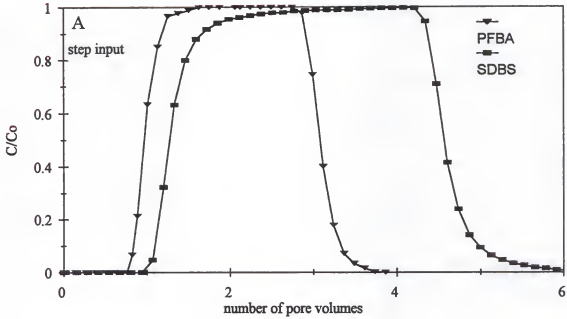

Figure 2-8 Breakthrough curves from IFT-D experiment

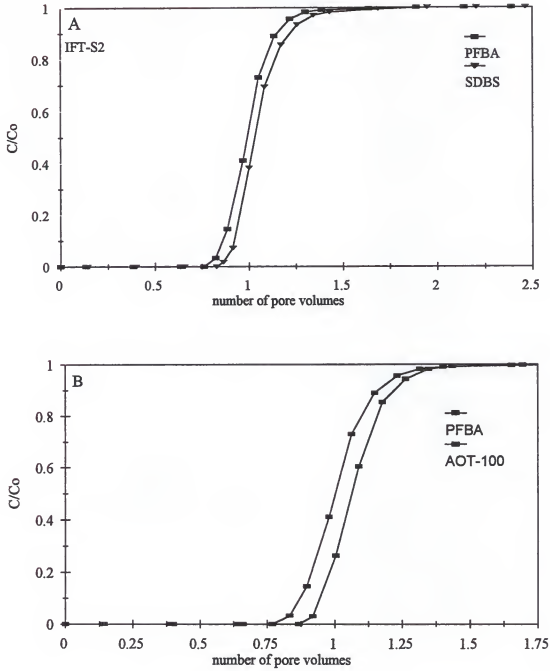

Figure 2-9 Breakthrough curves from (A) IFT-S2-1 and (B)IFT-S2-2 column experiments

value of 61 $Å^2$ for SDBS at decane-water interface, from a γ -C plot, using Wilhelmy plate technique (Fig. 2-3). The a value used in this work for valeric acid and SDBS at JP-OIL - water interface were 25 and 60$Å^2$ respectively. Further, an a value of 60$Å^2$ was used for AOT-100 at decane-water interface, and SDBS at the PCE-water and FC-40-water interafces as well.

In Table 2-2, a horizontal line separates the experimental data between two different modes of NAPL loading: 'water-wet first' mode and 'NAPL-wet first' mode. In the former mode, the dry sand (or glass bead) column pack was fully saturated with water, a part of which was later displaced by the NAPL, which should result in a truly non-wetting NAPL distribution. In contrast, in the 'NAPL-wet first' mode, the dry pack was filled with NAPL first, a large part of which was displaced by water later. This latter mode appears to have resulted in a partially NAPL-wet residual saturation distribution, as seen from the significantly larger a_{nw} values, as discussed in the following sections.

Assuming smooth, cubical particles and typical grain size distributions, the specific surface area of porous media in our experiments can be estimated by geometric analysis to be in the range 300 to 500 cm^2/cm^3 (Gregg and Sing, 1982). Irregular shape and surface roughness of particles can result in a higher specific surface area as measured by chemisorption techniques (Rosen, 1978; Anbeek, 1993; Gregg and Sing, 1982). In the case of IFT-A, IFT-FC40 and IFT-D columns, the NAPL appears to have partially wet the dry solid surfaces as films. In the case of IFT-FC40 column containing FC-40 oil, the residual saturation of oil was only 7.5%, due to the low interfacial tension between the oil and water. The a_{nw} for this column was 332 cm^2/cm^3, using an a value of 60 $Å^2$ for SDBS monomers at

Table 2-2. Results of interfacial tracer experiments in porous media columns

Experiment	Interfacial Tracer	R_{ift}	a_{nw}, cm^2/cm^3
mode of NAPL loading: *water-wet first*			
IFT-A	SDBS	1.061	86
IFT-JPOIL1	SDBS	1.065	68
IFT-JPOIL2	valeric acid	1.080	73
IFT-PCE	SDBS	1.090	92
IFT-T	SDBS	1.052	60
IFT-F	SDBS	1.090	91
IFT-S2-1	SDBS	1.063	89
IFT-S2-2	AOT-100	1.082	74
IFT-S1-P	SDBS	1.10	78
mode of loading: *NAPL-wet first*			
IFT-B	SDBS	1.169	218
IFT-FC40	SDBS	1.320	332
IFT-D	SDBS	1.247	233

the FC-40/water interface. In IFT-B and IFT-D, columns of same size packed respectively with glass beads and sand of similar particle size, the a_{nw} value measured at decane-water interface using SDBS agree closely, lending support to the consistency of technique. Further, the a_{nw} is about three times larger in column IFT-A than in IFT-B, both containing the same glass beads with different S_n values, but the former being wet by decane first and the later by water first. In the column wet by decane first, decane can be trapped primarily as wedges, films and pendular rings covering the particles (Mohanty *et al*, 1979; Schwille, 1981). In contrast, in a column wet by water first, decane cannot coat the water-wet solid surfaces, thus being trapped primarily within the pore spaces as large blobs (Wilson *et al*, 1990). As such, the a_{nw} for IFT-B column is only 40% of that of IFT-A column, where as their S_n values are not correspondingly different.

In the case of 'water-wet first' experiments, in which the NAPL form a truly nonwetting residual saturation consisting of ganglia of different shapes and sizes, the measured S_n for the NAPLs used was in the range of 15 to 25%, which is reasonable for trapped NAPLs in unconsolidated sands (Wilson *et al*, 1981). Interestingly, the measured a_{nw} value for these columns also was within a small range, between 60 to 90 cm^2/cm^3, for all of the NAPLs used. An a_{nw} value in this range for a hydrocarbon trapped at an average S_n of 20% (S_w of 80%) is in good agreement with several earlier theoretical predictions (Cary, 1994; Leverett, 1941; Bradford and Leij, 1995), particulary that of Leverett's thermodynamic model, as discussed in detail in Chapter 3. It should be noted here that sand particle size or pore size distribution and interfacial tension are the two characteristics that dictate the NAPL distribution. As such, the specific interfacial area (a_{nw}) value for

hydrocarbons, which possess similar interfacial tension values with water (40 to 50 dynes/cm), trapped in unconsolidated sands of similar NAPL entry pressures and pore size distributions, should be similar. As discussed above, the experimental results corroborate this prediction. A generic value or expression for a_{nw} that is common to many NAPLs and sands, would be extremely valuable in modeling of NAPL trapping and dissolution, and merits continued investigation. Finally, the a_{nw} values measured in the same experimental column using two different interfacial tracers agreed closely, as in the case of IFT-S2-1 & IFT-S2-2 and IFT-JPOIL-1& IFT-JPOIL-2 pairs. Overall, the results (a_{nw} values) are reasonable for the porous media and NAPLs used and are in agreement with the current understanding of immiscible fluid behavior in porous media.

In the case of solid-liquid interfaces, fine powdered adsorbents of known area, like graphon, are used to verify a technique proposed to measure specific surface. In contrast, it is very difficult to create a large fluid-fluid interface of known area in a flow experimental system. Further, no other methods currently are available against which to verify the proposed method. However, a considerable body of earlier work, conducted using surfactants in batch systems containing alkane-water emulsions, confirmed that the interfacial areas measured using surfactant adsorption and by an alternative (microscopic, drop size analysis) method were in agreement (Davis and Rideal, 1961; Haydon and Philips, 1957). Such evidence from earlier work confirms that the principle, assumptions and method of the interfacial technique are valid. Further, it will be seen that the measured a_{nw} results in interfacial tracer experiments in trapped saturation (this chapter) and the a_{nw}-S_w relationship measured in continuous NAPL saturation (Chapter 3) are in good agreement with the

theoretical predictions. Furthermore, the a_{nw} value changes monitored during mobilization of decane as a function of decreasing S_n, as will be shown in Chapter 4, are realistic. Finally, the interfacial tracers technique was also able to measure the significant increases in a_{nw} due to emulsification (chapter 3), an observation supported by the theory of emulsion science (Gopal, 1967). Adamson (1982) emphasizes that interfacial area of porous solids and (a_{nw} of fluids distributed in such solids, by the same token) should be regarded as relative than absolute quantities, owing to the fractal nature of the surfaces and uncertainties in the measurements involved. Such measurement uncertainties in tracer adsorption methods in fact are less in the case of liquid-liquid interfaces than in the case of solid-liquid interfaces, as the former are much more homogeneous, where monolayer adsorption and homogeneous packing of the tracer are assured, unlike at the solid-liquid interface. In light of these considerations, it is appropriate to conclude that interfacial tracers technology is adequate to provide a measure of the specific NAPL-water interfacial area a_{nw}.

Adsorption Isotherms

As can be seen from Gibbs equation (Eqn. 2-7), γ-C relationship is required to relate the surface concentration of the interfacial tracer to the bulk phase concentration. In the present work, the γ-C relationship was measured for SDBS adsorption at the decane-water interface using the Wilhelmy plate apparatus (Fig. 2-3(A)). Interfacial tension at a typical hydrocarbon-water interface starts at an initial value (γ_o) of 45 to 50 dynes/cm in the absence of any surface excess, and drops with increasing surfactant concentration (excess) at the interface to a final, asymptotic value (γ_{min}) of about 5 dynes/cm near the critical micellar

concentration (CMC) of the surfactants. Further increase in C does not cause appreciable change in γ. For the SDBS-decane-water system, the measured γ_o and γ_{min} values were 45 and 3.5 dynes/cm respectively, the measured γ-C relationship being shown as a γ^*-Ω plot in Fig. 2-3 (B). In this plot, γ^* and Ω are defined as

$$\gamma^* = \frac{\gamma - \gamma_{min}}{\gamma^* - \gamma_{min}} \qquad (2\text{-}12)$$

and

$$\Omega = C/CMC \qquad (2\text{-}13)$$

Using the measured γ-C data, the area per SDBS molecule, a, at the decane - water interface was found to be 61Å^2.

It is useful to obtain a functional relationship between γ-C, which can be differentiated to obtain the value of the slope $d\gamma/dC$ as a function of C, and hence convert the Gibbs equation to an isotherm (Γ-C) form. Following power function was obtained as a statistical best fit to the γ^*-Ω data of Fig. 2-3(B):

$$\gamma^* = 1 - (\Omega)^{0.185} \qquad (2\text{-}14)$$

Upon differentiation of Eqn. 2-14 and substitution into the Gibbs equation, the following isotherm equation was obtained for the adsorption of SDBS at the decane-water interface:

$$\Gamma = (5.43)10^{-10}\ C^{0.185} \qquad (2\text{-}15)$$

where C is molar concentration and Γ is expressed in moles/cm^2, measured at a temperature of 22°C and standard atmospheric pressure. The isotherm plots given by Eqn. 2-15 do resembel the typical isotherms for surfactant adsorption at hydrophobic fluid-water interfaces. However, it should be noted that Eqn. 2-15 is a model fit, obtained by differentiation of a γ-C function, which itself is another arbitrarily chosen model fit to the measured data. The isotherm equation (Eqn. 2-15) is extremely sensitive to the analytical function chosen to fit the γ-C data, a power function in case of Eqn. 2-14. We found that logaritmic and exponential functions, which appear to fit the γ-C data in lieu of a power function, fail to result in a meaningful adsorption isotherm (Γ-C plot). To the best of our knowledge, there were no reported attempts to model the γ-C relationship by rational or empirical means and translate it to isotherm models. Such exercise, though very useful, is difficult and involves arbitrary assumptions, as can be seen from the above discussion. Further investigation in this direction will be useful in the study of adsorption at liquid-liquid interfaces.

Experimental Results

To experimentally obtain the isotherm (γ-C relationship), a series of column experiments were conducted on IFT-T and IFT-D columns, both containing trapped decane in two different sands: IFT-T column containing S2 sand which did not adsorb SDBS appreciably, whereas IFT-D contained S1 sand that did adsorb SDBS significantly. A series of experiments also were conducted on IFT-S2 column, to obtain an isotherm for AOT-100 tracer. In plotting the isotherms of Fig. 2-10 and 2-11, it was assumed that the interfacial area a_{nw} does not change significantly due to contact with the surfactant (tracer). No mobilization

of residual decane was observed while using the surfactants in zero to *CMC* concentration range. Further, the retardation factor obtained using SDBS at a sub-*CMC* C_o value, before and after a similar experiment using C_o=*CMC* remained the same, confirming that a_{nw} did not change significantly due to SDBS contact wih the decane-water interface. Subsequently, the area a_{nw} for a given column was calculated as described earlier. The surface concentration G at any given C_o value was then obtained as the total mass adsorbed normalized to the measured a_{nw} value.

All of the experiments in this study were conducted in the absence of an electrolyte. As such, Gibbs equation will be applicable, with a factor of 2 in the denominator, i. e. as written in Eqn. 2- 6. However, the γ-C plot according to this equation, shown by a solid line in Fig. 2-11 underpredicts the G values at any given C by about 50%. Such discrepancy between the measured data and predicted Gibbs isotherm was observed earlier in the surface science literature as well. Isotherms obtained for adsorption of sodium lauryl sulfate and OT-100 surfactants at the oil-water interface in the absence of swamping amount of electrolyte, agreed well with the predictions by Gibbs equation, only when the factor 2 in denominator was omitted (Adamson, 1982; Osipow, 1962). This discrepancy was attributed to a phenomenon known as 'surface hydrolysis', whereby the H^+ ion, rather than the Na^+ ion, adsorbs at the interface (Osipow, 1962). An alternative explanation is that the undissociated surfactant, rather than the anion, is the adsorbing species, which obviates the need for using a factor of 2 in the denominator in Gibbs equation (Adamson, 1982). It should be emphasized here that the maximum surface excess values measured for SDBS at the decane-water interface, as measured in IFT-T and IFT-D experiments are in excellent agrrement with earlier

reported values for similar surfactants at the hydrocarbon-water interface (Rosen, 1978; Pethica, 1952; Haydon and Philips, 1957). The flow adosrption technique for the measurement of isotherms, as used in this work, will be useful in future investigations of adsorption at immiscible fluid interfaces.

The need for an isotherm in hydrologic applications of the interfacial tracers method arises from the term dG/dC required in Eqns. 2-2 and 2-4. As described earlier, there are alternative isotherm equations proposed specifically for the adsorption of long chain ions at oil-water interface. A Freundlich isotherm fit the measured G-C data from IFT-T and IFT-D experiments well, with K values of 1.617×10^{-8} and 2.775×10^{-8}, and q values of 0.577 and 0.69 respectively (Fig. 2-13). Pulse experiments were conducted in IFT-S2 column (IFT-S2-P experiment), using SDBS at a C_o value of 200 mg/L, at different pulse widths (1, 5, 10, 20 and 28 minutes, at a flow rate of 1.02 ml/min). The resulting breakthrough curves (Fig. 2-14) yielded retardation factors of 1.1, 1.13, 1.09, 1.11 and 1.1 respectively, indicating that the slight nonlinearity in SDBS adsorption, as represented by a Freundlic exponent q of 0.6, was not manifested in this experiment. A model prediction of the same breakthrough curves, produced using a one-dimensional numerical code (UFBTC) indicated that the pulse breakthrough curves obtained represent the sorption and transport of SDBS reasonably. The a_{nw} of 79 cm^2/cm^3, calculated using the R_{ift} value of 1.1 from these pulse experiments, agrees with the step experimental measurements. Further experimental investigation may lead to the development of a generic isotherm equation with K and q value ranges that are applicable across different surfactant classes and NAPL-water interfaces.

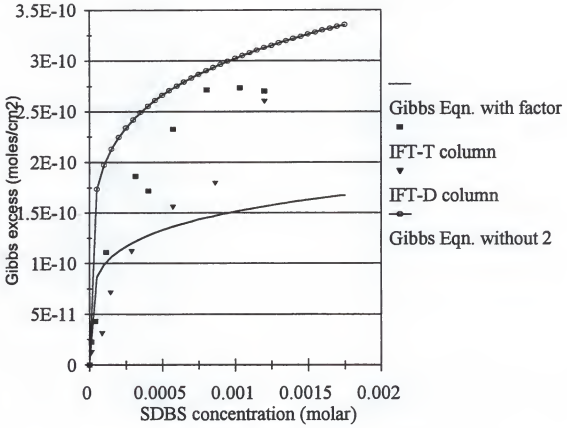

Figure 2-10. Isotherms for SDBS at decane-water interface measured from column experiments IFT-T and IFT-D & Gibbs equation fits

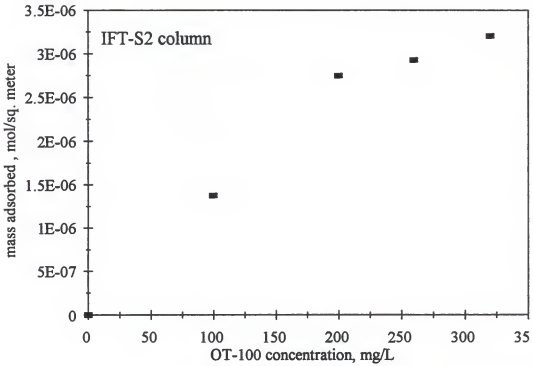

Figure 2-11 Isotherm for AOT-100 at decane-water interface, measured in IFT-S2 column flow experiments

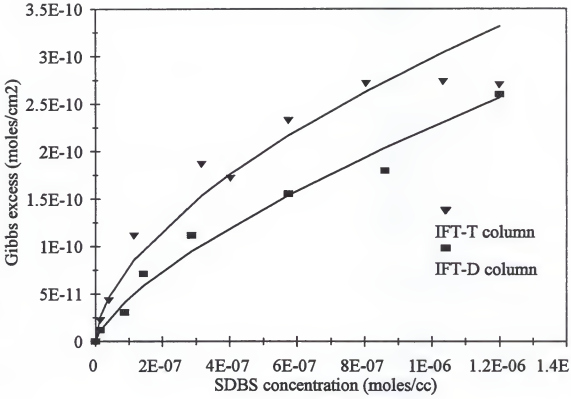

Figure 2-12 Isotherms obtained from column experiments IFT-T and IFT-D: Freundlich model fits to the measured data

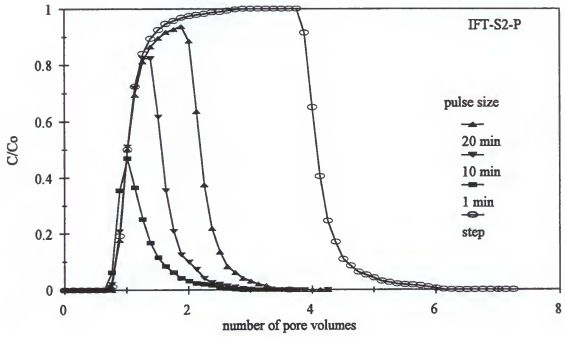

Figure 2-13 Breakthrough curves from IFT-S2-P pulse input experiments in IFT-S2 column

Further, it was observed (Fig.2- 14) that the isotherm can be approximated to be linear in the zero to 130 mg/l concentration range for SDBS and 0 to 280 mg/l range of AOT-100, a result in agreement with the state function approach. As such, for pulse tracer experiments conducted with a C_o value within the linear range of the isotherm, the slope K_i in Eqns. 2-2 and 2-4 can be treated as a constant. Furthermore, Eqn. 2-5 can be used to obtain a_{nw} as well, even in the case of tracer pulse experiments, as the retardation factor is independent of C_o. Isotherm linearty enables one to define the retardation factor as a linear function of a_{nw} according to Eqn.2-2, and thus simplifies the method application. Having measured R_{ift} from flow adsorption experiment and pore volume from a non-reactive tracer experiment, K_i is the only additional parameter required to estimate the a_{nw} of the porous medium using Eqn.2-2. The K_i value cannot be obtained from batch adsorption experiments, as it is very difficult to create a large liquid-liquid interface of known area in a batch vial. One way to measure K_i is to create a large interfacial area in a soil column and build an isotherm for interfacial tracer adsorption, as illustrated in the experimental section of this work. Alternatively, K_i value can also be obtained as the slope of the linear isotherm, as $1/Na'C'$, where a' is the area occupied per molecule at the maximum concentration limit C' up to which the isotherm is linear. For example, from Fig. 2-9, one observes that C' for SDBS at decane-water interface is about 130 mg/l, which is approximately equal to $CMC/3$. Alternatively, the a' value , which is typically obtained from a γ-C plot as explained earlier, can also be directly substituted in Eqn.2-5, to obtain the a_{nw} value.

In many porous media applications, one is interested in comparing interfacial areas among different systems, than absolute interfacial areas *per se*. For example, the proposed

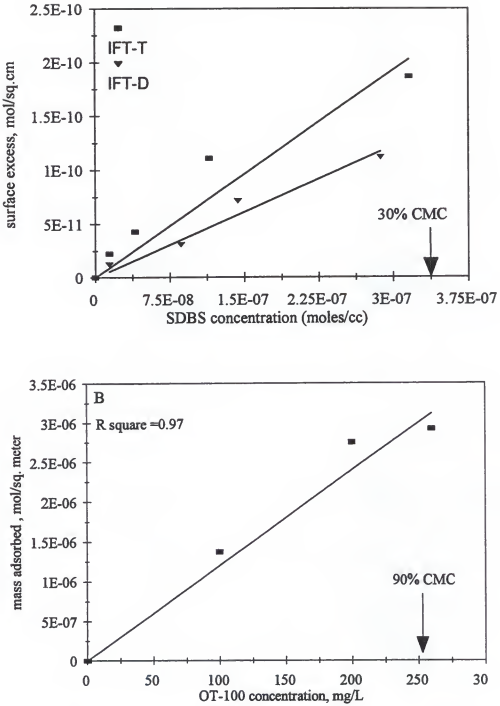

Figure 2-14 Linear ranges of adsorption isotherms for (A) SDBS and (B) AOT at decane-water interface

experimental technique can be used to define a NAPL morphology index, as the 'NAPL-water interfacial area to NAPL volume ratio' (I), which is an index of how thinly spread the oil is in a porous medium. Between two porous media having same NAPL saturation, the one containing many smaller NAPL blobs and films will have a higher I value, a result useful in the location of large pools of oils in aquifers and petroleum reservoirs. For example, the I values for the columns IFT-A and IFT-B columns in our experiments are 3028 and 1493 cm^{-1} respectively, clearly indicating the difference in NAPL morphology between systems containing decane at similar S_n values. Measurement and use of morphology index I are discussed more fully in Chapter 5.

Error Analysis

Measurement of specific interfacial area using interfacial tracers involves a tracer flow experiment. The interfacial tracer experimental method can be divided into four steps:

(i) measurement of the pore water volume in the test volume by direct gravimetric measurement and from a breakthrough curve (BTC) of a non-reactive tracer such as PFBA,

(ii) measurement of the interfacial tracer retardation factor, R_{ift}, from BTC of an interfacial tracer such as SDBS,

(iii) obtaining a value for the slope of the isotherm (K_i) for adsorption of interfacial tracer at the NAPL-water interface, at the initial concentration (C_o) of interest, and

(iv) obtaining a value for the slope of the isotherm (K_s) for adsorption of interfacial tracer at the soil-water interface, at the initial concentration (C_o) of interest.

The last step will be necessary for most of the natural soil surfaces, where the interfacial tracer is likely to adsorb significantly. In laboratory experiments using clean sands or glass beads, this step will not be necessary.

The primary data collected in interfacial tracer experiments lead to a breakthrough curve (BTC), which is a distribution of the normalized effluent tracer concentration (C/C_o) as a function of time (t). The product of time and steady volumetric flow rate yield the effluent flow volume at any given time. The time axis of BTC is usually transformed to 'number of pore volumes,' by normalizing the flow volume to one pore volume, which is obtained from the first normalized moment (μ_1) of the non-reactive tracer BTC. Subsequently, first normalized moment of the interfacial tracer BTC will yield the retardation factor, R_{fp}, which is a measure of the specific interfacial area a_{mn}, as seen in Eqn. 2-2.

Statistical uncertainty in the process of measuring a_{mn} thus consists of the uncertainty associated with the four experimental steps listed above. In step (i) and (ii), which involve similar tracer experiments, the possible experimental error is due to the physical measurement of the volumetric flow rate q and time t, and analytical measurement of C for each discrete sample that comprises a BTC. In addition, the possible mathematical error is due to moment analysis to find μ_1, which essentially involves a numerical integration of the area formed by the C-t distribution, whose accuracy is a direct function of the completeness and noise in the BTC data. A complete BTC is one in which there is no truncation of data, which is usually the case when there are no kinetic limitations to the reaction mediating retardation of the tracer (adsorption in the case of interfacial tracer). Interfacial tracer adsorption at the NAPL-water interface is reasonably fast (Davies and Rideal, 1969). As such, the resulting

BTCs are likely to be complete, if the NAPL-water interfaces are accessible. Noise in the BTC data is a function of the experimental technique. The experimental method and apparatus used in the present work have been used satisfactorily by several researchers before. Overall, the error associated with the BTC measurement and moment analysis in a standard laboratory setting is minimal.

However, if the first normalized moment of the interfacial tracer ($\mu_{1,if}$) is not significantly different from that of the non-reactive tracer ($\mu_{1,nr}$), then the resulting measurement of the retardation factor R_{if}, can have a high degree of uncertainty (or error) associated with it. A typical trapped NAPL distribution in soils, for a truly non-wetting NAPL, presents a low specific interfacial area, a_{nw}, (on the order of 100 cm^2/cm^3) which results in a difference of 10% only, between the measured $\mu_{1,nr}$ and $\mu_{1,if}$ values. This means that the corresponding R_{if} values are only on the order of 1.1, as can be seen from the results shown in Table 2-2. The R_{if} values are larger for a wetting NAPL, as shown also in Table 2-2, for a 'NAPL first' mode of loading. To test if the measured retardation factors in the experiments for the trapped NAPL case are significantly different from the non-reactive tracer retardation factor (R_{nr} =1 always), a student t-test was performed on the $_{if}$ R values measured in various trapped NAPL experiments (Table 2-2) using SDBS and AOT-100 as the interfacial tracers. Since the area per molecule (a) occupied by both SDBS and AOT-100 at several hydrocarbon-water interfaces is about 60 $Å^2$, and since the a_{nw} values presented by the hydrocarbon oils in the glass beads used were in a narrow range, they constitute a sample from one statistical population. (Valeric acid experiments, with a much smaller a value (25 $Å^2$) do not belong to this population). The results from t-test (mean R_{if} = 1.07, variance =

0.00023, calculated t equal to 12.45, which is larger than the two-tail critical t values of 1.94 and 2.44 respectively) indicate that mean R_{ift} value (1.07) is statistically different from 1.0, as shown by the large calculated t value. This is primarily because the standard deviation (a measure of error) in the measurement of R_{ift} was small (<2%), indicating that the small absolute difference between the mean R_{ift} and R_{nw} values was not due to error. Further, as will be seen in Chapter 3, the a_{nw} value in the range of 60 to 100 cm^2/cm^3 for trapped NAPL distributions is consistent with the earlier thermodynamic and geometric model predictions. Furthermore, a hydrodynamic based model presented in Chapter 4, relating a_{nw} and total trapping number N_T, also indicated that the a_{nw} values for a trapped NAPL distribution is on the order of 60 cm^2/cm^3. Finally, the R_{ift} values measured using interfacial tracers for NAPL of a morphology other than trapped, non-wetting ganglia (as continuously distributed NAPL at large S_n values or trapped wetting NAPL, for example) were large (from 1.25 to 2). This fact indicates that the relatively small R_{ift} values obtained in the case of a trapped, non-wetting NAPL are due to a low a_{nw} presented by that distribution, and do not necessarily reflect on the degree of error in the interfacial tracer technique itself. The laboratory column experiments, conducted using clean sands, liquid phases and interfaces under well controlled conditions do not represent the possible error in the measurement of a_{nw} value at field-scale, which is likely to be larger. An error propagation analysis to predict the error associated with the measurement of a_{nw} as a function of R_{ift} will be useful in this regard.

Error Propagation

The interfacial area a_{nw} is calculated as a function of the measured R_{ift} value, as can be seen from Eqn. 2-2:

$$R_{ift} = \frac{\mu_{ift}}{\mu_{nr}} = 1+\frac{a_{nw}}{\theta_w}(K_i)|_{Co,T} \qquad (2\text{-}2)$$

In Eqn. 2-2, the errors in the measurement of each of the four variables R_{ift}-1, a_{nw}, θ_w and K_i (where $K_i = G_d/C_o = 1/NaC_o$) can be referred to as δR, δa, $\delta\theta$ and δm respectively. Error in K_i is being referred to as δm (error in measuring the area per moleule value a), since C_o is known without error and N is a constant. Coefficient of Variation of a parameter x is defined as $CV = \sigma_x/\mu_x$, where μ and σ represent mean and standard deviation. Thus, CV is error in the measurement of a variable relative to its mean, and is an appropriate index to analyze the sensitivity of error in a dependent variable (a_{nw} in this case) to the errors in the independent variables (i. e. a_{nw}, K_i and θ_w). Assuming that the error $\delta\theta$ in water content measurement by gravimetric measurement and non-reactive tracer experiment is negligible, an error propagation equation can be developed to relate the variances among R_{ift}-1, a_{nw} and a_i using Taylor expansion (Bragg, 1974) as below:

$$(\sigma_a)^2 = (\sigma_{R-1})^2[\theta_w C_o Na]^2 + (\sigma_m)^2[\theta_w(R_{ift}-1)NC_o]^2 \qquad (2\text{-}16)$$

Using Eqn. 2-16, the coefficients of variation (CV) of these parameters can be related as

$$CV_a = \sqrt{CV_R^2 + CV_m^2} \qquad (2\text{-}17)$$

As was seen earlier from the t-test results, the error (variance) associated with the measurement of R_{jfi} -1 was small. The slope K_i and the area per molecule a are typically evaluated from a tangent graphically measured from either the interfacial tension plot or the measured (non-linear) isotherm, as was discussed in this chapter. The error associated with the measurement of K_i can be minimized by obtaining replicate data sets of γ_{nw}-C plots and verifying that the K_i value always corresponds to a meaningful area per molcule (a) value. These values (a) are documented in the literature for a number of surfactants and interfaces.

When the measured R_{jfi} values are small (i. e. $CV_R = 0$), it is reasonable to expect, from a modification of Eqn. 2-17, that CV_a is equal to CV_{nw}. This means that the fractional error in the measurement of a_{nw} will be approximately equal to that in the measurement of the isotherm slope K_i and the area per molecule a. A larger R_{jfi} value, which is possible in porous media containing large a_{nw} values, should also improve the accuracy of measurement of a_{nw}. Larger the absolute value of retardation factor in tracer experiments, smaller will be the error associated with that measurement (Jin, 1995). As such, it can be concluded that larger K_i and R_{jfi} values are desirable for an accurate measurement of a_{nw} in both laboratory and field settings. This can be accomplished by using interfacial tracer compounds that occupy a small area per molecule at the NAPL-water interface (e.g. valeric acid, a=25Å^2) and by using a swamping amount of electrolyte in the tracer carrier solution, which results in a tighter packing of the interfacial tracer at the interface. These measures result in a simultaneous increase of K_i and R_{jfi}. In conclusion, it is reasonable to note that the % error in the measurement of a_{nw} using interfacial tracers will be of the same order of magnitude as that in the measurement of R_{jfi}.

Summary and Conclusion

In the current work, use of the interfacial tracers method to measure the specific NAPL-water interfacial areas in porous media and its hydrologic application are discussed. The a_{nw} measured in column experiments using different interfacial tracers and NAPLs are reported. Trends in the measured a_{nw} (60-100 cm^2/cm^3 for 'water-wet first' systems and 200-330 cm^2/cm^3 for 'NAPL-wet first' systems), are in agreement with the current understanding of immiscible fluid behavior in porous media.

Investigation of adsorption isotherms revealed that the adsorption isotherms for typical interfacial tracers at the NAPL-water interface are slightly non-linear, described best by a Freundlich isotherm. For field applications, a linear isotherm approximation may be adequate. Error analysis revealed that the error in a_{nw} measurement is likely on the same order of magnitude as that related to R_{ift}. This error can be reduced by employing measures to increase retardation, such as the addition of electrolyte to the tracer input solution. The proposed technique finds immediate applications in groundwater remediation and unsaturated zone hydrology.

CHAPTER 3
SPECIFIC INTERFACIAL AREA OF CONTINUOUSLY DISTRIBUTED IMMISCIBLE FLUID INTERFACES IN POROUS MEDIA

Introduction

Behavior of immiscible fluids co-existing in porous media is of fundamental interest in several sciences and engineering applications. Of late, researchers have begun to recognize the specific interfacial area a_{nw} as a fundamental variable necessary to describe the status of immiscible fluids in porous media (Gray and Hassanizadeh, 1991; Hassanizadeh and Gray, 1993; Morrow, 1970). Equilibrium distribution of immiscible fluids in porous media corresponds to an energy status at which the total free energy is a minimum (Morrow, 1970). Surface free energy, an important component of total free energy, is directly proportional to the fluid interfacial area a_{nw}, just as the bulk phase free energies are proportional to the phase volumes or saturations.

Once the measurement of a_{nw} becomes widely available, constitutive relationships such as the soil moisture curves, can be described in terms of three fundamental variables: capillary pressure P_c, water saturation S_w and specific interfacial area a_{nw} (Gray and Hassanizadeh, 1991; Hassanizadeh and Gray, 1993). For any porous medium containing continuously distributed immiscible fluids, the relationships S_w - P_c , P_c - h, S_w - a_{nw} and a_{nw} - P_c ,where h is the hydraulic head, represent a complete knowledge of the static fluid behavior in the medium, atleast at a macroscopic (Darcy) scale. Several functions

available in the literature to describe the P_c - S_w relationship, notably among them the Brooks-Corey (1970) and Van Genuchten functions.

Because of the complex shapes and sizes the immiscible fluid interfaces assume, direct measurement of the specific interfacial area a_{nw}, and hence the a_{nw} - S_w , is difficult (Gray and Montemagno, 1995; Morrow, 1970; Pffankuch, 1984; Miller *et al*, 1990; Reeves and Celia,1996; Bradford and Leij, 1995). For the same reasons, mathematical modeling of the interfacial areas in porous media is often highly idealized, based on assumptions about pore geometry which may not necessarily be true (Leverett, 1941). Measurement of a_{nw} using interfacial tracers, and validation of the various a_{nw} - S_w model predictions will lead to a better understanding of the immiscible fluid statics and dynamics in porous media as well as several physico-chemical and biological processes at the fluid interfaces.

As described in Chapter 1, the specific interfacial area a_{nw} increases as the non-wetting phase saturation S_n increases and water saturation S_w correspondingly decreases. In the absence of tools to measure a_{nw}, past research focused on the development of mathematical models to describe the a_{nw} - S_w relationships. In the present work, the changes in a_{nw} were experimentally measured as a function of decreasing water saturation S_w , using the interfacial tracers technique. Using the resulting data, several available a_{nw} - S_w models are comparatively reviewed, and the similarities, applicability and unification of the various models discussed.

Experimental Methods

To confirm the earlier predictions that an increase in S_n results in a corresponding increase in a_{nw}, a first set of experiments was conducted using decane as the NAPL, in a short glass column, denoted as the ISH-A column (Kontes Co. 2.54 cm x 5 cm long, with Teflon end fittings). One end fitting was modified by inserting a stainless steel capillary barrier in the place of nylon filter. The decane entry pressure of the steel frit was much larger than that of the nylon filter. As such, the modification allowed decane to be retained in the cell at an S_n value much larger than the decane trapping saturation (around 20%, as shown in Chapter 2). The column was packed with dry glass beads (210 to 250 micron size) and saturated with distilled, deionized water in an upflow mode for several pore volumes. Using a 10 ml. glass syringe, decane was injected into the glass bead pack at the water inlet end (where the stainless steel frit was absent). Decane was trapped at an S_n of 43%, displacing a corresponding volume of water out of the column. Distilled water was flushed through the column at a slow flow rate (0.5 ml/min) for several pore volumes more, to remove any traces of decane in the effluent. At this stage, called 'ISH-A, Stage 1', interfacial tracer (SDBS) and nonreactive tracer (PFBA) breakthough curves (Fig. 3-1(A)) were obtained. The SDBS and PFBA concentrations in column effluent were analyzed using an in-line Ultraviolet (UV) detector at 260 and 254nm respectively. Subsequently, more decane was injected into the column, to achieve a higher decane saturation (S_n = 50%), and the tracer breakthrough curve experiments (Fig. 3-1(B)) were repeated to measure the increased a_{nw} value. The measured a_{nw} values at ISH-A1 and ISH-A2 stages were 131 and 177 cm^2/cm^3, respectively. These values are significantly larger than the a_{nw} measured in similar columns (chapter 2)

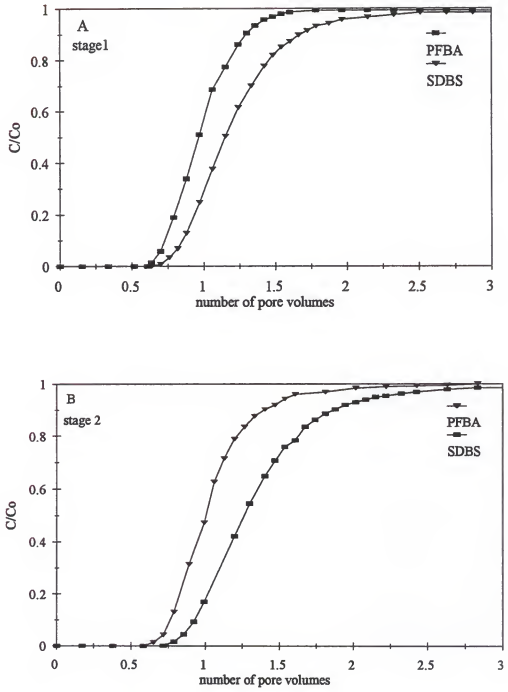

Figure 3-1 Breakthrough curves for PFBA and SDBS in ISH-D column at (A) stage 1 (S_n=43%) and (B) stage 2 (S_n=50%)

containing decane at a lower, trapped satuaration. Further, as can be seen from Fig. 3-2, trends in the measured a_{nw} - S_w relationship is in agreement with the earlier prediction.

Subsequently, a second set of experiments was conducted to establish the a_{nw} - S_n relationship. The experimental method essentially consisted of varying the capillary pressure in a short capillary cell containing decane and water in packed glass beads, to vary the fluid satuarations accordingly. Experiments were conducted using a specially designed modified capillary cell (Annable *et al*, 1992) that allows the retention and step-wise variation of S_n in a short soil sample in the cell, as a function of the external capillary pressure applied (Fig. 3-3). The stainless steel capillary barriers on either end of the cell allow only water to flow through. The glass bead packed cell was initially saturated with water. Some of the water was drained first by the entry of decane through the burette attached to the column into the pack, as the applied capillary pressure exceeded the decane entry pressure. A steady flow of water was applied at a low, steady flow rate to the top of the column. The cell outlet was kept at atmospheric pressure, using a hanging column of water. This produces a relatively uniform decane saturation content S_n in the short column. The NAPL saturation was increased by varying the total capillary pressure experienced at the center of the soil cell, by adjusting the decane level in the burette and the water in hanging column outlet. Locations of the hanging water column outlet and the decane level in the inlet burette were recorded at each stage of capillary equilibrium. These readings were used to calculate the average capillary pressure experienced at the center of the capillary cell. The cell inlet at the top and outlet at the bottom were used to conduct inert and interfacial tracer experiments, at a slow flow rate (0.5 ml/min). The slow flow was selected to avoid perturbation of the

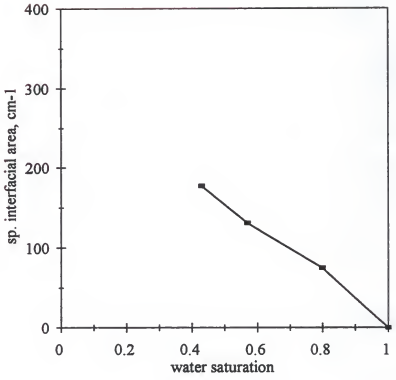

Figure 3-2 Change in specific interfacial area a_{nw} at decane-water interface in ISH-A column as a function of water saturation

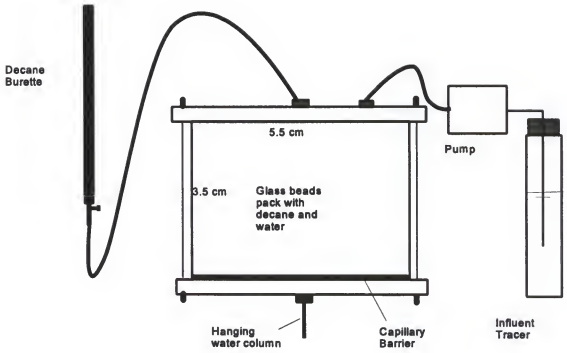

Fig. 3-3 Modified capillary cell used in ISH-C experiments

capillary pressure distribution along the cell length appreciably. Since the soil sample is short (3.4 cm high and 5.6 cm diameter), the NAPL saturation measure by volumetric balances represents an average saturation in the sample, at capillary equilibrium corresponding to the externally imposed capillary pressure value.

Experiments were conducted using decane as the NAPL phase and 210 to 250 micron size glass beads as porous media. By increasing the capillary pressure imposed on the system and allowing about 20 hours for equilibration, NAPL saturation was increased in a step-wise fashion. Using PFBA as a non-reactive tracer and SDBS as an interfacial tracer a_{nw} values were measured at each S_n value. In both SDBS and PFBA experiments, steady water flow was established using an HPLC pump (Gilson Co., Model 305) prior to injection of tracers. In separate experiments, a known pulse of interfacial tracers (SDBS) or non-reactive tracer (PFBA or bromide) was injected, foollowed by water injection. Experiments at low S_n values (0.13 and 0.25) were run using a step-input continuously until the effluent relative concentration reached unity. Discrete samples of effluent were collected continuously. The SDBS and PFBA concentrations in collected samples were analyzed using a UV spectrophotometer (Milton Roy Co., Spectronics 605) at 260 and 254nm respectively.

Shown in Fig. 3-4(A) through (G) are the SDBS and PFBA breakthrough curves at various saturation stages (stages ISH-C1 to ISH-C7) during the ISH-C capillary cell experiment. Results from analysis of these data were used to compare the measured trends in the a_{nw}-S_w relationship (Fig. 3-5(A)) with several earlier model predictions well, as will be shown in later discussion. Shown in Fig. 3-5(B) is the measured capillary pressure variation with decane imbibition and water drainage in the cell.

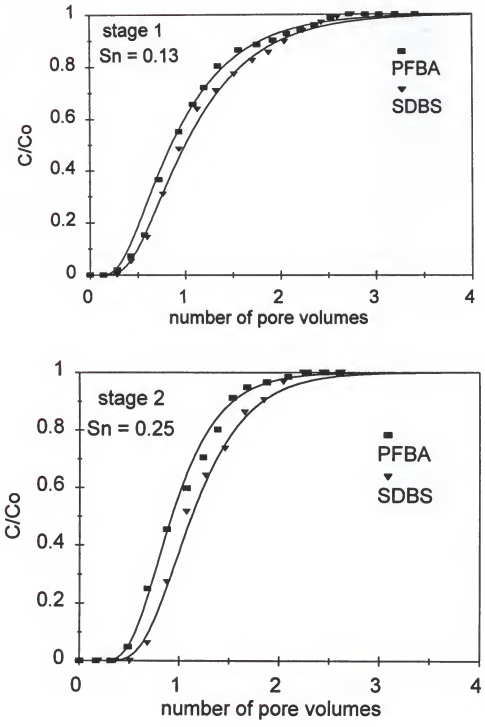

Figure 3-4 Breakthrough curves for SDBS and PFBA in ISH-B capillary cell at various stages of decane saturation

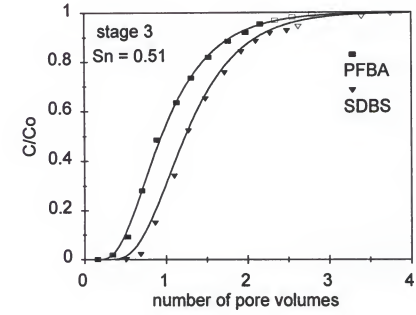

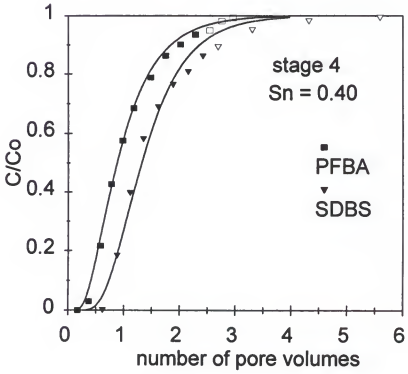

Figure 3-4 contd.

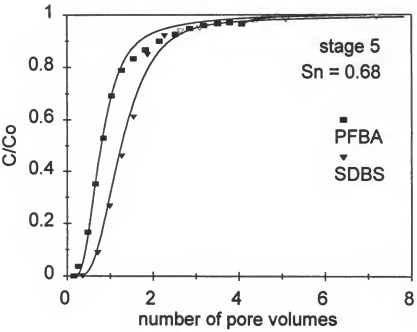

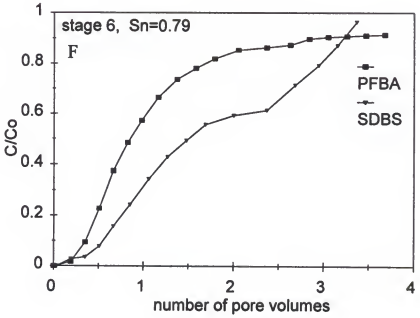

Figure 3-4 contd..

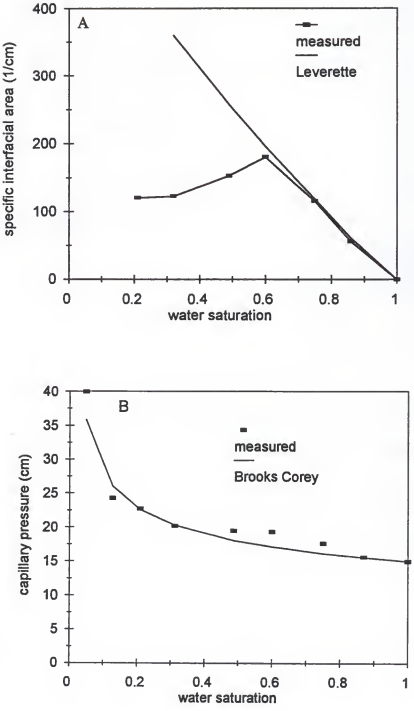

Figure 3-5 Results from capillary cell experiment ISH-C

Prediction of a_{nw} - S_w Realationship

Over the past several decades, many models were developed to predict a_{nw} as function of the fluid saturation and/or capillary pressure (Leverett, 1941; Morrow, 1970; Miller *et al*, 1990; Skopp, 1990; Cary,1994; Gvirtzman and Roberts,1991; Rose and Bruce, 1949; and Bradford and Leij, 1995). These models can be catagorized into (1) thermodynamic models (2) geometric models and (3) mixed empirical models. Geometric models often involve assumptions about the solid and pore geometry (Smith, 1933; Gvirtzman and Roberts, 1991), but do not invoke the concept of capillary retention of fluids in pores. In contrast, thermodynamic models (Leverett, 1941; Morrow, 1970; Bradford and Leij, 1995), which are based on the fundamental relationship between the capillary pressure across an immiscible fluid interface and the interfacial curvature, (the well-known Laplace equation), do not involve any geometric assumptions. Mixed empirical models use a combination of the thermodynamic and geometric approaches (Rose and Bruce, 1949; Cary, 1994; Skopp, 1990).

Thermodynamic Models

In a volume element containing two immiscible fluids, *n* (to denote nonwetting and/or NAPL phase) and *w* (to denote wetting or water phase), at capillary equilibrium the interfacial morphology corresponds to a state where the total free energy of the system is a minimum. The fundamental Gibbs' equation for change in Helmholtz free energy of a system containing the two immiscible fluids, *n* and *w*, is (Morrow, 1970):

$$dF = -EdT + \sum_{i=1}^{j} \mu_i dn_i - P_n dV_n - P_w dV_w + \gamma dA_{nw} \quad (3\text{-}1)$$

where the intensive quantities given on the right hand side of Eqn. 3-1 are entropy (E), chemical potential (μ), pressure in the bulk phase (P_w or P_n) and interfacial tension (γ) respectively. In Eqn. 3-1, i represents the species adsorbed at the *n-w* interface, n_i the number of moles of i adsorbed, A_{nw} the area of the *n-w* fluid interface, T temperature and V the phase volume respectively. The total Helmholz free energy of the system, F, is a sum of the bulk phase free energies, F_w and F_n and the interfacial free energy, F_s. For isothermal drainage and imbibition of incompressible fluid phases, when properties of the interface are independent of the total area A_{nw} it can be shown that the superficial surface free energy per unit interfacial area, f_s, is (Morrow, 1970):

$$f_s = \frac{F_s}{A_{nw}} = \sum_{i=1}^{j} \mu_i \Gamma_i + \gamma \quad (3\text{-}2)$$

where Γ_i is the Gibbs surface excess of component i. In the absence of any excess accumulation at the interface (i.e., no interfacial adsorption), Eqn. 3-2 leads to the definition of interfacial tension:

$$\gamma = \left(\frac{\partial F_s}{\partial A}\right)_{T,V,n} \quad (3\text{-}3)$$

Leverett (1941) extended the above described concepts of surface energetics to immiscible fluid interfaces in porous media. According to Leverett, the law determining the

shape of the interfacial surfaces is that the interfacial surface free energy should be a minimum, compatible with the volumes of fluids present and shapes of the restraining solid surfaces. Further, this global minimum in free energy (at Darcy scale) can be affected by a variety of local, pore-level minimum configurations (Mohanty, 1981; Gray and Hassanizadeh, 1993), which means that several a_{nw} values are possible for the same NAPL-soil system at the same fluid saturation.

Further, Leverett showed that the capillary pressure P_c at any location in the static column is the free energy increase δF accompanying the transfer of unit volume of water, V, from the sand to a zero curvature reservoir of water at the same level. Since an element of pore volume equal to one unit, $dV = -dS_w$, one writes

$$dF = P_c dV = -P_c dS_w \tag{3-4}$$

At this stage, Leverett proposed that the reversible work necessary to cause a change dS_w is equal to the difference in the free surface energies, ΔF, between the two saturation stages.

$$\Delta F = -\int_{S_{w1}}^{S_{w2}} P_c dS_w \tag{3-5}$$

Eq. 3-5 assumes that P_c and S_w are uniquely and continuously related, which is a valid assumption only in a certain range of S_w values and in the absence of hysteresis. These assumptions are reasonable when the fluids are continuous and do not experience draining-imbibition hysteretic cycles. Since the interfacial surface free energy (ΔF) per unit fluid-fluid interfacial area is by definition equal to the interfacial tension γ, an expression relating the

change in the interfacial area to the change in wetting phase saturation can be obtained as:

$$A_2 - A_1 = -\frac{1}{\gamma}\int_{S_{w1}}^{S_{w2}} P_c dS_w \qquad (3\text{-}6)$$

A_1 and A_2 being the total immiscible fluid interfacial area present in the sample, corresponding to water saturations of S_{w1} and S_{w2}, respectively. Leverett noted that Eq. 3-6 is valid in the intermediate water saturation regions only (i. e., the funicular region) where the solid-water interfacial area is reasonably constant and hence does not contribute to the overall change in free energy. Further, Eq. 3-6 is not valid for discontinuous nonwetting phase saturations, since the fluid saturations are insensitive to changes in capillary pressure in this region. At complete saturation of wetting phase, $S_w = 1$ and $A_1 = 0$, since no interface is present. When integrating to a limit of $S_w = 1$, Eq. 3-6 becomes

$$A_2 = \frac{1}{\gamma}\int_{S_{w2}}^{1} P_c dS_w \qquad (3\text{-}7)$$

The integral term in Eq. 3-7 represents the external work done on the system during drainage of water, and is equal to the increase in the surface free energy F_s when drainage is carried out isothermally. Payne (1953) used Eq. 3-7 to predict the specific solid surface areas of glass beads from P_c-S_w curves, integrated in the S_w range of 1 to S_{wr} . The predictions compared well with the actual specific surface areas.

Traditionally, interfacial curvature is regarded as the most significant property of a multiphase system from the standpoint of capillary behavior. Capillary pressure P_c is related to the interfacial tension γ and the principal radii of curvature R_1 and R_2 by the equation:

$$P_c = \gamma\left(\frac{1}{R_1}+\frac{1}{R_2}\right) \qquad 3\text{-}8$$

The net interfacial curvature is equal to $1/R_1 + 1/R_2$. For air-water and oil-water interfaces in porous media, the curvature is positive. Using Eq.3-8 as the basis, Leverett derived expressions relating P_c, S_w and a_{nw}, with reference to a water-wet porous medium in which two immiscible fluids exist under static equilibrium. In such systems, the capillary pressure P_c at any location in the column at a height h from an arbitrary datum where $P_c = 0$, is given by

$$P_c = \Delta\rho g h \qquad (3\text{-}9)$$

where $\Delta\rho$ is the difference in density between the two immiscible fluids. Using results from long column experiments with different sands containing air-water interface, Leverett proposed a relationship between the capillary head and water saturation, known as the Leverett's J-function, as below:

$$J(S_w) = \frac{P_c}{\gamma}\,[K_{sat}/\epsilon]^{0.5} \qquad (3\text{-}10)$$

where K_{sat} is the saturated hydraulic conductivity of the medium, $J(S_w)$ is a dimensionless

function of wetting phase saturation, ε is porosity and (K/ε) represents the 'average pore radius'. Eq. 3-10 can describe the P_c-S_w relationship in any clean, unconsolidated sand.

Capillary Pressure-Saturation Relationships

As seen from the thermodynamic analysis above, the nature of a_{mw} - S_w relationship is a strong function of the P_c - S_w relationship. Earlier researchers (e.g. Smith, 1933) also showed that the P_c - S_w relationships can be derived from a purely geometric analysis, without recourse to thermodynamics. It is instructive to briefly summarize the relevant P_c - S_w relationships here. In the literature, several semi-empirical functions are available to model the P_c - S_w relationship, prominent among them the Brooks-Corey (1985) and Van Genuchten (1980) functions. Brooks and Corey (1970) suggested an empirical function for the P_c - S_w relationship, as below:

$$S_e = [\frac{P_d}{P_c}]^{\lambda} \qquad (3\text{-}11)$$

where S_e is effective wetting phase saturation, P_d is non-wetting phase entry pressure and λ is a pore-size distribution index of the sand. For media having a uniform pore size, λ could approach a very large value. On the other hand, for media with a wide range of pore sizes, λ is a small number and can approach zero. Eq. 3-11 is valid for capillary pressure larger than P_d and saturation values larger than the residual saturation. When the λ value approaches infinity for a soil of uniform particle size, the Brooks-Corey prediction will agree with that of Smith (1933), which was derived for uniform spheres.

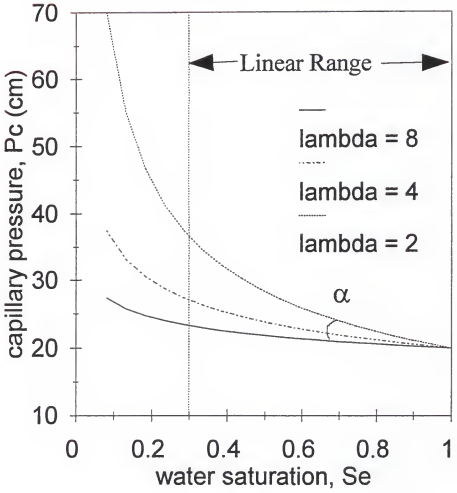

Figure 3-6 Hypothetical Brooks-Corey curves to illustrate the linear range approximation in P_c-S_e relationship

Van Genuchten (1980) model describes the P_c - S_w relationship in the entire range of capillary pressures and saturations. It is given by the following equation:

$$P_c = 1/\omega[(1/S_e)^{1/m}-1]^{1/n} \quad (3\text{-}12)$$

where ω is equal to $1/h_d$, the reciprocal of NAPL entry pressure head, and m and n are empirical constants characteristic of the sand. The parameters m and n are related (m=1-1/n), and it is possible to relate them to the grain and pore size distributions of sands used (Van Genuchten, 1980). It should be possible to derive a set of Van Genuchten parameters as well, that will correspond to the Smith's assumptions. An agreement among these different models with the analysis of smith would lend support to the physical meaning of the model parameters, such as λ. Similarly, using the Leverett's J-function as a basis, expressions can be developed to represent the a_{nw} - S_w relationship for any unconsolidated sand, in a generic fashion.

Leverett's analysis above considers the free energy contributions due to the *n-w* interface alone, assuming a completely wettable solid surface. However, many of the natural soils are mixed-wet in nature. To model the capillary behavior in such soils more fully, free energy contributions due to other interfaces, viz., the solid-water and solid-NAPL interfaces, must be included. Bradford and Leij (1995) undertook such complete analysis. In a porous medium containing two immiscible fluid phases and a solid phase, three phase interfaces are possible: solid-water, solid-NAPL and NAPL-water interfaces, which possess different interfacial tensions. The change in Helmholtz free energy of such a system with any perturbation can be given by a modification of Eqn. 3-1 (Bradford and Leij, 1995):

$$dF = -EdT + \sum_{i=1}^{3}\gamma_i dA_i - \sum_{p=1}^{3}P_p dV_p \qquad (3\text{-}13)$$

where γ and A represent the interfacial tension and the interfacial area at any interface i. In Eq. 3-13, it is assumed that there is no surface excess of species at any of the interfaces. For an isothermal system (dT=0) with incompressible phases, dF is equal to the net change in the surface free energies alone, i. e., $\sum\gamma_i dA_i$. This change in free energy in the system due to an external perturbation, such as the drainage of water to cause changes in NAPL and water saturations, dS_n and dS_w, is equal to the external work done on the system:

$$dW_{ext} = P_n \epsilon V_b dS_n + P_w \epsilon V_b dS_w = -P_c \epsilon V_b dS_w \qquad (3\text{-}14)$$

where V_b is the bulk volume of the porous medium and $dS_n = -dS_w$. Combining Eq. 3-13 and 3-14, and dividing the resulting equation by V_b, we obtain:

$$-P_c dS_w = \gamma_{nw}\cos(\phi_{snw})da^*_{sn} + \gamma_{nw}da^*_{nw} \qquad (3\text{-}15)$$

where ϕ_{snw} is the equilibrium contact angle at the *s-n-w* contact line. Thus, Eq. 3-15 relates observable changes in capillary pressure and fluid saturation to the changes in the specific interfacial areas per unit pore space a^*_{nw} and a^*_{sn}. For the case of complete wetting of the solid by water, a^*_{sn} and ϕ_{snw} are equal to zero, and Eq. 3-15 simplifies to:

$$-P_c dS_w = \gamma_{nw}da^*_{nw} \qquad (3\text{-}16)$$

which is the same as Eq. 3-6, as proposed by Leverett. Bradford and Leij (1995) propose that, upon integration between two limits of water saturation 1 and S_w, Eq. 3-16 should be

wrritten as:

$$a^{*}_{nw} = \frac{\Phi_{nw} + C_{nw}}{\gamma_{nw}} \qquad (3\text{-}17)$$

where Φ_{nw} is the area under the P_c - S_w curve between the water saturation values 1 and S_w, and C_{nw} is the constant of integration, equated to the a^{*}_{nw} value at the trapped residual saturation of the NAPL phase. This assumption leads to a discontinuity in the a^{*}_{nw} - S_w relationship between the trapped and continuous NAPL saturation regions. In addition, since the trapped individual ganglia coalesce as S_w decreases, Eq. 3-16 may over predict the a^{*}_{nw} values. The constant of integration in the integration of Eq. 3-7 bewteen the limits 1 and S_w gets canceled out. As such, for a NAPL-water system with completely water-wet solid, the expression:

$$a^{*}_{nw} = \frac{\Phi_{nw}}{\gamma_{nw}} \qquad (3\text{-}18)$$

as proposed by Leverett, is adequate.

The Φ_{nw} term in Eq. 3-18 can be obtained from direct integration of a P_c - S_w function, such as the Brooks-Corey (Fig. 3-4(B)) or Van Genuchten functions. Substitution of the Brooks-Corey function in Eq. 3-18 yields the required a_{nw}-S_w relationship as below:

$$a_{nw} = \frac{P_d}{\gamma(1-1/\lambda)}[1 - S_w^{(1-1/\lambda)}] \qquad (3\text{-}19)$$

It can be seen from Eqn. 3-19 that the NAPL entry pressure P_{d}, pore distribution index λ and interfacial tension γ are the parameters that dictate the a_{nw}-S_w relationship.

Shown in Fig. 3-5 are the measured capillary pressure as a function of water saturation in the cell, and a Brooks-Corey model fit. Shown in Fig. 3-6 are the Leverett's model prediction derived using Eq. 3-19, and the measured data (ISH-C experiments) for the a_{nw} - S_w relationship, for three different porous media (of different λ values). Results shown in Fig. 3-6 indicate that the measured trends in the a_{nw}-S_w relationship agree with the thermodynamic model of Leverett in the water saturation range of 55 to 100%. Below 55%, the tracer method reported a decreasing trend in interfacial area, contrary to the model predictions. The interfacial tracers report an a_{nw} value that is accessible to and sensed by the advective flow only. At high S_n values, the bulk of the pore networks, especially those comprising of larger pores, is filled with NAPL. Since the solid surfaces are wetted by water, there is likely a thin film of water present between the NAPL and solid surfaces, even at very high NAPL saturations. This water film, while sufficient to create increasing NAPL-water interfacial areas, should present severe mass transfer limitations to tracer adsorption via advective flow. Such mass transfer limitations due to the limited accessibility of the adsorbing interfaces through the immobile water regions, were widely reported in the literature on sorption in soils. Thus, at higher NAPL saturation, the a_{nw} values reported by interfacial tracers represent the fraction of the total interfacial area that is accessible to the advective flow.

Further, observation of several experimentally measured P_c - S_w functions (Busby *et al*, 1995; Guarnaccia *et al*, 1992; Demond and Roberts, 1989; Wilson *et al*, 1990; Leverett,

1941) reveals that the function has a linear nature in the high and intermediate S_w ranges, especially when λ is a large number (i. e. uniform porous media). As such, we propose a linearization of the P_c - S_w function in the insular and funicular saturation ranges (S approximately 1 to 0.3), by introducing a lever angle α (Fig. 3–6). Such linearization simplifies the a_{nw} - S_w analysis, as below:

$$S_e = \frac{P_d - P_c + \tan\alpha}{\tan\alpha} \tag{3-20}$$

and, according to Eqn. 3-18,

$$a_{nw}(S_e) = \frac{S_e}{2\gamma}[2P_d + (1 - S_e)\tan\alpha] \tag{3-21}$$

In the above model, the lever angle α and entry pressure P_d are the two parameters that dictate the nature of the a_{nw}-S_w relationships. Lever angle α can be shown to be a function of pore size and particle size distribution. Shown in Fig. 3-7 are a_{nw}-S_w curves predicted by the linearized Leverett model (Eq. 3-21) for sands with different α values.

Rose and Bruce (1949) developed an expression relating a_{nw} and capillary pressure, using the fundamental capillary rise equation:

$$P_c = \Delta\rho g h = \frac{2\gamma}{R_h} \tag{3-22}$$

together with the definition of hydraulic radius in a porous medium as $R_h = \varepsilon/A_s$, where ε is

porosity and A_s is the solid surface area per bulk volume, to obtain

$$A_s = \frac{\epsilon P_c}{\gamma} \tag{3-23}$$

The term A_s in the above equation is the solid or interstitial surface area; Rose and Bruce proposed a similar expression for the fluid interfacial area, a_{nw}, in terms of the water saturation S_w as below (Rose and Bruce, 1949; Miller *et al*, 1990):

$$a_{nw} = \frac{\epsilon S_w P_c}{\gamma} \tag{3-24}$$

Eq. 3-23 and 3-24 are useful to predict the general trends in the a_{nw}-S_w relationship. They are based on an explicit assumption due to Carman (1941) that the capillary rise in complex porous media such as random-packed, non-spherical sands can be obtained by using twice the hydraulic radius as the R_h value in Eq. 3-22, and a tacit assumption by Rose and Bruce that the specific interfacial area a_{nw} is proportional to A_s, the solid surface area, the proportionality being dictated by the capillary pressure status of the interface. This later assumption is not supported by any mechanistic explanation. Further, the pore size for the entire porous medium is represented by an average hydraulic radius. Even in hypothetical sand packs of uniform spherical particles, the pore size distributions are complex. It follows that the nonwetting phase interfaces, which are strongly dictated by the pore size distribution, also are complex. There is mounting evidence to support this observation. The model of Rose and Bruce can be modified topredict a_{nw} more realistically, by rewriting Eq. 3-24 as

$$a_{nw} = \frac{\epsilon}{\gamma}\sum P_{ci} \tag{3-25}$$

where i =1 to n represent pore size fractions ranging from the largest size pores of radius R_1 to smallest size pores of radius R_n that are successively filled by the nonwetting fluid as the capillary pressure increases. The capillary pressure P_{ci} corresponding to any pore of radius R_i is defined P_c=2γ/R_i. However, since the capillary pressure measured at Darcy scale is only a space-averaged value, Eqn. 3-25 cannot be used at present. A comparison of Eq. 3-7 and 3-24 reveals the similarities and differences between the models of Leverett and Rose and Bruce. Both models predict the a_{nw} to be directly proportional to the term P_c/γ. Leverett's model accomplishes the space averaging described above, to represent the various pore sizes in the medium, by using the integral term in Eqn.3-7, and hence predicts the interfacial area as a nonlinear function of S_w depending on the P_c-S_w function. This function, in turn, depends mainly on the entry pressure and pore size distribution of the soil, as represented by the parameter λ (Brooks-Corey) or n and ω (Van Genuchten). Due to its space-averaging character, Leverett's model is more realistic to predict the a_{nw} in porous media.

Eq. 3-24 of Rose and Bruce can be written in terms of wetting fluid saturation, by substituting Eqn. 3-11 (Brooks-Corey model):

$$a_{nw} = \frac{\epsilon P_c}{\gamma} = \frac{\epsilon P_d}{\gamma} S_e^{-1/\lambda} \tag{3-26}$$

Further, just as the solid specific surface A_s can be related to porosity ϵ, the fluid interfacial

area a_{nw} can be related to the nonwetting fluid saturation, S_n to define the appropriate hydraulic radius. To do this, consider a hypothetecal, rhomboidal or spherical pore with the nonwetting phase trapped as a spherical globule at the center. Each side of the equilateral rhomboid or the diameter of the sphere is equal to twice the hydraulic radius R defined by Rose and Bruce. Then, in the case of the pore and nonwetting phase globule being modeled as concentric spheres, the modified equation for specific interfacial area is given as:

$$a_{nw} = S_n^{2/3} \frac{\epsilon}{\gamma} P_d S_e^{-1/\lambda} \tag{3-27}$$

Instead, if the pore is considered to be an equilateral rhomboid, with a spherical nonwetting phase globule at the center, then by a similar derivation, it can be shown that

$$a_{nw} = 0.714 S_n^{2/3} \frac{\epsilon}{\gamma} P_d S_e^{-1/\lambda} \tag{3-28}$$

Shown in Fig.3-8 are the a_{nw}- S_w curves, for a soil of uniform pore size, (represented by a λ value of 4 in the Brooks-Corey function), using the Bruce and Rose model and the modified Bruce and Rose model, respectively.

Geometric Models

Behavior of immiscible fluids can be elucidated by modeling the solid particles, pores and the fluid elements as regular geometric solids (Smith, 1933). The resulting models,

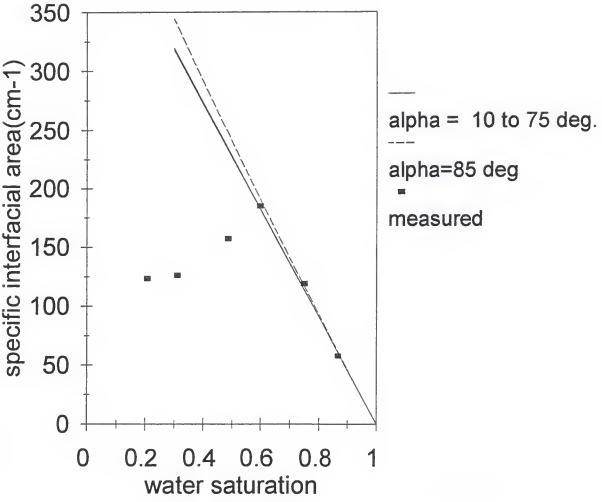

Figure 3-7 Linearized Leverette model prediction and measured data for ISH-C capillary cell experiment

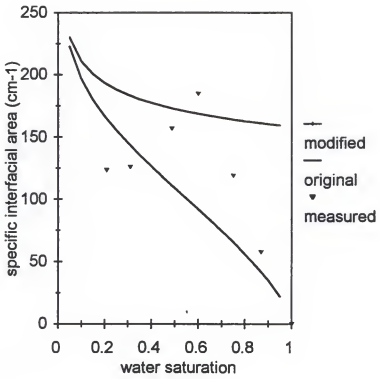

Figure 3-8 Measured data and model predictions using Rose and Bruce function for ISH-C capillary cell experiment

while highly idealistic, can offer valuable insights into the various phenomena; further, as the system tends towards ideal geometry (e. g. spherical glass beads), geometrical model predictions can closely represent the reality, as was demonstrated by Smith (1933). We propose a simple 'pore singlet model', which effectively captures the nature of the a_{nw}- S_w relationship. In this model, the pore space formed between spherical beads of uniform size is modeled as a rhombohedron of equal side a. The nonwetting phase occupies the rhombohedron at low S_n values as a small concentric sphere of radius r, which grows as the S_n increases. This growth in the NAPL sphere will continue till it begins to touch the pore wall, at $r = 0.288\ a$ (for a complete derivation, please see appendix A). The growing NAPL glob then begins to loose its spherical shape, assumes a progressively rhomboidal shape until it mimics the shape of the pore itself, at S_{wr}. The predicted a_{nw}- S_w relationship, as shown in Fig. 3-9 (A), closely agrees with the measured trends. The model can be slightly improved by considering coalescence of individual NAPL blobs with increasing S_n values. The model predictions are reasonable even when the blob coalescence is ignored, because, in a pack with high aspect ratios, the contribution of blob connections (at the pore throats) to a_{nw} is not significant.

Gvirtzman and Roberts (1991) proposed a geometric model to predict the spatial distribution of immiscible fluids and immiscible fluid interfacial areas in ideal sphere packs as a function of the wetting phase saturation. The model is derived from a geometric analysis of the shape and sizes of pendular rings of the wetting phase that form at the spherical particle contact points. By assuming that the solids of revolution formed by identical pendular rings at each such contact point as the basic geometric block that forms the wetting phase

saturation (volume) and interfacial area, the model predicts interfacial areas as a function of sphere packing arrangement, solid-fluid contact angle and sphere radius. A schematic of the model prediction for a rhombohedral packing of 0.25 mm sphere radius is shown in Fig. 3-9(B). As shown in this figure, the model predicts an increase in a_{nw} with increasing S_w in the 'insular' region of water saturation (approximately 100 to 70% of S_w) and a decreasing trend in the a_{nw} - S_w curve in the 'pendular' saturation range (approximately 25 to 0% S_w). The a_{nw} - S_w relationship is undefined in the funicular saturation range. The model's prediction of an increasing trend in the insular region agrees well with that of the thermodynamic models (Leverett, 1941; Morrow, 1970; Miller et al, 1990; Bradford and Leij, 1996). However, the prediction in the pendular region, i. e., a decrease in a_{nw} with decreasing S_w is opposed to the thermodynamic model predictions. This apparent difference is due to the fact that the geometric model of Gvirtzman and Roberts (1991) models the interface formed near the solid surface, at low water saturations, by a molecularly thick water film as a solid-air interface rather than a water-air interface. Thus, with increasing S_n or decreasing S_w in the pendular region, more a_{sn} is uncovered, lowering the a_{nw} correspondingly. The thermodynamic models assume that the solid-NAPL (or air) interfacial area, a_{sn}, is zero, if the solid surfaces are completely wettable by water. Thus, the interfacial area formed by the molecularly thin water film adhering to the solids must be counted as a contribution to a_{nw} alone.

Our results, shown in Fig. 3-5(A), suggest that the trend in the measured a_{nw} - S_w relationship using interfacial tracers agrees with the model prediction of Gvirtzman and

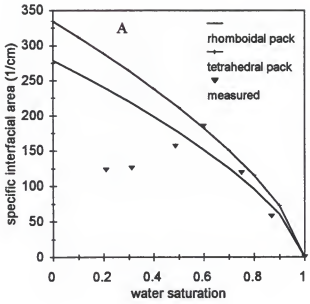

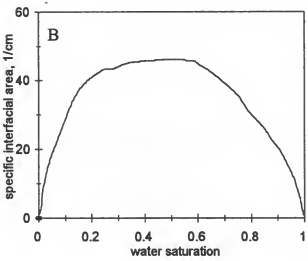

Figure 3-9 Geometric approaches to model a_{nw}-S_w relationship
(A) Pore Singlet Model (B) Gvirtzman and Roberts (1991)

Roberts (1991). However, we attribute the measured decreasing trend in a_{nw} with decreasing S_w in the low water saturation range to the inaccessibility of the *n-w* interface formed by the molecularly thick water films and NAPL, as advection of the interfacial tracer is not possible through these water films.

Mixed Empirical Models

Cary (1994) proposed a model for the specific fluid interfacial area of two continuous immiscible fluids in a porous medium. Use of this model requires fluid saturations, specific solid surface area A and a capillary pressure-saturation relationship. To derive the model, Cary assumed a cylindrical nonwetting phase bubble or blob in a cylindrical pore of length l and radius r. The pore radius r is chosen such that all pores with an effective radius less than r are filled with water, while those equal to or greater than r are lined with a very thin film of water, and otherwise filled with air. The basic equations describing the interfacial area and water content are:

$$\Delta a_{nw} = 2\pi l r \tag{3-29}$$

and

$$\Delta\theta = \pi l r^2 \tag{3-30}$$

where θ is cm^3 of pore space per cm^3 of porous medium. Combining the two equations yields

$$a_{nw} = \sum \Delta a_{nw} = 2\sum \frac{\Delta\theta}{r} \tag{3-31}$$

the summation being carried over the range of radii r to r_∞ where r_o is the pore radius corresponding to the air entry pressure, and θ_o is equal to porosity, ε. To relate θ and r, Cary used the relationship

$$r_o/r = (\theta_o/\theta)b[\beta(\theta_m/\theta)+1] \qquad (3\text{-}32)$$

where θ_m is the volumetric water content when only a monolayer of adsorbed water is present and β is a fitting factor that is fixed by the specific surface areas of the solids and b is a porosity index. Justification for the use of this relationship is given by Cary *et al* (1994), from the basic capillary pressure - capillary radius relationship $P_c=2\gamma/r$.

Substituting Eq. 3-31 in Eq. 3-32 yields the final expression for the specific interfacial area as:

$$a_{nw} = (2\frac{\theta_o^{\,b}}{r_o})[(-\beta\ \theta_m/b)(\theta_o^{\,-b}-(\theta^{-b}))+\frac{1}{(1-b)}(\theta_o^{\,1-b}-(\theta^{1-b})] \qquad (3\text{-}33)$$

Substitution for volumetric water content $\theta = S_w\,\varepsilon$, and saturated water content $\theta_o = \varepsilon$, Eqn. 3-33 can be expressed as

$$a_{nw} = (2\frac{\epsilon^b}{r_o})[(-\beta\ \theta_m/b)(\epsilon^{-(b+1)}-(1-S_w^{\,-b}))+(\frac{\epsilon^{1-b}}{(1-b)}(1-S_w^{\,1-b})] \qquad (3\text{-}34)$$

The second term on the right hand side of the Eq. 3-34, containing β, converges rapidly to a negligible value. Shown in Fig. 3-10 are a_{nw}- S_w curves as predicted by Eqn. 3-34.

In a study of oxygen mass transfer in the root zone, Skopp (1985) developed an expression for the specific air-water interfacial area a_{mv} in a soil, starting from an assumption that the wetting phase (water) in a capillary tube of variable radius, with both end menisci contributing to the air-water interfacial area. Interfacial area considered is due to the two menisci only. Thus, the interfacial area in a single pore is given as

$$A = 4\pi r^2 f \tag{3-35}$$

where f is the frequency of pores having a radius r.

$$f(r) = V\theta_v \int_{l_{min}}^{l_{max}} [g(l)/Q(l,r)]dl \tag{3-36}$$

Where $g(l)$ is the fraction of all pores having a length l, and Q is the volume of a single pore of effective radius r and length l. The term $g(l)$ is normalized such that

$$\int_{a_{min}}^{a_{max}} g(a)\, da = 1 \tag{3-37}$$

Skopp(1985) chose the Dirac delta function for $g(a)$, such that

$$g(a) = \delta(a-r) \quad \text{and} \quad a = r$$

Substituting Eqns. 3-36 and 3-37 and the identity $Q = \pi r^2 a + 2\,\pi r^3/3$ in Eqn. 3-35, Skopp obtained an expression for the specific air-water interfacial area as

$$a_{nw} = 12\theta_v/5r \quad (3\text{-}38)$$

To express the pore radius r in terms of water saturation θ_v/ϵ , Skopp used the capillary rise model (Campbell, 1974):

$$\psi_m = -d(\theta_v/\epsilon)^{-\tau} \quad (3\text{-}39)$$

where ϵ is the total porosity, and d and τ are empirical coefficients. Value of τ is typically <1 for coarse, sandy materials and >1 for finer materials. The significance of d or typical values used was not clear in Skopp (1985). Upon substitution of Eq. 3-39 in 3-38, the final expression for a_{nw} is obtained as:

$$a_{nw} = 6d\rho\epsilon/5r\ (\theta_v/\epsilon)^{1-\tau} \quad (3\text{-}40)$$

where ρ is the density of water. Using values for m ranging from 0.1 to 1.6 (for coarse to fine sands) and an unspecified value for d, Skopp presented a_{nw} -S_w plots. These plots (Fig. 3-11) indicate that, for a coarse textural sand the specific air-water interfacial area monotonically decreases from a finite value at complete saturation to zero at complete dryness. For a medium textured sand, the interfacial area is predicted to be a constant, independent of the degree of saturation. For a finer sand (τ=1.6), interfacial area increases exponentially with decreasing water saturation. These predictions do not appear to agree with the physical reality. Several researchers had predicted a zero interfacial area at complete saturation and complete dryness, as there is no interface present in either case. With the drainage of water due to air (or NAPL) entry, the water saturation progressively decreases, the air/oil saturation

correspondingly increases, with a concomitant increase in the interfacial area. Researchers predicted a maximum value in the specific interfacial area in the intermediate to high nonwetting phase saturation range. In light of these considerations, the results obtained by using Eq. 3-40 (shown in Fig. 3-11) are not realistic.

In the development of Eq.3-40 although the visualization of air-water interfaces as the menisci of the capillary water column is rather simplistic, the resulting expression for a_{nw} should still predict the trends in a_{nw}-S_w relationship realistically. One reason why Eq. 3-40 fails to do so is the omission of the contribution of interfaces other than the air-water menisci at the ends of the visualized capillary water column. A more realistic approach would be to consider the contribution of longitudinal surfaces of air (or oil) ganglia, in addition to the menisci. It is well recognized in the literature that the nonwetting phase is separated from the solid surface by a wetting phase (water) film of at least a few molecular layers thickness. The film's contribution to a_{nw} can be added by modifying Eq. 3-38 to include the area $2\pi rl = 2\pi r^2$, Since $l=r$. Further, Eq. 3-39 can be replaced by a Brooks-Corey function (Eqn. 3-11), noting $\theta_w/\epsilon = S_e$, to obtain:

$$a_{nw} = \frac{6\epsilon P_d}{5\gamma} S_e^{\frac{\lambda-1}{\lambda}} \qquad (3\text{-}41)$$

In Eq. 3-41, pore size distribution index replaces the d and τ parameters. The a_{nw}- S_w relationship predicted by Eqn. 3-41 (Fig. 3-11) agrees more closely with the measured trends.

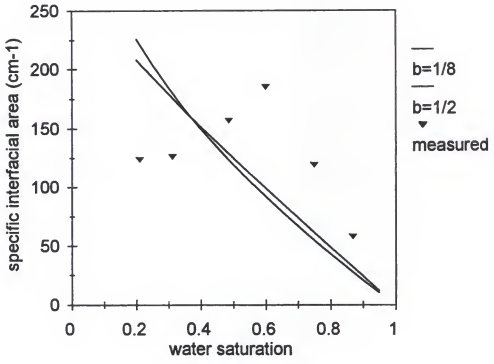

Figure 3-10 Measured data and model predictions using Cary (1990) model for ISH-C capillary cell experiment

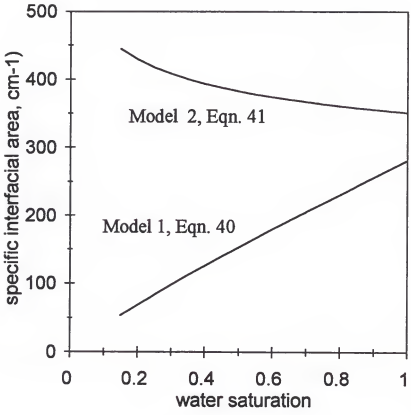

Figure 3-11. Original and modified Skopp (1985) model predictions

Earlier Experimental Investigation of a_{nw} -S_w Relationships

In the literature, there were no reports of measured data representing the a_{nw}-S_w relationships, owing to the difficulty in the measurement of a_{nw}. Using toluene in glass bead columns, Miller *et al* (1990) measured the Sherwood number *Sh* related to the NAPL mass transfer versus S_n at different Reynolds number values, as shown in Fig. 3-12. Sherwood number is defined by the equation

$$Sh = \frac{k_l a_{nw} d_p^2}{D_m} \tag{3-42}$$

where d_p is the grain size diameter, D_m is the molecular diffusion coefficient of NAPL solute in water and k_l is an intrinsic mass transfer coefficient. As such, for a given NAPL in a porous medium of given particle size, Sherwood number is directly proportional to a_{nw} alone. Thus, the relationship between *Sh* and S_n can be converted into an a_{nw} - S_w relationship, as shown in Fig. 3-12, obtained by transforming the data of Miller *et al* (1990). Trends in these curves agree with the model predictions of Leverett. The data also indicate an increasing *Sh* with increasing *Re*. Given that the increases in *Sh* and *Re* are obtained by changes in a_{nw} and v (flow velocity) respectively, the results of Miller *et al* (1990) suggest an increase in either k_l or a_{nw} with increasing flow velocity. There is no mechanistic basis to believe that the interfacial area increases with increasing aqueous flow velocity. Thus, the intrinsic mass transfer coefficient, k_l, is likely the sole reason for increase in *Sh* with increase in v. Experimental results of Miller *et al* (1990) confirmed that *Sh* increases with *Re* in the range of *Re* = 0 to 0.12 and then begin to level off, from which they concluded that the

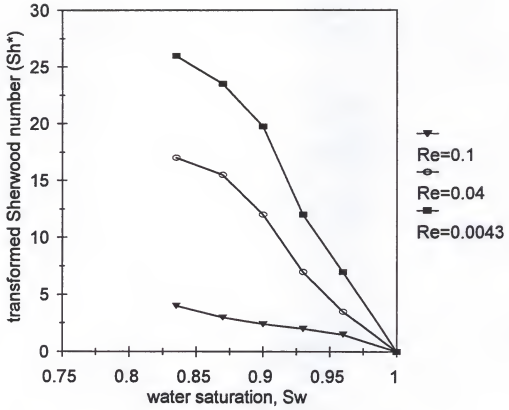

Fig. 3-12. Transformed Sherwood number (Sh*) as a function of water saturation, data from Miller *et al* (1990)

mass transfer coefficients increase with velocities in a certain range of velocities. If the Sh-S_n relationships shown in Fig. 3-12 are normalized using different k_l values using the Sh-Re plots of Miller *et al* (1990), then the resulting a_{nw} - S_w relationships are found to be independent of the Reynolds number values used. Further research, with independently measured a_{nw} and k_l values, will lend a rational basis for the modeling of mass transfer at the NAPL-water interface.

Summary and Conclusions

Among the various models discussed, the thermodynamic models and some mixed empirical models (which are based upon realistic assumptions of pore and blob geometry) are found to model the a_{nw} - S_w relationship adequately. Using a generic P_c - S_w relationship, such as the Leverett's J-function or Brooks-Corey function, an analytical expression is developed, to predict the a_{nw} - S_w relationship for unconsolidated sands, as a function of the interfacial tension, pore size parameter and NAPL entry pressure. Use of an appropriate a_{nw}- S_w model makes it possible to model the NAPL dissolution, mass transfer and hence the contaminant transport, more fully.

CHAPTER 4
MEASUREMENT OF INTERFACIAL AREA CHANGES DURING REMEDIATION BY CHEMICAL FLOODING

Introduction

At many of the contaminated sites and petroleum reservoirs, NAPL exists in soil as a trapped or residual, nonwetting phase. As such, understanding the mechanisms of NAPL residual trapping and its removal is important to various remediation technologies. The NAPL passing through a water saturated soil is trapped in relatively larger sections of the pores as disconnected ganglia, which grow in size with increasing capillary pressure, invading increasingly small pores within the pore networks, finally to form a nonwetting phase fully connected across the length of the medium. Water flooding a soil containing NAPL at high saturations will lead to a reduction in the NAPL saturation to a relatively low value, called the trapped or residual saturation, at which the NAPL exists as disconnected ganglia. Nonwetting phase trapped saturation, the focus of this chapter, can vary from 0 to 35% or more, depending on the soil's pore size distribution, clay content, texture and surface characteristics (Chatzis *et al*, 1988). Typical residual NAPL saturations (S_n) reported in the environmental literature are about 20% (Wilson *et al*, 1990; Mercer and Cohen, 1990). Earlier research in this area focussed on understanding the capillary trapping of oil in soil pores as a discontinuous, non-wetting phase. The related literature is large, and yet incomplete, since the mechanisms are complicated by the interrelated properties of complex porous media structure, fluid properties and applied conditions (Stegemeier, 1977; Dullien,

1979). The literature typically deals with trapping and release of nonwetting phases under equilibrium conditions, in pore body and structure typically found in sands and sandstones.

Character of the porous medium itself, including pore shape and size, largely determines the trapped saturation and its morphology. Such trapping occurs in unique and statistically reproducible patterns , which are controlled by capillary, viscous and buoyancy forces (Mohanty, 1980; Stegemeier, 1977). Capillarity is due to the unbalanced force resulting from cohesion within each fluid phase and adhesion between the solid phase and each of the fluids. The capillary force is proportional to the interfacial tension at the fluid-fluid interface and the strength of fluid wetting the solid surface, and inversely proportional to the pore size. Viscous or dynamic forces are proportional to the permeability and the pressure gradient across the porous medium. Buoyancy is a gravitational force proportional to the density difference between the fluids. At typical groundwater flow rates, capillary forces often dominate over viscous and buoyancy forces.

Theoretical investigations and experimental works using micro models, pore network models and flow experiments suggest that the magnitude and morphology of the trapped nonwetting phase is a strong function of the ratio of pore body to pore neck radii, called the 'aspect ratio', interfacial tension and potential gradient. At the pore level, two trapping mechanisms have been identified. One is 'snap-off' or 'choke-off', whereby the nonwetting front displacing water in a pore neck becomes unstable and ruptures (Roof, 1970; Mohanty, 1980). High pore aspect ratio was shown to cause snap-off with the resulting blob occupying single pore bodies (Morrow and Heller, 1985), the blob shape being nearly spherical. High pore aspect ratios generally lead to high residual saturations of nonwetting phase, causing the

recovery during water flooding to come only from the pore throats. At lower pore aspect ratios, NAPL is bypassed by water in multiple pore structures, resulting in larger ganglia.

Characterization During Remediation

In order for any NAPL remediation method to be effective, NAPL zones must be properly characterized (Mackay and Cherry, 1989). Fluid saturations and specific interfacial areas are two characteristics important in such characterization. Knowledge of these parameters is also necessary to understand the fate, transport and morphology of NAPLs in porous media, as well as the heat, mass and momentum transfer processes at the fluid-fluid interfaces. A few different methods are available for the characterization of fluid saturations. In the laboratory, fluid saturations in a contaminated soil core can be found by liquid extraction, volume/mass balance and the partitioning tracers technique (Jin *et al*, 1994). In contrast, no methods were available till recently to measure the specific NAPL-water interfacial area, a_{nw}, which is defined as the NAPL-water interfacial area per unit porous medium volume (Saripalli *et al*, 1995).

Using partitioning and interfacial tracers in tandem, the S_n and a_{nw} values of a NAPL zone can be measured, and hence the NAPL zones adequately characterized at any stage of the remediation process. Pre- and post-remediation characterization is very important for obvious reasons; characterization during a remediation process by various processes is important for a better understanding of the same. Many of the current NAPL remediation technologies were developed or adapted only in the recent past. Monitoring the changes in S_n and a_{nw}, and hence the morphology index I, is a good means for such chatracterization.

The resulting knowledge can be used for optimization, decision making and comparative evaluation of the various remediation methods and development of new technologies. For example, if characterization during surfactant flushing of a NAPL reveals that the a_{nw} is increasing dramatically during the process, the resulting enhancement in mass transfer may be advantageous in a subsequent enhanced dissolution step. Cosolvent flooding followed by a brief surfactant pre-treatment, to increase a_{nw}, is an example of such step-wise treatment. This approach, known as 'treatment trains' approach, is a recent development, which can be effectively investigated using characterization during remediation. Thus, use of tracers provides a powerful tool to characterize the NAPL content and morphology in soils during remediation process. Such tool can be used in trouble shooting during remediation as well. For example, a dramatic increase in a_{nw} during chemical flooding can trigger hydrodynamic challenges, such as clogging of pores. Characterization during remediation using tracers, even if at the laboratory scale alone, can help foresee such developments.

Furthermore, characterization of NAPL distributions during chemical flooding offers an excellent experimental method to validate and advance the current theoretical predictions about multiphase flow in porous media, such as the concept of oil blob size distributions, for example. Interfacial tension (γ) at the oil-water interface is the single most important characteristic that governs the behavior of multiphase fluids in porous media. In a step-wise flooding of an initial trapped NAPL distribution with chemical adjuvants, such as surfactants, the flood composition can be altered suitably to cause a step-wise change in the interfacial tension. Characterization of the resulting changes in NAPL distribution, by measuring S_n, a_{nw} and I, will offer and validate fundamental insights about the influence of γ on multiphase fluid

behavior in porous media. Solubilization parameter is analogous to the interfacial tension, which can be used in similar studies on processes enhancing dissolution, such as co-solvent flooding.

Capillary Number

Recently, there has been interest focused on the mobilization of residual NAPL by chemical adjuvants, such as surfactants and cosolvents. Capillary number and Bond number are useful indices developed to model such mobilization process (Taber, 1969; Morrow *et al*, 1988). Several researchers proposed various forms of capillary number and S_n-N_{Ca} relationships, to effectively describe the mobilization of residual NAPL (Taber, 1978). Using interfacial tracers, changes in the specific interfacial area a_{nw} can be measured as a function of capillary and bond numbers.

Capillary number is a generic term for the ratio of viscous to capillary forces. Several researchers have observed that mobilization of NAPL commences when the capillary number exceeds a critical value. Theoretical support for this observation can be established by considering a force balance on a NAPL singlet. Shown in Fig. 4-1(A), a NAPL singlet of length l_b aligned with the flow direction, and radii of curvature r_1 and r_2 at the trailing edge (point 1) and leading edge (point 2) respectively. Pressure in the water and NAPL phases at these two points are represented by P_{w1}, P_{w2} and P_{n1}, P_{n2} respectively. At points 1 and 2, capillary equilibrium dictates that:

$$P_{n1} = P_{w1} + \frac{2\gamma_{nw}}{r_1} \qquad (4\text{-}1)$$

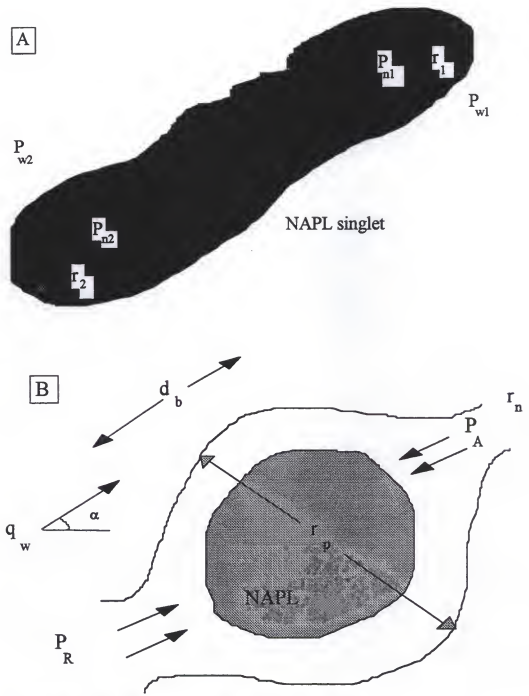

Figur 4-1 Schematic pictures of NAPL singlets for developing (A) equation 4-10 and (B) equation 4-16 (Pennell *et al*, 1995)

$$P_{n2} = P_{w2} + \frac{2\gamma_{nw}}{r_2} \quad (4\text{-}2)$$

Subtracting Equation 4-1 from 4-2,

$$P_{n1} - P_{n2} = 2\gamma_{nw}[1/r_2 - 1/r_1] + P_{w2} - P_{w1} \quad (4\text{-}3)$$

Further, for a stable blob (Pascal's law):

$$P_{n2} = P_{n1} \quad (4\text{-}4)$$

Combining Equation 4-3 and 4-4, we obtain the condition for equilibrium:

$$P_{w1} - P_{w2} = 2\gamma_{nw}(1/r_2 - 1/r_1) \quad (4\text{-}5)$$

Equation 4-5 is the condition required for trapping of the blob within the pore. Any perturbation, such as an increase in the differential water pressure or a decrease in the interfacial tension, will prompt the blob to move out of the pore. An increase in the net water pressure produces an increase in the Darcy flow gradient:

$$\frac{dP}{dx} = \frac{P_{w1} - P_{w2}}{l_b} \quad (4\text{-}6)$$

As such, Eqn.4-5 can be written in terms of the externally imposed head gradient, as:

$$\frac{dP}{dx} = \frac{2\gamma_{nw}}{l_b}(1/r_2 - 1/r_1) \quad (4\text{-}7)$$

Considering Darcy flow velocity, V_w as

$$V_w = -\frac{kk_{rw}}{\mu_w}\frac{dP}{dx} \quad (4\text{-}8)$$

Substituting Eqn.4- 8 into 4-7 and rearranging

$$\frac{V_w\mu_w}{\gamma_{nw}} = [\frac{2}{l_b}kk_{rw}(1/r_2-1/r_1)] \quad (4\text{-}9)$$

The dimensionless group $V_w\mu_w/\gamma_{nw}$, which is a ratio of the viscous forces to capillary forces, is known as the capillary number. Since Eqn. 4-9 represents the condition for equilibrium of the blob, the critical capillary number required for NAPL mobilization is defined as:

$$N_{ca}^{crit} = \frac{kk_{rw}}{l_b}[2(1/r_2-1/r_1)] \quad (4\text{-}10)$$

The above analysis demonstrates the use of capillary number as an index of mobilization of NAPL in porous media. Experimental data from several works confirm the usefulness of capillary number. For NAPL trapped in unconsolidated sands, the critical capillary number ranges from 10^{-5} to 10^{-3}. Residual NAPL blobs in porous media are not all singlets; while a fraction of them are singlets, the rest follow a blob size distribution (Mayer and Miller, 1992; Chatzis *et al*, 1983). Equation 4-10 is used with respect to all blob shapes and sizes, l_b being considered the characteristic length of such complex blobs. In media made of randomly packed, equal sized spheres of radius R, the characteristic length was observed

to be proportional to R:

$$l_b = nR \tag{4-11}$$

where n is a constant representing the packing of spheres. With respect to the force balance equation (Eqn. 4-10), Morrow and Heller (1985) observed that, from similarity considerations, the relative permeability k_{rw} should be independent of the bead size in uniform bead packs. As such, relationships between the capillary number and residual saturation (N_{ca}-S_n) should follow a universal curve for systems of different permeability but similar bead size and geometry. Chatzis *et al* (1982) experimentally confirmed the existence of such generic S_n-N_{ca} curve.

Pennell *et al* (1995) derived an expression for 'total trapping number', which is a sum of the capillary number and Bond number N_B, from a similar force balance. The NAPL singlet considered in their analysis, shown in Fig.4-1(B), is slightly different from that shown in Fig. 4-1(A), in that the flow direction is considered to be at an angle α to the horizontal, and, N_B and N_{ca} are derived in terms of the pore neck radius (r_n) and pore body radius (r_p). Thus, in Laplace equation defining the capillary pressure, r_p and r_n are considered the principal radii of curvature. Their analysis defines the criterion for NAPL mobilization as

$$N_{Ca} + N_B \sin\alpha = \frac{2\beta k k_{rw}}{l_b r_n} \tag{4-13}$$

where β is the ratio $1-r_n/r_p$ and capillary and Bond numbers are defined as:

$$N_{Ca} = \frac{q_w \mu_w}{\gamma_{nw} \cos\theta} \quad (4\text{-}14)$$

$$N_B = \frac{\Delta\rho g k k_{rw}}{\gamma_{nw} \cos\theta} \quad (4\text{-}15)$$

where $\Delta\rho$ is the density difference between NAPL and water and θ is the contact angle of wetting. Equation 4-13 offers a mobilization criterion based on the combined influence of viscous, capillary and buoyancy forces. This equation suggests that, the effect of buoyancy forces on mobilization is the greatest when the flow is vertical and may be unimportant when the flow is horizontal.

Equations 4-10 and 4-13 are derived considering only a NAPL singlet in a single pore with two throats. However, in natural porous media, pores contain many throats aligned along many directions. Further, the NAPL ganglia can be complex in shape and size, ranging over several grains. Thus, a more general formulation is necessary for assessing the criteria for mobilization in a natural porous medium. Pennell *et al* (1995) presented one such formulation, called the total trapping number (N_T):

$$N_T = \sqrt{N_{Ca}^2 + 2N_{Ca} N_B \sin\alpha + N_B^2} = \frac{2kk_{rw}\beta}{r_n l_b} \quad (4\text{-}16)$$

where l_b is a characteristic length of the blob. It the special case of horizontal flow (α =0), Eqn. 4-16 reduces to:

$$N_T = \sqrt{N_{Ca}^2 + N_B^2} \quad (4\text{-}17)$$

and, for vertical flow (α =90°):

$$N_T = |N_{Ca} + N_B| \quad (4\text{-}18)$$

Equation 4-16 is predicated on a force balance at a Darcy scale (typically several times larger than a pore scale) between the advancing pressure force and a resisting 'average' capillary force acting to retain the organic liquid. Space averaging of the pressure head, as represented by Darcy's law is a generally agreed concept in the literature. Right hand side term of Eqn. 4-16 represents an average capillary pressure experienced by a complex blob of arbitrary characteristic length d_b. This concept is in agreement with the observed fact that the pore to neck radius ratio, of which β is a measure, plays a critical role in the mobilization of trapped NAPL (Stegemeier, 1977; Wilson *et al*, 1990) via the 'snap-off' and 'by passing' mechanisms of ganglia formation. Inspection of Equation 4-16 also reveals that the blob size l_b decreases as the trapping number N_T increases. This fact was observed by other researchers as well (Mohanty, 1980). Further, β/r_n is a useful pore-level parameter that governs mobilization. By definition,

$$\frac{\beta}{r_n} = \frac{r_p - r_n}{r_p\, r_n} \quad (4\text{-}19)$$

If $r_p >> r_n$ then β/r_n can be approximated as $1/r_n$. Thus, a small neck radius implies difficult

mobilization. Experimental investigations using porous media of different types of packing and degrees of compaction can elucidate the dependence of N_T on aspect ratio and blob size.

As described earlier, capillary number was shown to be a useful index to predict the criteria for NAPL mobilization. Mobilization of petroleum from sand stones and laboratory sand packs was shown to occur in the N_{Ca} range of 10^{-5} to 10^{-3} (Chatzis, 1980; Chatzis and Morrow, 1984). Pennell *et al* (1995) showed that the mobilization of PCE in Ottawa sand packs occurred in the N_T range of 10^{-5} to 10^{-3} as well. Thus, it is reasonable to assume that the mobilization of typical, non-wetting NAPLs in contaminated soils occurs in this N_T range. Unfortunately, the low groundwater velocities and relatively high interfacial tension values in contaminated soils present low N_T and N_{Ca} values that are not conducive to mobilization. This observation explains why mobilization of NAPLs by water at contaminated sites is a difficult task.

For example, a NAPL of density 1.6 gm/cc and interfacial tension of 48 dynes/cm trapped in a hypothetical sand of k = 1.4e-07 cm^2 and k_{rw} = 0.6, with q_w = 20 cm/hr presents an an N_{ca} = 11.05e-07, N_B = 10.3e-07 and N_T = 21.35e-07. Clearly, the low values are not sufficient to cause mobilization. Examination of Eq. 4-13 through 4-18 reveals that the Darcy flux (q_w), NAPL-water interfacial tension (γ_w) and liquid density difference ($\Delta\rho$) are the parameters that can be controlled to achieve the high N_T values necessary to mobilize trapped NAPL. An increase of two to three orders of magnitude in N_{Ca} and N_T is necessary for the mobilization of such NAPL. Increasing q_w by more than an order of magnitude requires high pressure pumping systems, which could lead to the fracture of the formation and hence is not feasible in laboratory experiments as well as in the field. The fluid density difference can be

changed by adding chemical additives such as alcohols and xanthan gum to the NAPL, which contribute to the Bond number component of N_T. However, such additions could adversely impact the viscosity of flood. Further, changes induced by such density alteration to N_B are marginal. Further, it can be shown that the contribution of N_B itself to N_T is marginal in typical NAPL remediation scenarios. The alternative of changing interfacial tension is a very attractive option. Ultra low NAPL-water interfacial tensions can be achieved by adding chemicals such as surfactants, co-solvents and a combination of surfactants and salts to the NAPL-water-soil system. Such lowering of interfacial tension, by two to three orders of magnitude, causes a corresponding increase in both N_B and N_{Ca}, and hence in N_T.

Ultra-low interfacial tensions

In the petroleum engineering literature, several researchers reported that successful immiscible oil displacement depends on the existence of a very low interfacial tension between the oil and water phases (Taber, 1969; Melrose and Brander, 1974). A value of 0.001 dynes/cm or less is required to mobilize the trapped oil (Morgan *et al*, 1977). Ultra low interfacial tensions can be arbitrarily defined as 2×10^{-3} dynes/cm or lower. In a water/oil/surfactant/electrolyte system, the important variables affecting the achievement of ultra-low interfacial tension are: the surfactant molecular weight and structure, surfactant concentration, electrolyte concentration and type, oil phase average molecular weight and structure, system temperature and age of the system (Morgan *et al*, 1977). Thus, for a given surfactant-NAPL system, surfactant concentration and salt concentration are the two variables that can be deliberately controlled to achieve ultra low interfacial tensions. Several studies have confirmed that the presence of electrolyte in the surfactant solution in a critical

concentration range leads to ultra-low interfacial tensions (Noronha, 1980; Morgan *et al*, 1977). Using isomerically pure alkyl benzene sulfonates of concentration well above the CMC, NaCl as electrolyte and different alkanes as oils, Noronha (1980) showed that ultra-low interfacial tensions are attained at an optimum salt concentration. Shown in Fig. 4-2 is a schematic of the results from Noronha (1980) for an n-decane/water/NaCl system. As can be seen from Fig. 4-2, the interfacial tension at the decane-water interface is about 0.5 dynes/cm in the presence of 1% AOT surfactant. The interfacial tension decreases with the addition of NaCl to the surfactant solution and reaches a minimum of 5×10^{-3} dynes/cm at a salt concentration of 0.4%. Further increases in the salt concentration lead to an increase in the interfacial tension. These results indicate that the aqueous solutions containing AOT and NaCl can be used to study mobilization of residual decane.

In the current work, experiments were conducted to measure the changing a_{nw} as a function of S_n and N_T during mobilization of residual decane in sand column experiments. The intent of these experiments was to measure and model the a_{nw} -N_T and a_{nw} -S_n relationships, which offer valuable insights for elucidation of the changing NAPL morphology, mass transfer and mobilization of trapped NAPL. In addition, the resulting information will be useful in the characterization of NAPL waste sites, design, trouble shooting and performance assessment of remedial technologies. For example, a knowledge of the a_{nw} -N_T relationship can be used in the design of a remediation 'treatment train', wherein a large a_{nw} is created first by a surfactant-salt flush at the appropriate N_T, followed by cosolvent flushing. A large a_{nw} enhances dissolution of NAPL and hence remediation

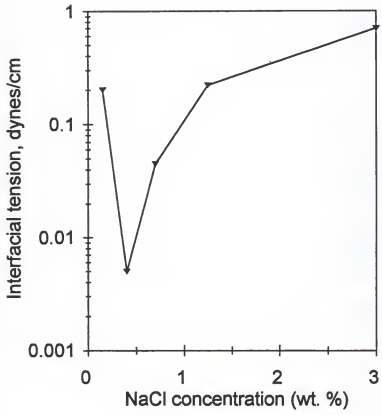

Figure 4-2 Ultra-low interfacial tensions at decane- 1% AOT surfactant solution interface (after Noronha, 1980)

performance during co-solvent flushing. Deliberately increasing the a_{nw} is likely to enhance the performance of other technologies, such as bioremediation, soil vapor extraction, oxidation treatments and surfactant flushing as well.

Experimental

Soil column flushing experiments were conducted using n-decane as the trapped NAPL phase in glass columns (Kontes 2.54 cm i. d. x 5 cm long with teflon end fittings) packed with clean glas beads or clean sand. Four sets of mobilization experiments were conducted, each set consisting of the measurement of S_n and a_{nw} at various stages of decane mobilization. Decane saturation S_n was measured using volumetric measurements as well as partitioning tracer breakthrough experiments. Interfacial area a_{nw} was measured at every stage, by conducting tracer breakthrough curve experiments using pentafluorobenzoic acid (PFBA) as a non-reactive tracer and sodium dodecyl benzenesulfonate (SDBS) as an interfacial tracer. The resulting breakthrough curves were analyzed to obtain the retardation factor for SDBS with respect to PFBA, which can be related to a_{nw} as discussed in chapter 2, Eqn. 2-2.

Glass beads in the size range of 150 to 350 μ (Cataphote Corporation, MS) washed several times with methanol/water, and hydrochloric acid/water and baked at 100 °C for several hours, were used as porous media in the experiments. Decane was introduced into the water saturated porous media, using a syringe pump at a flow rate of 0.2 ml/min. A part of the decane was later removed by injecting water into the columns, at a flow rate of 1 ml/min. At the end of loading, pore spaces in the columns were filled partially with oil at a

saturation S_n. Steady volumetric water flow was established using an HPLC pump (Gilson Co., Model 305) prior to injection of tracers. In separate experiments, interfacial tracer (SDBS) and non-reactive tracer (PFBA) were injected continuously until the relative concentration C^* in the effluent reached unity. Effluent from the column was analyzed for SDBS or PFBA using an in-line UV spectrophotometer, at 260 and 254 nm respectively.

Single Stage Flooding Experiments

An initial set of experiments was conducted using two chemical floods, a 1% Igepal-70 solution (IFT-S2) and a cosolvent mixture of 50% ethanol, 2% pentanol and 48% water (IFT-CS1), to investigate how interfacial area changes during flushing by a surfactant and a cosolvent solution. In IFT-S2 experiment, a 1% Igepal solution, presaturated with decane, was flushed through decane trapped in a clean sand pack, at an S_n of 17%. No decane was mobilized out of the column or solubilized, as the surfactant flush was presaturated with decane. Shown in Fig. 4-4 are breakthrough curves for SDBS and PFBA in IFT-S2 column, measured both before and after the surfactant flushing. The interfacial area a_{nw}, measured both before and after the surfactant flush, was 93 and 338 cm^2/cm^3 respectively. This 3.6 fold increase in the interfacial area, although the S_n was maintained constant, can be attributed to emulsification of decane during surfactant flushing. In contrast, in the experiment IFT-CS1, where similar sand pack with 16% decane trapped decane was flushed with decane-presaturated cosolvent solution (48% water, 50% ethanol and 2% pentanol) caused a decrease in the a_{nw} value from 85 to 12 cm^{-1}. Shown in Fig. 4-5 are BTCs for SDBS and PFBA a_{nw} after cosolvent flushing indicates that the residual decane may have been

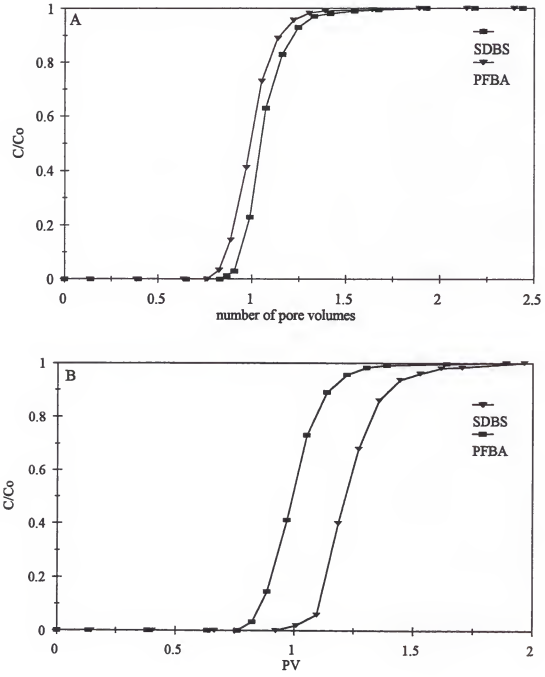

Figure 4-3 Breakthrough curves in IFT-S2 column experiments (A) before and (B) after emulsification of residual decane using 1% Igepal-70 solution

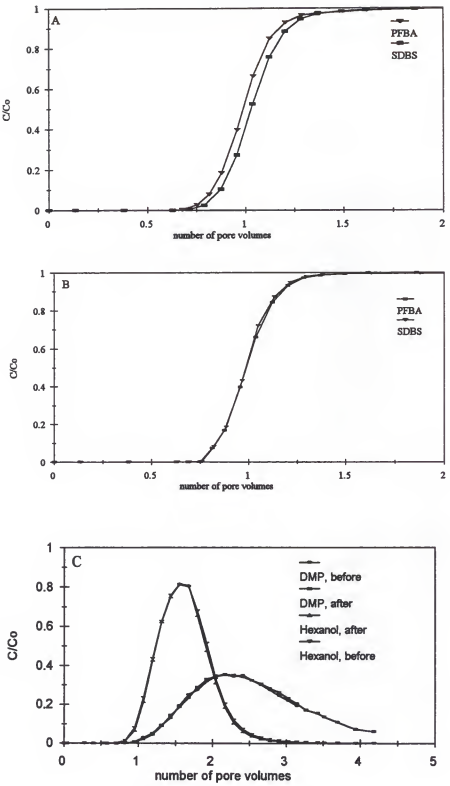

Figure 4-4 Breakthrough curves in IFT-CS1 column experiments (A) before and (B) after cosolvent flooding of residual decane (C) partitioning tracer experiment

redistributed inIFT-S2 column, measured both before and after the surfactant flushing. The reduction in a_{nw} is possible because of blob coalescence. No decane was removed during cosolvent flush, as seen from partitioning tracers (Fig. 4-5(C)). Further work is necessary to elucidate the mechanism by which cosolvent flushing causes a reduction in a_{nw}.

Multi -stage Flooding Experiments

Subsequently, IFT-SN1 and IFT-SN2 experiments were conducted, using aqueous solutions of Aerosol-OT 100 (an anionic surfactant, sodium dioctyl sulfosuccinate) and varying concentrations of NaCl. Varying the NaCl concentration from 0 to 3% allowed the variation of decane-water interfacial tension by three orders of magnitude, from 44 to 0.005 dynes/cm (Noronha, 1980) thus allowing a similar variation in N_T as well. The intent of these experiments was to monitor the changes in the decane-water interfacial area (a_{nw}) with increasing N_T and decreasing S_n values.

The experiment IFT-SN1 was carried out in stages, a measured amount of the initial (2.3 ml) decane present in the column being removed at each stage by means of an AOT-NaCl flood. At each stage, tracer breakthrough curve experiments were conducted using inert, partitioning and interfacial tracers, to measure the changed pore volume, decane saturation and interfacial area. Glass beads were packed dry in a glass column (Kontes 2.54 cm i. d. x 5 cm long). The resulting bead pack was saturated by pumping several volumes of distilled, deionized, deaired water in an upflow mode at a high flow rate. Using a syringe pump, 6.3 ml of decane were injected into the water saturated column in a down-flow mode, at a flow rate of 0.2 ml/min. This was the maximum volume of decane that could be retained in the

water wet pack. Subsequently, water was pumped through the column at a flow rate of 1.08 ml/min, in an upflow mode, to remove 4 ml. of the 6.3 ml decane retained. The remaining 2.3 ml of decane in the column formed a trapped saturation of 20%, corresponding to Stage 1. The column was flushed with several pore volumes of distilled, deionized water, which did not remove any significant amount of decane, as its water solubility is very low. A non-reactive tracer (pentafluorobenzoic acid, PFBA) breakthrough curve experiment was conducted on this column, to measure the pore water volume in the column. A partitioning tracer experiment, using an aqueous solution of methanol, pentanol and 2,2 dimethyl -3-pentanol, at concentrations of 1000, 700 and 600 µl/l was conducted to measure the decane initial residual saturation. The measured S_n value agrees well with the volumetric loading measurement (20 %). Further, an interfacial tracer experiment also was conducted, to measure the initial NAPL-water interfacial area a_{nw} in the column to be 78 cm^2/ cm^3. A 250 mg/L solution of sodium dodecyl benzenesulfonate (SDBS), an anionic surfactant, was used as the interfacial tracer solution. The retardation of the interfacial tracer relative to the nonreactive tracer is a measure of the NAPL-water interfacial area.

At this point, the column was flushed with three pore volumes of SDBS at 418 mg/L, which causes the decane-water interfacial tension to decrease from 44 dynes/cm to 5 dynes/cm. This corresponds to Stage 2 of the experiment. Breakthrough curve response of the SDBS was monitored during the flushing, as it can be used to measure the interfacial area as well. No decane was removed from the column as a result of this flush. Subsequently, an interfacial tracer experiment using 250 mg/L SDBS was conducted. The a_{nw} value measured in both experiments (418 and 250 mg/L SDBS) agreed closely.

Subsequently, Stage 3 through 6 experiments were conducted on the column, by flushing with a 1% AOT and varying NaCl concentration solutions, as shown in Table 4-1. The surfactant/salt flush was injected for approximately 2 pore volumes in all cases, sufficient to cause the required mobilization of decane, without excessive solubilization. To avoid salt gradients while flushing, the AOT/NaCl flush was followed, in stead of pure water, by two more pore volumes of salt solution of same salt concentration as in the preceding AOT/salt flush, which removed all of the AOT remaining in the column. Water flush followed immediately after this salt water flush, after which breakthrough curve experiments using inert, interfacial and partitioning tracers were conducted as usual. Procedure for the next stage of experiment was the same, except that a different salt concentration was used, to affect a different interfacial tension (γ_{nw}) value. During and after each AOT/NaCl flush, the effluent was observed for signs of mobilization and any emulsification. The mobilized decane was volumetrically measured. Results from various stages in IFT-SN1 experiment are shown in Fig. 4-1.

Another experiment, IFT-SN2, which was similar to IFT-SN1, was conducted in a similar column (2.54 cm i. d. x 5 cm long) which was packed dry with glass beads and saturated first with water. Loading of decane with a syringe pump in a fashion similar to the loading of IFT-SN1 column resulted in a final decane volume of 1.7 ml. This corresponds to an initial S_n of 17%. The experiment IFT-SN2 also was carried out in stages, a measured amount of the initial decane present in the column being removed at each stage by means of an AOT-NaCl flood. At each stage, tracer breakthrough curve experiments were conducted using, inert, partitioning and interfacial tracers, to measure the changed pore volume, decane

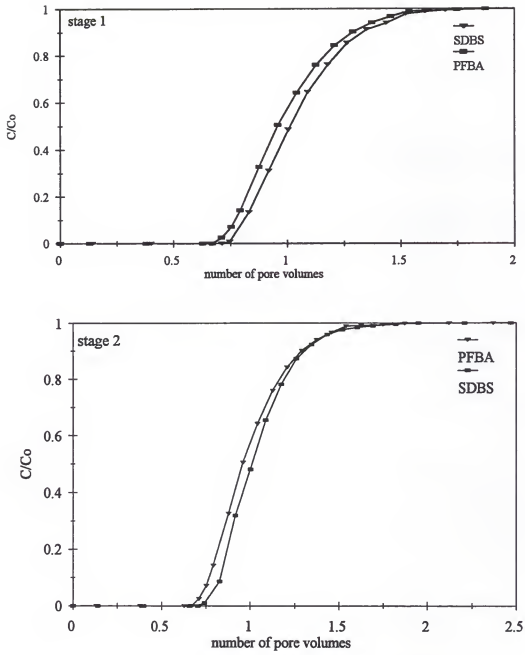

Figure 4-5 Breakthrough curves for PFBA and SDBS during decane mobilization experiment sIFT-SN1

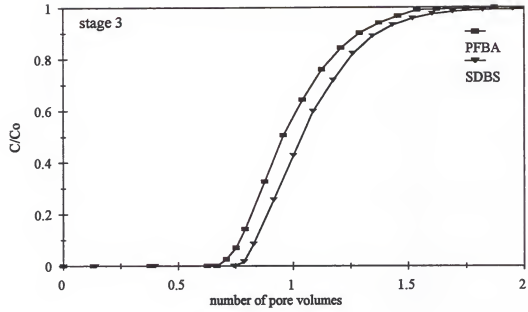

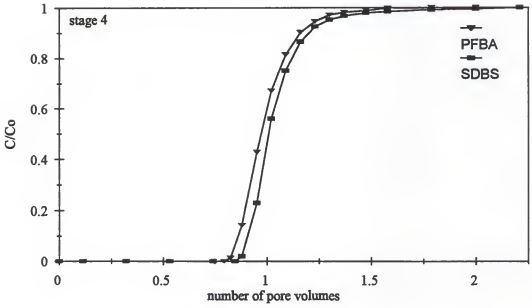

Figure 4-5 contd..

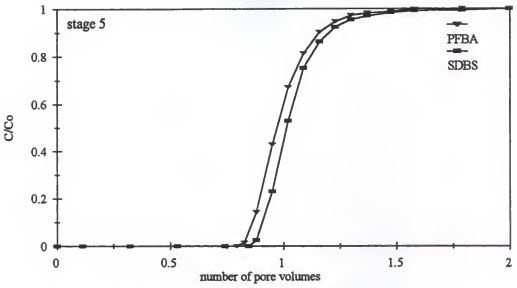

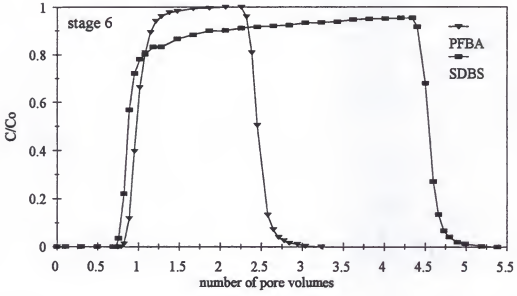

Figure 4-5 contd..

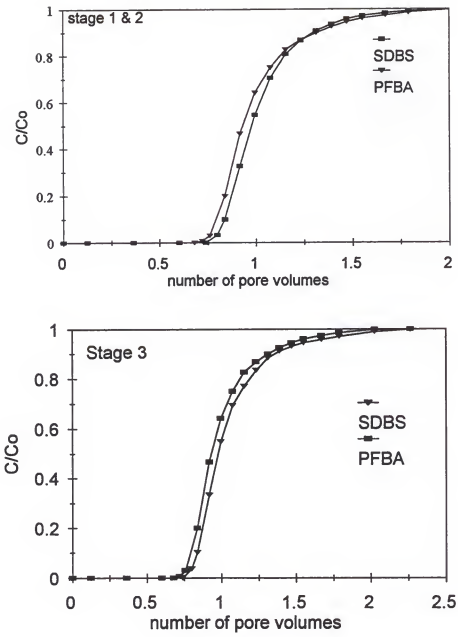

Figure 4-6 Breakthrough curves for PFBA and SDBS during decane mobilization experiment IFT-SN2

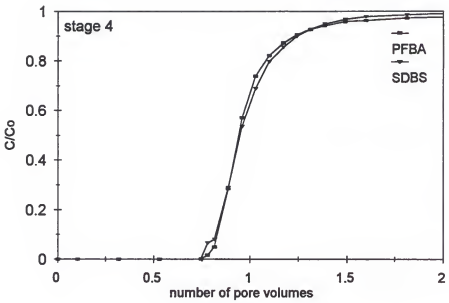

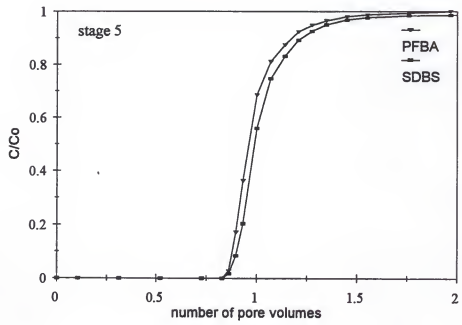

Figure 4-6 contd..

saturation and interfacial area. Results from various stages in the experiment IFT-SN2 are shown in Fig. 4-6.

Results from both experiments (Table 4-1) show similar trends in the S_n-N_T and a_{nw}-N_T relationships. The N_T values were calculated using measured γ_{nw} values from Noronha (1980), measured flow rate and estimated k_{rw} values using a S_n-k_{rw} correlation (Corey, 1994) with a measured λ value of 4 (Chapter 3). Use of predicted relative permeability values was shown to be adequate in studies concerning NAPL behavior in soils (Hunt and Sitar, 1991). There was no mobilization of decane in the N_T range of 1e-06 to 2e-05 and the residual decane saturation remained equal to the initially loaded value (20% and 17% for IFT-SN1 and IFT-SN2, respectively). Further increase in trapping number caused rapid removal of decane in the 0.0001 to 0.001 range. The measured data in both experiments agree with the S_n-N_T relationships observed and predicted earlier (Pennell *et al*, 1995; Taber, 1981). The initial a_{nw} was 78 cm^{-1} in IFT-SN1 column and 45 cm^{-1} in IFT-SN2 column. The lower interfacial area in the case of IFT-SN2 could be due to its lower initial S_n of 17%, when compared to IFT-SN2. Earlier work predicted that a_{nw} in the trapped saturation range may be larger for higher S_n values (Miller *et al*, 1990).

The specific interfacial area, a_{nw}, in both cases remained constant in the N_T range of 1e-06 to 1e-03, indicating that the a_{nw} was insensitive to increase in N_T in this range, even as S_n begins to decrease as N_T approaches 0.0001. The constancy of a_{nw} with N_T in the relatively low N_T value range is reasonable, as there is no change in S_n. The interfacial tension reduction in this range was insufficient to either remove a part of the trapped decane or cause changes in the blob morphology. However, as N_T approached 0.0001, decane

Table 4-1. Stages in IFT-SN1 and IFT-SN2 surfactant flushing experiments

Stage	Flood	γ_{mw} Dynes/cm	S_n%	N_{ca}	N_B	N_T	a_{mw} Cm^{-1}
				{← x 10^{-6} →}			
IFT-SN1 Experiment							
1	water	44	20	0.72	0.32	1.04	85
2	SDBS 0.7 mM	5	19	1.55	0.64	2.10	85
3	SDBS 1.2 mM	20	20	6.33	2.80	9.13	84
4	1%AOT + 3% NaCl	0.58	8	54	241	82	80
5	1%AOT + 0.2% NaCl	0.09	2	352	160	510	78
6	1%AOT + 0.4% NaCl	0.005	~0	7000	2800	9800	142
IFT-SN2 Experiment							
1	water	44	17	0.72	0.32	1.04	51
2	SDBS 0.7 mM	5	17	1.55	0.64	2.10	51
3	1%AOT + 3% NaCl	0.58	16	54	241	82	51
4	1%AOT + 0.2% NaCl	0.09	12	352	160	510	21
5	1%AOT + 0.4% NaCl	0.005	2	7000	2800	9800	74

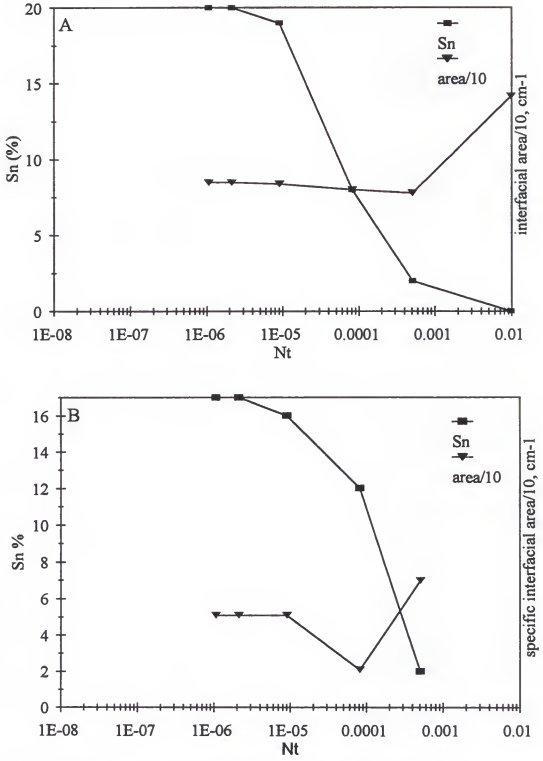

Figure 4-7. Changes in decane saturation and decane-water a_{nw} with N_T in experiments (A) IFT-SN1 and (B) IFT-SN2

mobilization commenced and the S_n began to decrease slowly. In experiment IFT-SN1, reduction in S_n from 18% to 9% in the 1e-05 to 0.0001$_T$$N$ range did not result in any appreciable change in a_{nw}, indicating that the decane volume removed corresponds to large ganglia, whose contribution to a_{nw} must be negligible. Decane being the nonwetting phase was preferentially trapped in the larger pore bodies. Increasing N_T values should have mobilized the decane in the larger pore channels first, as even a low N_T value (i.e. a relatively high interfacial tension) is sufficient to mobilize decane from the larger pores, according to the capillary trapping theories (Schwille, 1988; Wilson, 1990; Taber, 1969; Stegiemeir, 1977). Such mobilization of large blobs caused a reduction in S_n but no corresponding significant reduction in a_{nw}, as the contribution of the large (low surface area) ganglia to a_{nw} was small to begin with. Further removal of decane, at relatively low (ultra-low) interfacial tensions and high N_T values, was from the relatively smaller pore channels, which contain smaller ganglia. Thus, decane removed in this phase contributed significantly to the a_{nw}, even though its contribution to S_n was relatively small, owing to the high interfacial area/volume ratio of decane in the small pores. This explains the reduction in a_{nw} in the N_T range of approximately 0.00005 to 0.0001for IFT-SN1 and 0.0001 to 0.0005 range for IFT-SN2. The reduction in a_{nw} was significant in the case of IFT-SN2, indicating that the decane removal in this region corresponded to a large fraction of high surface area/volume ratio blobs. Even though the particle size and dimensions of IFT-SN1 and IFT-SN2 columns were the same, the resulting morphologies of trapped decane can be significantly different, as the morphology is a complex function of pore size distribution and compaction of pack, which cannot be maintained identical among different columns.

Interestingly, in both experiments, after passing through a minimum the a_{nw} value dramatically increased with further increases in N_T, caused by ultra-low interfacial tensions. This increase indicates that there was a significant change in the decane morphology, very likely due to the break up of large blobs into smaller blobs or droplets via emulsification. When there is sufficient energy input and ultra low interfacial tensions are present, NAPLs in porous media can be emulsified (Gopal, 1967; Sutheim, 1947). In single stage experiments (IFT-S2) with decane and a 1% Igepal-70 surfactant flush indicated that surfactant flood can cause emulsification and a 3.6 fold increase in the a_{nw} value.

In summary, the experiments and theory together indicated that the a_{nw}-N_T relationship can be described best by dividing the curve into two regions: a 'mobilization' region and an 'emulsification' region (Fig. 4-7). Mobilization of NAPL is initiated, due to sufficient reduction in the capillary forces, only when the N_T value exceeds a 'mobilization threshold'. In the mobilization region, the a_{nw} value initially remains unchanged even after the trapped NAPL mobilization commences and a large portion of the initial S_n removed. Further increases in N_T lead to a reduction in a_{nw} commensurate with the morphology of ganglia trapped in smaller pores and reaches a minimum. This minimum, referred to as the 'emulsification threshold' in Fig. 4-7, represents the transition zone between the mobilization and emulsification regions. Further increases in N_T cause dramatic increases in a_{nw} due to emulsification, as explained above. If the NAPL removal is complete (100%), then, the a_{nw} value must return to a zero value, as the NAPL-water interface disappears. However, complete removal is seldom possible and the a_{nw} reported by interfacial tracers remains high, as shown by the results from the final stage in IFT-SN1 and IFT-SN2 experiments (Fig. 4-8).

Modeling the a_{nw}-N_T Relationship

Remediation of NAPL contaminated soils by surfactant flushing is accomplished by mobilization of the NAPL and its enhanced solubilization into the aqueous phase. A knowledge of the specific interfacial area a_{nw} and the 'area-volume ratio index', I, is very useful in understanding the morphology changes and NAPL transport in the case of mobilization and interfacial mass transfer in the case of enhanced solubilization. As described earlier, the total trapping number N_T is a useful index that can describe the process of NAPL volume removal by means of S_n-N_T relationship. Modeling and experimental measurement of the a_{nw}-N_T and a_{nw}-S_n relationships would be a useful contribution to the study of both mobilization and enhanced solubilization of NAPLs using surfactants, as well as other chemical adjuvants, such as co-solvents. The physico-chemical processes involved in such enhanced remediation are additive-specific, however. For example, the reduction in interfacial tension achieved by surfactants and co-solvent flushing in the same NAPL-soil-water system can be very different in magnitude and mechanism. As such, models representing the a_{nw}-N_T, S_n-N_T and a_{nw}-S_n relationships will be specific to a class of adjuvants, such as surfactants.

In the following analysis, a relationship between the a_{nw}-N_T relationship is developed. Consider Eqn. 4-16, with respect to a vertical column, as below:

$$N_T = |N_{Ca}+N_B| = \frac{2kk_{rw}\beta}{r_n l_b} \qquad (4\text{-}21)$$

Equation 4-21 indicates that the blob length l_b has to decrease with an increase in N_T, in a linear fashion. Mohanty (1981) confirmed that l_b decreases with N_T, and offered a linear

relationship between l_b and N_T. Terms on the left hand side of equation 4-21 are all evaluated at a macroscopic or Darcy scale. In contrast, the right hand side term is a combination of the pore level parameters β, r_n, l_b and the Darcy level parameters k and k_{rw}, depends on the pore topography and blob size. While the terms on the LHS are unique and measurable, the terms on RHS, except k and k_{rw} are neither unique nor easily measurable. As such, Eqn. 4-21 is not an exact equality among uniquely defined quantities, but an empirical 'criterion' to indicate whether mobilization occurs.

A rigorous application of force balance equations such as Eqn.4-21 require measurement of the pore level parameters β, r_n and l_b. All of these porous media parameters (pore neck size, ganglion length and β) have distributions rather than unique values (Mayer and Miller, 1992; Dullien, 1979; Mohanty, 1980). Since the development of Equation 4-21 is based on the fundamental capillary equation (Eqn. 4-6) and since changes in N_T are primarily affected by changes in γ_{nw}, it is reasonable to propose several trapping number ranges, each range corresponding to the removal of ganglia of a certain size range and emptying (by mobilization) of a certain pore size range. It is a well known fact in soils literature that, in the drainage of soil water out of a saturated column, pores in the largest size range empty first, followed by the smaller pores and so on (Hillel, 1981). Mobilization of NAPL should follow a similar pattern, largest ganglia mobilizing first in the low N_T range, followed by the smaller ganglia, until emulsification commences. Experimental results from the IFT-SN1 and IFT-SN2 experiments support this conclusion. In light of these observations, Equation 4-21 can be modified to incorporate the statistical concept of N_T, β, r_n and d_b distributions as below:

$$\sum N_T \quad = \quad \sum |N_{Ca} + N_B| \quad = \quad \sum \frac{2kk_{rw}\beta}{r_n \, l_b} \qquad (4\text{-}22)$$

The summation in Eqn. 4-22 represents the fact that each size range of pore level parameters corresponds to a range in N_T. The pore level parameters β, r_n and l_b are interrelated. For example, β, which is a measure of the pore aspect ratio, has a strong influence on l_b, larger aspect ratios leading to smaller l_b.

Research effort to quantify and interrelate these pore level parameters has begun only in the recent past. Mohanty (1981) presented a relationship that predicts a linear decrease in l_b as a function of N_T. To develop a functional relationship between a_{nw} - N_T, an average, constant aspect ratio for the bead pack, r_n / r_p, may be assumed as 0.1. Then, the β value will be 0.9. It follows that:

$$N_T \quad = \quad \frac{18kk_{rw}}{r_p l_b} \qquad (4\text{-}23)$$

Since volume is proportional to the third power of radius, the oil saturation can be approximated as

$$S_n \quad = \quad r_b^3 / r_p^3 \qquad (4\text{-}24)$$

where r_b is the NAPL blob radius. Implicit in Eqn. 4-24 is an assumption that the NAPL ganglia can all be represented by a single blob of radius r_b, which is not a fully realistic assumption. The use and limitations of this assumption are discussed later. To proceed with

the model development, the specific NAPL-water interfacial area can be approximated as the total number of spherical blobs at any given saturation times the surface area of each blob:

$$a_{nw} = 2S_n \epsilon / r_b \quad (4\text{-}25)$$

where ε is porosity of the soil. Substituting Eqn. 4-24 in 4-23 and rearranging:

$$N_T = \frac{18 k k_{rw} (S_n)^{1/3}}{r_b l_b} \quad (4\text{-}26)$$

And, substituting Eqn. 4-25 in 4-26, to expel the term r_b and to introduce a_{nw}, and rearranging we obtain:

$$a_{nw} = \frac{N_T \epsilon l_b S_n^{2/3}}{9 k k_{rw}} \quad (4\text{-}27)$$

Finally, to obtain a relationship between a_{nw} and N_T that excludes any pore level parameters that are difficult to measure, the following expression relating l_b and N_T was substituted in Eqn. 4-27:

$$l_b = J - sN_T \quad (4\text{-}28)$$

where J represents l_b corresponding to the longest blob initially present and s an empirical constant. Equation 4-28 is based on the observation that the average blob length l_b decreases

with increasing N_T, in an approximately linear fashion. Works of Mohanty (1981) and Pennell *et al* (1995) portend such relationship. In porous media literature, it is coustamary to characterize the blob length l_b in terms of number of pores occupied. The length of largest blobs (i. e. J value) observed were typically ten pores long (Dullien, 1974). Equation 4-28 is meaningful only in the critical trapping number range (usually 0.0001 to 0.001) within which mobilization occurs and l_b changes.

Upon substitution of Eqn. 4-28 in 4-27 and rearranging, one obtains:

$$a_{nw} = \frac{N_T \epsilon(J - sN_T) S_n^{2/3}}{9kk_{rw}} \qquad (4\text{-}29)$$

Equation 4-29 is dimensionally consistent and predicts that a_{nw} is relatively insensitive to increases in N_T in the relatively low N_T value range (i. e. in 1e-05 to 0.0001 range) and decreases with further increases in N_T (Fig. 4-10). The predicted a_{nw} - N_T curve in Fig. 4-10 was obtained with reference to the glass bead packs used in IFT-SN-1 and IFT-SN-2 experiments. A J value of 2.5 cm (ten times the average bead diameter of 250 microns) and an s value of 2700 were used, based on an assumption that l_b decreases with increasing N_T in the critical N_T range in a linear fashion. Predicted trends are in agreement with the measured trends, in the 'capillary mobilization' region. Eqn. 4-29 fails to predict the sudden increase with further increases in N_T, (i.e. in the 'emulsification' region), as the assumptions of capillary trapping that led to the definition of N_T become inoperative in this region.

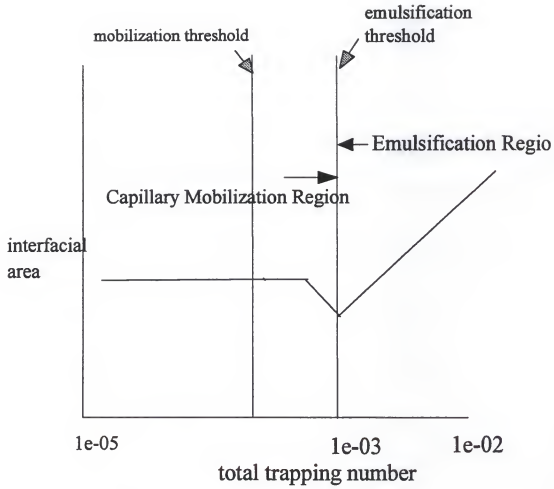

Figure 4-8 A shematic representation of the a_{nw} - N_T model (Eqn. 4-28)

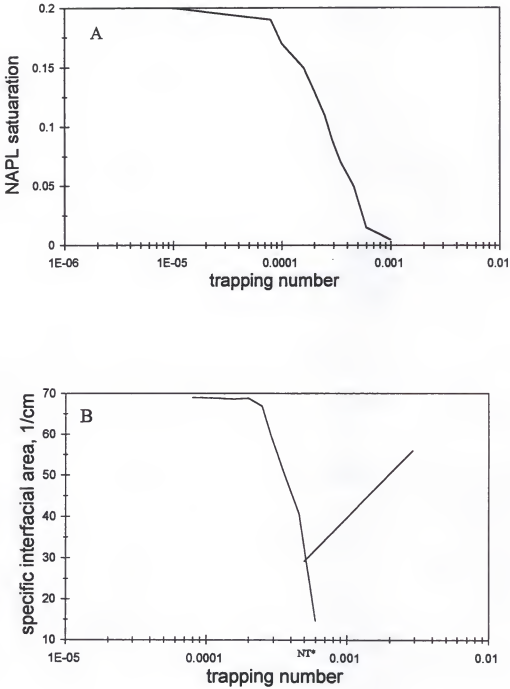

Figure 4-9 Illustration of (A) an S_n-N_T curve and
(B) the corresponding a_{nw} - N_T curve

Emulsions are intimate mixtures of two immiscible fluids, one of them being dispersed in the other, in the form of fine droplets. NAPL in porous media can be emulsified when there is sufficient energy input and/or sufficient lowering in γ_{nw} to create the new interface. The work of emulsification, W, is proportional to the newly created NAPL-water interfacial area, A_{nw}, according to the following equation:

$$W = \gamma_{nw} A_n \tag{4-30}$$

In the present mobilization experiments, volumetric water flow rate was maintained constant and, as such, the term W was a constant. Therefore, an increase in γ_{nw} should cause a linearly proportional increase in A_{nw} (and hence a_{nw}), according to Eqn. 4-30. The measured data in the emulsification region agree with this prediction of linear increase in a_{nw} due to emulsification. To account for such emulsification, the a_{nw}-N_T model, presented by Eqn. 4-29, can be extended as below:

$$a_{nw} = \frac{N_T \epsilon(J - sN_T) S_n^{2/3}}{9kk_{rw}}; \qquad for \quad N_T < N^*_T \tag{4-31a}$$

and

$$a_{nw} = a^*_{nw} + m[N_T - N^*_T] \tag{4-31b}$$

where a^*_{nw} the interfacial area at the minimum corresponding to the emulsification threshold (N^*_T) and m is slope of the a_{nw}-N_T curve in the emulsification region, equal to W/γ_{nw}.

Summary and Conclusions

Experimentally measured a_{nw}-N_T curves were presented, using interfacial tracers and surfactant-flushing as a means of mobilization. It was found that, during mobilization of decane using AOT-100 surfactant, a_{nw} initially remained insensitive to increase in N_T, decreased and passed through a minimum with further increases in N_T, to dramatically increase with further, final increase in N_T, due to emulsification. It was proposed that the total N_T range during mobilization be divided into two regions, a 'capillary mobilization' range and an 'emulsification' range. In addition, a simple analytical model to predict the same relationship also is presented. The model, though simplistic, successfully predicts the trends in the a_{nw}-N_T in the low to moderate capillary number range. A modification of the model, to incorporate the effects of emulsification, allows model predictions in the high N_T (emulsification) region as well. Future measurements and models relating the pore level parameter l_b and r_b to the trapping number N_T can be incorporated in this model, to place it on a more rational basis.

CHAPTER 5
USE OF INTERFACIAL TRACERS TO CHARACTERIZE NAPL MORPHOLOGY IN POROUS MEDIA

Introduction

When a nonaqueous phase liquid (NAPL) is introduced into the subsurface, gravity causes it to migrate downwards towards the water table, while a portion of it is retained in the vadose zone by capillary trapping. Once the NAPL reaches water table, it either floats on the water table or sinks further into the aquifer, depending on whether it is lighter than water (an LANPL) or denser than water (a DNAPL). In the case of a DNAPL also, a part of the liquid is retained in both vadose and saturated zones, and the rest, if available in sufficient volume, migrates further towards the bed rock. The fraction of NAPL left behind by the migrating free phase is entrapped in the aquifer pore spaces mainly under the influence of capillary forces under ambient groundwater flow conditions. This fraction, known as the trapped or residual NAPL saturation, exists in the subsurface as isolated, discontinuous ganglia of complex shapes and sizes. Residual NAPL source zones can contaminate large volumes of groundwater for long periods of time, owing to the low water solubility of their constituents, and thus create large plumes of contaminated water. Further, the drinking water standards for many NAPL constituents are orders of magnitude lower than their water solubility, which implies that dilution of the NAPL saturated plumes can not easily abate

contamination. Thus, even a small NAPL source zone can pose a large and persistent risk to groundwater quality. Various technologies were developed over the years to enhance NAPL remediation.

In order for any NAPL remediation method to be effective, NAPL zones must be properly characterized (Mackay and Cherry, 1989). The task of delineating contamination at these sites presents unprecedented difficulties to the scientific, engineering and regulatory communities. These difficulties are often exacerbated when the conventional characterization techniques based on drilling are used, due to remobilization of NAPL and possible displacement of contamination, which render the samples unreliable (Feenstra *et al*, 1995). Determination of the "nature and extent" of contamination, a regulatory requirement in the site investigations, is difficult to meet in practice, because of the complex nature of NAPL distribution.

At the laboratory scale, researchers have used physical methods such as blob casting and visual techniques such as CAT-SCAN, to study the NAPL morphology (Chatzis *et al*, 1988; Mayer and Miller, 1992). Information gained from such techniques is semi-quantitative at best. In contrast, tracers have the potential to offer a simple, non-destructive standard method to delineate the NAPL morphology. Tracer methods offer an attractive alternative or addition to the conventional methods of characterization. Use of tracers for characterization of the sub-surface involves the input of a known quantity of a reactive tracer, which can be a chemical, organism or energy that reacts with the sub-surface in a specific way, and comparing its output response to that of an inert, non-reactive tracer. By suitably designing the tracer, the necessary hydrodynamic and geochemical information of interest

about the subsurface can be obtained. For example, use of dyes as tracers to locate the groundwater stream lines is a standard tracer method in sub-surface hydrology. In the remediation of NAPL contaminated sites, apart from the aquifer properties, the basic information necessary includes chemical composition and quantity of NAPL present, its spatial distribution or morphology. Quantity of NAPL in the subsurface is typically measured in terms of NAPL saturation, S_n, which is the ratio of NAPL volume to soil pore volume. Traditionally, NAPL in soil have been quantified using liquid extraction and mass/volume balances. At the field scale, core sampling, cone penetrometer testing, geophysical logging and tracer test methods are the techniques available for characterization. Among these methods, partitioning tracers technique (Jin *et al*, 1994) is more effective at both laboratory and field scales, in terms of larger sample volumes represented, accuracy, convenience and replicate data sets obtained by using a suit of tracers in a single experiment. Partitioning tracers have been successfully used to measure the fluid saturations in both laboratory (Jin *et al*, 1994) and contaminated aquifer (Annable *et al*, 1994) settings. Using interfacial tracers, together with inert and partitioning tracers, the morphology of a NAPL source zone can be characterized more fully.

Morphology of Irregular Source Zones

In the study of morphology of three dimensional objects like NAPL ganglia, shape, size, location, volume, interfacial area and the area-to-volume ratio are the important characteristics. Methods to delineate the morphological distribution of NAPL would greatly add to the site characterization; such methods are not currently available. Use of multi-level

samplers (MLS) in tracer experiments can provide information about the spatial location of NAPL source zones (Annable *et al*, 1994). Thus, measurement of NAPL saturation S_n, specific interfacial area a_{nw} and area to volume ratio (I) using multi-level sampling approach, can provide information to characterize the NAPL source zone morphology adequately. For example, in a test volume containing heterogeneously distributed NAPL source zones, the spatial distribution of S_n can be mapped from partitioning tracers MLS data: the MLS locations in which partitioning tracers exhibit high retardation factors correspond to a zone of high NAPL saturation. Similarly, the spatial distribution of a_{nw} can be mapped from interfacial tracers MLS data: the MLS locations in which interfacial tracers exhibit high retardation factors correspond to a zone of high NAPL-water interfacial area. High a_{nw} values in a source zone can be a result of high S_n values. Alternatively, they can be a result of thinly spread out nature of a NAPL existing at a fairly low saturation, as explained earlier. For example, a source zone containing emulsified NAPL at a low S_n values will yield very high a_{nw} values. Thus, knowledge of either S_n or a_{nw} alone can not offer an adequate description of the source zone morphology.

However, information from the S_n and a_{nw} distributions can be combined into a single morphology index (I), which is the NAPL 'area-to-volume ratio', as below:

$$I = \frac{Total\ NAPL\text{-}water\ interfcaial\ area}{Total\ NAPL\ volume} = \frac{a_{nw}}{\epsilon\, S_n} \qquad (5\text{-}1)$$

where ε is the soil porosity. In contaminated soils, NAPL present at the same saturation can present vastly different interfacial areas, as shown in Fig. 5-1. Shown in Fig. 5-1(A) and (B)

are two different soil samples, contaminated with NAPL at the same average S_n value, the NAPL morphology being very different, however. In Fig. 5-1(A), the NAPL exists as a relatively few, large ganglia, as opposed to that in Fig. 5-1(B), where the NAPL is spread out as many small ganglia. Clearly, the specific NAPL-water interfacial area as well as the I index are much larger in the latter case. Thus, the I index is a useful index to describe the 'spread out' nature of NAPL among different regions of a contaminated aquifer or among different aquifers. Further, I is a more appropriate index to describe the morphology than is a_{nw}, because interfacial area alone cannot quantify the 'spread out' nature of ganglia as effectively the area-to-volume ratio. Using inert, interfacial and partitioning tracers in tandem, NAPL saturations (S_n), specific NAPL-water interfacial areas (a_{nw}) and I index, can be monitored before, during and after the remediation process. This method offers a valuable technology essential in the characterization of waste sites, remediation planning, design, evaluation and risk assessment.

Further, it can also be useful in the study of immiscible fluid behavior in porous media, at the laboratory scale, in such disciplines as groundwater and vadose zone hydrology and petroleum engineering. In hydrology research, there is currently an awareness that the constitutive relationships, known as the 'soil moisture curves' or P_c-S_w curves, are inadequate to describe multi phase flow (Gray and Hassanizadeh, 1991; Hassanizadeh and Gray, 1993), as they represent the changes in bulk phases alone. Inclusion of the interfacial area in such relationships will lead to more complete descriptions of the multi phase phenomena. The morphology index I could be an additional parameter useful in such revisions.

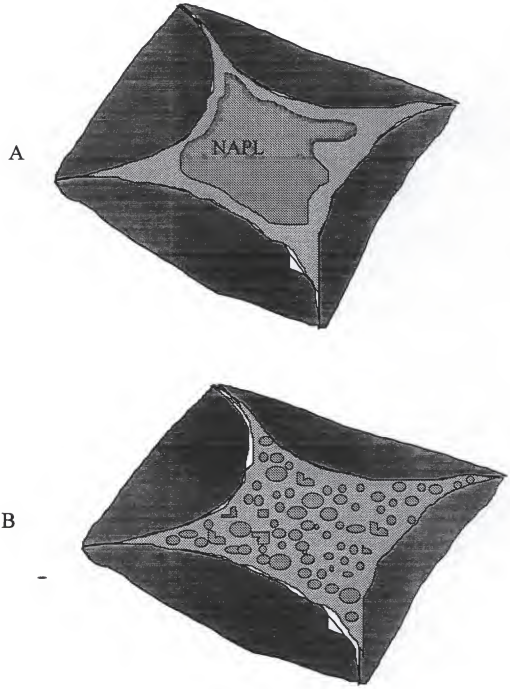

Figure 5-1 Morphology of a NAPL ganglion trapped in a pore (A) before and (B) after emulsification

Experimental

The primary objective of the experimental work was to create different morphological distributions of NAPL in sands, and characterize the same using interfacial tracers. To this end, several soil column flow through experiments were conducted. Changes in NAPL morphology were affected by three different experimental techniques, namely: (1) Dry versus wet NAPL loading (2) Emulsification and (3) Capillary pressure alteration. The three experimental techniques are described in the following sections.

(1) Dry versus wet NAPL loading Experiments

NAPL loaded differently into clean sand packs can present different morphological distributions, because of wettability differences. For example, Schwille (1988) observed that NAPL accumulate as ganglia at the pore centers when loaded into an initially water saturated medium, but form wedges at pore corners when loaded into an initially dry sand, followed by water flushing. It was found in our experiments also that the same NAPL, such as decane or PCE, at comparable saturations, exists in significantly different morphological distributions, depending on whether the NAPL is loaded into an initially dry sand or initially water saturated sand. Accordingly, different modes of loading of NAPL (dry loading and wet loading) were used as means to change NAPL morphology. In the dry loading case, glass columns (Kontes 2.54 cm i. d. x 5 cm long with teflon end fittings) packed with clean glass beads or clean sand were loaded with the NAPL in an upflow mode, at a flow rate of 0.2 ml/min, using a syringe pump. The column then was flushed with distilled, deionized, deaired water (DI water), using a syringe pump at a flow rate of 1.04 ml/min, in an upflow mode in the case of an LNAPL and

downflow mode in the case of a DNAPL, to facilitate the drainage of NAPL. Water was flooded through the column for several pore volumes, to ensure that no traces of free phase NAPL was draining out of the column. The NAPL retained in the column forms a uniform average residual saturation S_n, which was measured by monitoring the influent and effluent volumes. In the case of wet loading, the procedure was the same, except that NAPL was imbibed into an initially water saturated column, rather than being drained by water imbibition. The resulting residual saturation (S_n) values were consistently lower for the 'dry loading' case (Table 5-1). Miscible displacement experiments were conducted on the columns, using PFBA as a nonreactive tracer and SDBS (Sodium dodecyl benzenesulfonate) and/or Aerosol-OT-100 as interfacial tracers. The specific interfacial area a_{nw} and morphology index I were calculated using Eqn. 5-1 and 5-2, respectively.

(2) Emulsification

Emulsification of NAPL in porous media can cause dramatic changes in the NAPL morphology by breaking up the ganglia into smaller droplets. Such break up causes a dramatic increase in the specific interfacial area a_{nw} at any given S_n value, if the NAPL is not mobilized out of the coulmn in the process of emulsification. In our experiments, emulsification was used as a means to cause changes in NAPL morphology. Glass columns were packed with clean sand as described earlier, and NAPL was loaded in a wet loading mode, to form a residual NAPL saturation. Subsequently, the column was flushed with a 1% Igepal-70 solution saturated with decane. The intent of presaturating the surfactant solution with decane was to prevent loss of decane by solubilization during flushing. Batch

experiments using decane and 1% Igepal-70 solution confirmed that the lowering of interfacial tension causes emulsification of decane upon contact with the surfactant solution. In the column flushing experiment, although emulsification occurred, no mobilization of the decane was observed. After flushing three pore volumes of DI water through the column containing emulsified decane, tracer experiments were conducted using PFBA as a nonreactive tracer and SDBS as an interfacial tracer. In addition, an experiment was also conducted using a cosolvent mixture of 50% ethanol, 2% pentanol and 48% water (IFT-CS1), rather than a surfactant solution, to cause changes in NAPL morphology.

(3) Capillary pressure alteration

In the same porous medium, NAPL present at different S_n values presents different morphologies. The NAPL saturation S_n can be changed by changing the capillary pressure (P_c) across the sand pack sample. Based on this principle, experiments were conducted using a modified capillary cell (Annable, 1990) that allows the entrapment and step-wise variation of S_n in a short soil sample in the cell, as a function of the external capillary pressure applied (Fig. 3-3). The stainless steel capillary barriers on either end of the cell allow only water to flow through. The NAPL saturation is increased by varying the total capillary pressure experienced at the center of the soil cell, by adjusting the levels of the NAPL level in the burette and the hanging column at the outlet. Further, the cell contains an inlet at the top and outlet at the bottom, which are used to conduct inert and interfacial tracer experiments. Since the soil sample is short (3.4 cm high and 5.6 cm diameter), the NAPL saturation measured represents a uniform, average saturation in the sample, at capillary equilibrium.

Experiments were conducted using decane as the NAPL phase and 60 to 70 size glass beads as porous media. By increasing the capillary pressure imposed on the system and allowing about 20 hours for equilibration, NAPL saturation was increased in a step-wise fashion. Using PFBA as a non-reactive tracer and SDBS as an interfacial tracer, both at a concentration of 100 mg/L, a_{nw} and I values were measured corresponding to each S_n value.

Results and Discussion

Characteristics of the experimental columns used in the four sets of experiments and the results are tabulated in Table 5-1. Decane, perchloroethene (PCE), FC-40 (a synthetic, inert fluorinated hydrocarbon, a DNAPL) and an LNAPL from a contaminated aquifer in Utah were used as the NAPLs in the experiment. SDBS and AOT-100 were used as interfacial tracers. In the first two sets of experiments, glass columns were used. In the capillary pressure alteration experiments, a specially designed capillary cell that is amenable to tracer experiments was used (Annable, 1991). As can be seen from Table 5-1, although the NAPL residual saturations varied from 12 to 23%, the morphology index I values ranged from 71 to 7000, indicating that similar NAPL saturations (S_n) in porous media can present vastly different morphologies. (It should be noted that the very high S_n values presented in section IV of Table 5-1 represent continuous NAPL saturations, not residual trapped saturations).

Table 5-1. Results from interfacial tracer experiments using four different techniques to change NAPL morphology

column	length/dia	medium	tracer used	NAPL	S_n %	a_{nw}	I cm^{-1}	Remarks
1. Dry Vs. Wet Loading Technique								
IFT-O	5 x 2.54	GB1	SDBS	none	0	0	0	Control
IFT-A	15 x 2.54	GB1	SDBS	decane	21.8	218	2941	Dry loading (NAPL first)
IFT-B	5 x 2.54	GB1	SDBS	decane	16.4	86	1542	Wet loading (water first)
IFT-D	5 x 2.54	sand	SDBS	decane	20.4	233	3359	
IFT-FC40	5 x 2.54	GB1	SDBS	FC-40	7.4	332	13195	Dry loading (NAPL first)
IFT-PCE	5 x 2.54	GB1	SDBS	PCE	24.0	78	956	
IFT-S2	5 x 2.54	sand	AOT	decane	19.6	74	1110	
IFT-JPOIL1	5 x 2.54	GB1	SDBS	JP-OIL	23.0	68	869	wet loading (water first)
2. Emulsification technique								
IFT-S2	5 x 2.54	S1	SDBS	decane	17	93	547	before 1% Igepal flush
IFT-S2	5 x 2.54	S1	SDBS	decane	17	338	1988	after 1% Igepal flush
IFT-CS1	5 x 2.54	S1	SDBS	decane	17	85	500	before cosolvent flush
IFT-CS1'	5 x 2.54	S1	SDBS	decane	17	12	71	after cosolvent flush
IFT-SN2-A	5 x 2.54	GB1	SDBS	decane	12	68	567	before AOT-100 flush
ISH-SN2-A'	5 x 2.54	GB1	SDBS	decane	2	140	7000	after AOT-100 flush
3. Capillary Pressure Alteration Technique								
ISH-C1	5.6 x 3.4	GB2	SDBS	Decane	0	0	0	capillary head = 15cm
ISH-C2	5.6 x 3.4	GB2	SDBS	Decane	0.13	58	1312	capillary head = 15.6 cm
ISH-C3	5.6 x 3.4	GB2	SDBS	Decane	0.25	120	1411	capillary head = 17.6 cm
ISH-C4	5.6 x 3.4	GB2	SDBS	Decane	0.4	186	1367	capillary head = 19.3 cm
ISH-C5	5.6 x 3.4	GB2	SDBS	Decane	0.51	158	911	capillary head = 19.5 cm
ISH-C6	5.6 x 3.4	GB2	SDBS	Decane	0.68	127	549	capillary head = 20.2 cm
ISH-C7	5.6 x 3.4	GB2	SDBS	Decane	0.79	124	462	capillary head = 22.7 cm

The difference in morphology between the 'Dry versus Wet Loading' experiments is striking. Among IFT-A and IFT-B columns, which were run in the same glass bead packs containing decane at similar Sn values, the only difference being that IFT-B was wet by water first, whereas IFT-A was 'wet' by decane first. The fact that I index is more than an order of magnitude larger for IFT-A indicates that decane existed in this column in a much more spread out manner than in IFT-B. It is well established in the literature that NAPL that truly are nonwetting exist in porous media as ganglia at the center of pore spaces. By a simple geometric analysis, assuming spherical ganglia at centers of pore spaces, it can be shown that the a_{nw} and I values of IFT-B column are consistent with the classical explanation of decane ganglia entrapment at the pore centers. However, in case of IFT-A, the inordinately high a_{nw} and I values do not support the view that decane exists as ganglia at pore centers in this case (decane loaded first into dry sand, followed by water). On the contrary, the high a_{nw} and I values in this case can be explained if the porous medium is treated as a decane-wet, or at least a mixed-wet system. Mixed wetting of the glass bead surfaces is possible in principle, because when decane is drained off of the glass bead surfaces by water imbibition, a part of it can still be trapped as films wedges at pore corners, which offer strong capillary resistance to dewetting. This observation is consistent with the earlier theoretical predictions about the morphology of a nonwetting phase displaced by a from porous media by a wetting fluid (Mohanty *et al*, 1979). Schwille's (1988) visual experiments support this view. In such scenario, the final morphology of decane in the case of IFT-A should consist of both wedges in the pore corners as well as ganglia in the pore

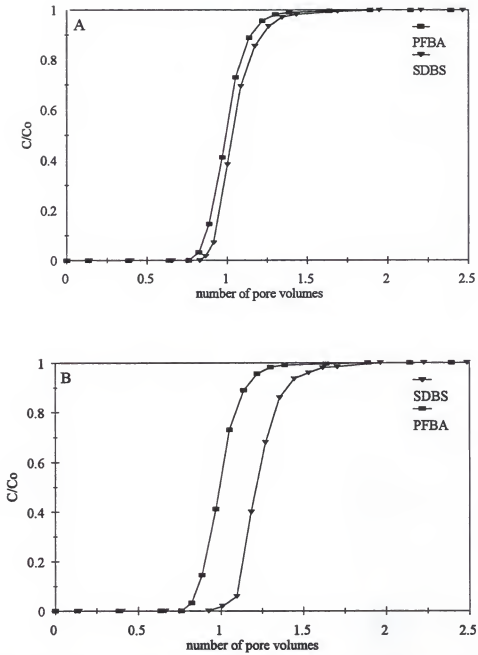

Figure 5-2 Breakthrough curves for PFBA and SDBS in IFT-S2 column (A) before and (B) aftercontact of trapped decane with a 1% Igepal-70 solution, in the absence of mobilization

centers, as opposed to ganglia alone in IFT-B. In addition, decane may also have been trapped on the bead surfaces due to micro-capillaries on the molecularly rough glass surface, which will be sensed as 'decane-water interface' by the interfacial tracer, as even a monolayer of decane adsorbed to the solids can present a large additional interfacial area. If this were true, then the a_{nw} value must be nearly equal to the specific surface of the solids itself. Nitrogen adsorption measurements on the glass sand indicated that its specific surface is in the order of 1000 cm^{-1}. Accurate measurement of the same was not possible, the available specific surface was too small for nitrogen adsorption measurement. The fact that the measured a_{nw} is much less than the sand's specific surface, together with the fact that decane, a nonpolar hydrocarbon, must be truly nonwetting on clean glass points against the microwetting of surfaces with decane. The alternative explanation that decane existed as both ganglia at pore centers and wedges and films at pore corners seems to be more reasonable. The same can be said to be true in the cases of IFT-FC1, IFT-F and IFT-P1 experiments as well, where the different NAPLs were loaded in a 'NAPL-first' mode.

The difference in morphology between the two modes of loading has major implications for the study of NAPL transport and remediation, especially in the unsaturated zone. In this zone, NAPL spills on dry top soil correspond exactly to the 'NAPL first' type loading, which presents much larger a_{nw} and I values than what is predicted by the ganglia hypothesis. Consequently, the larger interfacial areas at any given saturation in the unsaturated zone offer larger contamination risks than in the saturated zone. By the same token, clean up of the spread out NAPL could be more difficult in the unsaturated zone. Such predictions are only speculation at this point, as the study of the influence of NAPL

Such predictions are only speculation at this point, as the study of the influence of NAPL morphology on transport, fate and remediation of NAPLs has not even been initiated yet, for want of experimental techniques. The interfacial tracer methods presented in this work will be useful in such future studies.

In light of the above discussion, it can be seen from Table 5-1 that emulsification also caused a dramatic increase in the a_{nw} and I values. The data presented in section II, for experiments IFT-S2 &IFT-S2', IFT-CS1&IFT-CS1' and IFT-SN2-A &IFT-SN2-A' represent data obtained by interfacial tracer experiments conducted on three different experiments, before and after (represented by a prime, eg: IFT-S2') flushing with a high concentration surfactant or co-solvent solution as means of changing NAPL morphology. The experiments IFT-S2 and IFT-SN2-A indicate that the surfactant flushing caused severe emulsification of decane in the column, resulting in large a_{nw} and I values. In the case of IFT-S2 experiment, flushing of trapped decane using a 1% Igepal-70 solution presaturated with decane caused an increase in a_{nw} but no reduction in S_n. It is not clear why the emulsified decane was not mobilized out of the sand in this experiment. One reason could be an unfavorable hydrodynamic situation, caused due to plugging of pore spaces by the emulsified decane. In the case of IFT-SN2-A experiment, a different surfactant solution (AOT-100 in 0.2%NaCl, not presaturated with decane) caused both emulsification and mobilization of decane. The post flushing tracer experiment (IFT-SN2-A') revealed that emulsified decane even at 2% S_n can present a large interfacial area and I values. In contrast to the surfactant flushing experiments, flushing of trapped decane with a 48% ethanol, 2% pentanol, 50% water cosolvent presaturated with decane caused a reduction in the a_{nw} and I values and no removal

within the column. In principle, such coalescence is plausible, as the reductions in interfacial tension due to the presence of cosolvents may be sufficient for internal reorientation of the ganglia, while it is certainly insufficient to cause emulsification. Alternatively, it could represent an unknown artifact in the interfacial tracers experiment conducted in IFT-CS1' phase. The presence of even trace amounts of pentanol or ethanol in the column, after the cosolvent flush, can change the adsorption behavior of interfacial tracer at the decane-water interface. More work is necessary before it can be concluded that cosolvent flushing causes blob coalescence, thus leading to a reduction in the a_{nw} and I values.

Observations from these emulsification experiments can be useful in understanding and improving the chemically enhanced remediation of NAPL in soils. For example, since solubilization efficiency is a direct function of the a_{nw}, cosolvent remediation experiments can be conducted in sequence with surfactant flushing experiments. In this scenario, a single pore volume of appropriate surfactant precursor can be used to emulsify the NAPL in-situ and thus cause a dramatic increase in its a_{nw}, which now can be solubilized using fewer cosolvent pore volumes. Similarly, if the cosolvent flushing indeed causes blob coalescence and NAPL bank formation, then the NAPL bank so formed can be recovered as a free product. These two hypothetical examples illustrate how knowledge about NAPL morphology and its control can be used to improve NAPL remediation technologies.

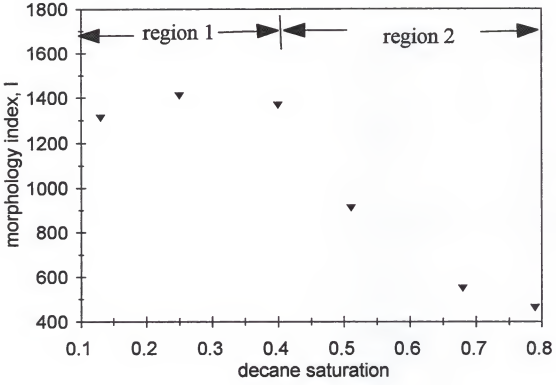

Figure 5-3 Variation of morphology index, *I*, measured in ISH-C capillary cell experiments as a function of decane saturation

In section III of Table 5-1, results from the capillary pressure alteration experiments are reported. As explained earlier, the experiments ISH-C1 through C7 represent seven stages of capillary pressure and NAPL saturation in the same capillary pressure cell, affected by changing the decane and water levels in the burettes (Fig. 3-3). In Fig. 5-4, the morphology index I, plotted against S_n indicates that the I index is insensitive to changes in S_n in the 0 to 50% S_n range. This is the range where the NAPL ganglia grow in size due to an increase in volume. Beyond 50% NAPL saturation, the NAPL-water interface and the solid particle walls are separated by only a thin film of water a_{nw} values observed at higher saturations represent the fraction of total interfacial area that is accessible to the interfacial tracers. In Chapter 3, it was shown that the thermodynamic (Leverett, 1941) and geometric (Gvirtzman and Roberts, 1991) model predictions as well as experimentally measured data indicate a nearly linear increase in a_{nw} with increasing S_n . This fact implies that the morphology index I, which is the ratio of a_{nw} to S_n, should remain insensitive to S_n in the continuous NAPL saturation range (Fig. 5-2). This observation can serve as a basis for predictions about the shape of the NAPL phase boundary, the required condition being a constancy of I. For example, a perfectly spherical ganglion fails to satisfy this condition, as its I index is not insensitive to its volume, but increases with the one-third power of volume. Thus, the phase boundary must be a complex geometric shape that satisfies the condition that I is independent of S_n.

Summary and Conclusions

A complete NAPL source zone characterization requires knowledge of the physico-chemical character, location and volume of the NAPL ganglia, their shape, size and morphologic distribution. Volume of NAPL is represented by residual saturation S_n, which can be measured in-situ using recent tracer methods such as partitioning tracers. The properties that can adequately describe the morphology of any object are its location, volume, specific interfacial area and the area-to-volume ratio. Neither experimental tools nor theoretical methods are available in the literature, to study the NAPL morphology in porous media. In the current work, we proposed the specific NAPL-water interfacial area a_{nw} and the NAPL area-to-volume ratio I, termed the morphology index, as two useful indices that can adequately describe the NAPL morphology. Using interfacial tracers, new experimental methods were developed to measure the a_{nw} and I indices for NAPL in unconsolidated sands. Several experiments were conducted, using several different NAPLs and surfactants as interfacial tracers, which demonstrate the use of morphology index I to effectively capture such differences in morphology, both in the trapped saturation and continuous saturation regions of S_n. Study of the differences in NAPL morphology as measured by the I index can be used to better characterize the NAPL sites and improve their remediation design. The methods and results presented here have potential applications in the characterization, remediation design and assessment of NAPL sites and petroleum reservoirs, as well as in multi-disciplinary research concerning immiscible fluid behavior in porous media.

CHAPTER 6
SUMMARY AND CONCLUSIONS

Conclusions

The central objective of this study was to develop an experimental technique to measure the specific interfacial area of immiscible fluids, such as NAPL and water, distributed in porous media. Accordingly, a tracer experimental method, called 'interfacial tracers technique', was developed and used to address relevant questions about characterization of immiscible fluid interfaces in porous media. The specific conclusions of this study are :

1. Interfacial tracers technique offers a simple method for the measurement of the specific NAPL-water interfacial area (a_{nw}) in porous media. The a_{nw} values measured in trapped, continuous and chemically altered NAPL saturation scenarios are in agreement with the current understanding of immiscible fluid behavior in porous media.

2. Use of interfacial tracers can present an effective new method for a more complete characterization of the NAPL source zones in the sub-surface. Isotherms for adsorption of interfacial tracers were found to be linear in low concentration ranges, and feebly non-linear in a larger range. A linear adsorption isotherm simplifies the field application of interfacial tracers.

3. The flow experimental methods used in this study will likely be useful in the study of adsorption at the immiscible fluid interfaces.

4. The thermodynamic model predictions of Leverett (1941) agreed with the measured trends in a_{nw} as a function of fluid saturation in continuously distributed immiscible fluid systems in porous media, in an S_w range of 0 to 55%.

5. For a given NAPL-water distribution in an unconsolidated sand, the NAPL entry pressure, NAPL-water interfacial tension and a pore size distribution index together can adequately describe the a_{nw} distribution.

6. The interfacial area a_{nw} for a given NAPL in a given sand at the same saturation can be significantly different between a NAPL-wet and a water-wet conditions. Interfacial tracers technique can offer a new tool for the study of wettability of porous materials.

7. Interfacial tracers technique can effectively capture the changes in a_{nw} during chemically enhanced remediation, such as surfactant and co-solvent flushing applications. The resulting information can be used in remediation design, trouble shooting and the development of new approaches in remediation.

8. An analytical model presented adequately predicts the changes in a_{nw} as a function of total trapping number (N_T) during the mobilization of a trapped residual NAPL.

9. The interfacial area to NAPL volume ratio, termed the 'morphology index (I)', can effectively capture the differences in NAPL morphology.
10. The methods presented in this work can be useful in the characterization of NAPL source zones and petroleum reservoirs, and in the performance assessment of various remediation technologies.

Recommendations

Interfacial tracers technique has potential applications in the study of mass, heat and momentum transport processes across immiscible fluid interfaces, wettability and morphology of NAPL in porous media. Accordingly, recomendations for future work include:

1. Experiments and modeling of constituent mass transfer across the NAPL-water interface with a knowledge of measured residual NAPL values, which will elucidate the mass transfer process.
2. Use of interfacial tracers to investigate wetting of porous media by NAPL under different wettability conditions, which may lead to a new experimental method for the characterization of rock wettability.
3. Use of interfacial tracers to investigate the influence of NAPL-water interfacial area (a_{nw}) on relative permeability (k_{rw}) in soils.
4. Use of interfacial tracers in three immiscible fluid systems, to measure the specific surface areas of the three fluid interfaces.

5. Use of inert, partititioning and interfacial tracers to locate and characterize heterogeneously distributed NAPL source zones in porous media.
6. Use of interfacial tracers and partitioning tracers in tandem, to probe the interfaces and bulk phases of immiscible fluids for a better understanding of non-equilibrium of interfacial and inter-phase mass transfer.
7. Use of interfcial tracers in bioremediation of NAPL, to investigate the observation that the extent of bioremediation is proportional to a_{nw}, as bacteria prefer to thrive at the substrate-water interace.
8. Use of interfacial tracers in the characterization of pitch, which is a persistent fraction of NAPL remaining after the remediation is complete.
9. Use of interfacial tracers in fractured media to quantify the extent of contamination,
10. Use of interfacial tracers in combined experimental-modeling efforts to include a_{nw} as a fundamental characteristic, together with capillary pressure and fluid, saturations, in constituitive relationships describing immiscible fluid distributions.
11. Use of interfacial tracers for a better understanding of heat/energy transfer across the NAPL-water interface and its application in thermal enhancement based remediation processes, such as steam strpiing and soil vapor extraction.
12. Use of interfacial and partitioning tracers in development of 'treatment trains'for remediation of NAPL contaminated sites.

APPENDIX A

PORE SINGLET MODEL

Nearly spherical solid particles packed as a porous medium form prismoidal pore spaces that are bounded by the spherical walls, as shown in Fig. 1-1. To demonstrate the trends in the a_{nw}-S_w relationship, this pore singlet can be modeled as a rhomboidal prism (Fig. A-1, stage 1), of base a and height $\sqrt{3}a/2$ and volume $a^3/8$. At low NAPL saturations, the NAPL ganglion exists at the center of the pore as a spherical blob of radius r. At any blob radius r, the NAPL saturation S_n can be expressed as a ratio of volumes of spherical blob and prismoidal pore singlet, as:

$$S_n = \frac{V_s}{V} = \frac{33.51\ r^3}{a^3} \qquad \text{(A-1)}$$

The blob radius increases with decreasing S_w until it almost touches the pore walls, separated by only a thin film of water. The maximum blob radius corresponding to this stage, R_{max}, can be shown (Fig. A-1, stage 2) to be equal to 0.5 a tan η, where η is the median angle at the pore corner, equal to 30 degrees for the present case (rhomboid). Thus, R_{max} is equal to 0.288 a for the present case, which corresponds to a blob volume maximum, V_{max}:

$$V_{max} = 4/3\pi(0.288\ a)^3 = 0.1\ a^3 \qquad \text{(A-2)}$$

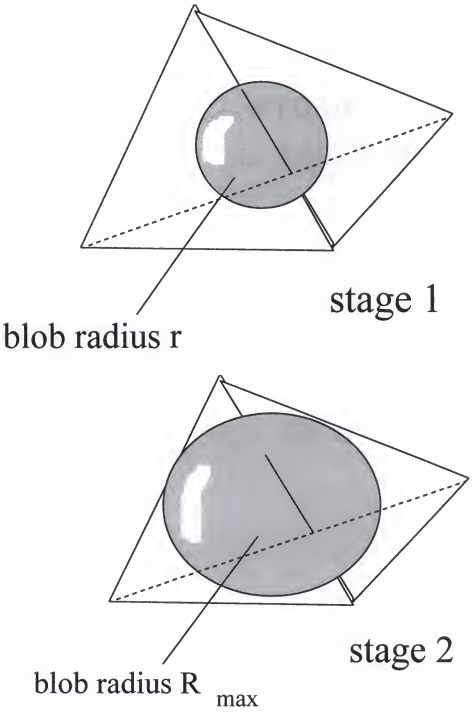

Figure A-1. Schematic development of Pore Singlet Model

Interfacial area corresponding to this stage is

$$A_{max} = 4\pi(0.288\ a)^2 = 1.04\ a^2 \qquad \text{(A-3)}$$

The maximum S_n value corresponding to R_{max} is equal to 0.8 or 80%. Beyond this saturation, the NAPL blob begins to loose its sphericity and progressively assume the shape of the pore until it mimics the shape of the pore itself, at S_{wr}. Thus, between S_n values of 0.8 and 1, the NAPL-water interfaccial area corresponds to a prismoid with rounded (spherical) corners. In the S_n range of 0 to 80%, the NAPL-water interfacial area within the pore singlet is equal to:

$$A_{nw} = 4\pi r^2 \qquad \text{(A-4)}$$

In a rhombohedral packing of beads, the number of pores formed per unit cell of side $2a$, called the grain coordination number, is 12. Therefore, in a soil volume of side $2R_b$, where R_b is the radius of solid beads, 12 NAPL blobs grow progressively with increasing S_n. In a rhombohedral packing of beads, the side of pore, $2a$, is approximately related toR_b as (Iwata *et al*, 1981):

$$a = 0.6\ R_b \qquad \text{(A-5)}$$

where R_b is the bead radius. Further, porosity of a rhombohedral pack is equal to 0.26.

In a soil volume of one cubic centimeter, the number of such singlet blobs is equal to 0.26/V or $0.26*8/a^3$ or $9.63/R_b^3$. Thus, the specific NAPL-water interfacial area, which is

the interfacial area per one c.c. of soil, can be written as:

$$a_{nw} = \frac{9.63}{R_b^3} * 4\pi r^2 \qquad \text{(A-6)}$$

A modification of Eqn. A-1 yields:

$$r = a\,[\frac{S_n}{33.51}]^{1/3} \qquad \text{(A-7)}$$

Upon substitution of Eqn. A-5 and A-7 in A-6, we obtain:

$$a_{nw} = \frac{4.19 S_n^{2/3}}{R_b} \qquad \text{(A-8)}$$

For a bead radius of 150 microns, the a_{nw} is given as 508 $S_n^{2/3}$. For tetrahedral packing also, a similar equation can be derived as:

$$a_{nw} = \frac{5.02 S_n^{2/3}}{R_b} \qquad \text{(A-9)}$$

As shown in Fig. 3-12 , the model predictions agree reasonably with the measured trends. The model can be slightly improved by considering coalescence of individual NAPL blobs with increasing S_n values. The model predictions are reasonable even when the blob coalescence is ignored, because, in a pack with high aspect ratios, the contribution of blob connections (at the pore throats) to a_{nw} is not significant.

GLOSSARY

Roman

a	Area occupied per tracer molecule at the interface, L^{-2}
a_{nw}	Wetting-nonwetting phase interfacial area per unit porous medium volume, L^{-1}
a^*_{ns}	Solid-nonwetting phase interfacial area per unit pore space, L^{-1}
a^*_{nw}	Wetting-nonwetting phase interfacial area per unit pore space, L^{-1}
a^e_{nw}	Specific NAPL-water interfacial area at emulsification threshold, L^{-1}
A_s	Specific solid surface area, L^{-1}
A_{nw}	Total interfacial area of the immiscible fluid interface, L^2
b	Porosity index (dimensionless)
C	Aqueous phase concentration, Molar
C_{nw}	A constant of integration (dimensionless)
C_s	Aqueous phase concentration in equilibrium with NAIL, moles L^{-3}
C_o	Aqueous phase tracer input concentration, moles L^{-3}
d_p	Soil particle diameter, L
D_m	Molecular diffusion coefficient, L^2T^{-1}
E	Entropy
f	Frequency of pores of radius r (dimensionless)
F_s	Superficial surface free energy, ML^2T^{-2}
f_s	Superficial surface free energy per unit interfacial area, MT^{-2}
F	Helmholtz free energy, ML^2T^{-2}

g Acceleration due to gravity, LT^{-2}

G Sorbed phase concentration at the immiscible fluid interface, moles L^{-2}

h Static head, L

h_d Nonwetting phase entry pressure head, L

I NAPL area-to-volume ratio(morphology index), L^{-1}

J Blob length at mobilization threshold, L

$J(S_w)$ Leverett's J function

k_w Relative permeability to water (dimensionless)

K Freundlich isotherm coefficient (dimensionless)

K_i Linear adsorption coefficient for interfacial tracer at the fluid interface, L^{-1}

K_s Linear adsorption coefficient for interfacial tracer at the solid-water interface, L^{-1}

k Intrinsic permeability, L^2T^{-1}

K_l Apparent mass transfer coefficient, L^2T^{-1}

K_{sat} Saturated hydraulic conductivity, L^3T^{-1}

k_l Intrinsic mass transfer coefficient, T^{-1}

l Length of cylindrical pore, L

l_b Length of NAPL blob, L

λ Brooks-Corey Pore Distribution Index (dimensionless)

β A fitting factor in Cary (1994) model (dimensionless)

m Empirical exponent in Van Genuchten soil characteristic function (dimensionless)

M Total mass adsorbed, M

n Empirical exponent in Van Genuchten soil characteristic function (dimensionless)

n_i Number of moles of species I (dimensionless)

N Avogadro's number (dimensionless)

N_T Total trapping number (dimensionless)

N_T* Total trapping number at emulsification threshold (dimensionless)

N_B Bond number (dimensionless)

N_{Ca} Capillary number (dimensionless)

p Hydraulic head, L

P Pore water volume, L^3

P_c Capillary pressure, $ML^{-1}T^{-2}$

P_{co} Capillary pressure at datum, $ML^{-1}T^{-2}$

P_w Wetting phase (water) pressure, $ML^{-1}T^{-2}$

P_{nw} Nonwetting phase (NAPL) pressure, $ML^{-1}T^{-2}$

P_d Nonwetting phase (NAPL) entry pressure, $ML^{-1}T^{-2}$

q Freundlich isotherm exponent (dimensionless)

Q_w Volumetric water flow rate, L^3T^{-1}

r Radius of cylindrical pore, L

r_p Radius of pore body, L

r_n Radius of pore neck, L

r_b Radius of NAPL blob, L

R Univerasal gas constant, $ML^2T^{-2}mol^{-1}\ ^oK^{-1}$

R_1 Principal minor radius of curvature at the interface, L

R_2 Principal major radius of curvature at the interface, L

R_h Hydraulic radius, L

R_e Reynolds number (dimensionless)

R_{rfi} Retardation factor for interfacial tracer (dimensionless)

R_{nr} Retardation factor for nonreactive tracer (dimensionless)

R_b Bead radius, L

s Empirical constant in I_b-N_T relationship (dimensionless)

S Sorbed phase concentration of interfacial tracer at the solid-water interface, moles L^{-2}

S_w Wetting phase saturation, %

S_n Nonwetting phase saturation, %

S_r Residual wetting phase saturation, %

S_e Effective wetting phase saturation, %

Sh Sherwood number

t Time, T

t_s Tracer pulse input duration, T^{-1}

T Temperature (°)

v Water flow velocity, LT^{-1}

V Volume, L^3

V_p Volume of phase p, L^3

V_b Bulk volume of porous medium, L^3

V_w Darcy flow velocity, LT^{-1}

x Length, L

Greek

γ Interfacial tension, MT^{-2}

γ_o Interfacial tension in the absence of interfacial tracer, MT^{-2}

γ_{min} Interfacial tension in the presence of interfacial tracer at *CMC*, MT^{-2}

γ^* Normalized interfacial tension (dimensionless)

Ω Concentration normalized to CMC (dimensionless)

ε Porosity (dimensionless)

ρ Water density, ML^{-3}

ρ_w Wetting phase density, ML^{-3}

ρ_{nw} Wetting phase density, ML^{-3}

μ_w Viscosity of water, $M^{-1}LT^{-1}$

μ_{nr} Area integral from a nonreactive tracer breakthrough curve (dimensionless)

μ_{ift} Area integral from an interfacial tracer breakthrough curve (dimensionless)

Γ Gibbs surface excess, moles L^{-2}

θ Pore space per unit medium volume (dimensionless)

τ Empirical constant (dimensionless)

ϕ_{snw} Equilibrium contact angle at the *snw* contact line (radians)

Φ_{nw} Area under the P_c-S_w curve, L

θ_w Volumetric water content (dimensionless)

μ_i Chemical potential of species *I*, $ML^2T^{-2}mol^{-1}$

α Lever angle in the linearized Leverett model (radians)

REFERENCES

Adamson, A. W. (1982) *Physical Chemistry of Surfaces,* John Wiley & Sons, New York.

Anbeek, C. (1993) "The Effect of Natuaral Weathering on Dissolution Rates," *Geochimica et Cosmochimica Acta*, 57: 4963-4975.

Annable (1991) "Aqueous Phase Transport in Soils Contaminated with Multicomponent Liquid Hydrocarbon and Subjected to Vapor Flow," Ph. D. Dissertation, Michigan State University, East Lansing, MI.

Annable, M. D., Rao, P. S. C., Hatfield, K., Graham, W. D., Wood, A. L. and Enfield, C. G. (1996) "Use of Partitioning Tracers for Measuring Residual NAIL: Results from a Field-scale Test," submitted to *ASCE Journal of Environmental Engineering*

Atlas, R. M. (1988) "Biodegradation of Hydrocarbons in the Environment," in *Environmental Biotechnology* (G. S. Omenn, Editor), pp. 211-220, Plenum Press, New York.

Binks, B. P. (1993) "Surfactant Monolayers at Oil-Water Interfaces," *Chemistry & Industry*, July 1993: 537-541.

Bradford, S. and Leij, F. (1995) "Estimating Interfacial Areas for Multi-fluid Soil Systems," unpublished manuscript.

Bragg, G. M. (1974) *Principles of Experimentation and Measurement*, Prentice-Hall, Inc., Engelwood Cliffs, NJ.

Busby, R. D., Lenhard, R. J. and Rolston, D. E. (1995) "An Investigation of Saturation-Capillary Pressure Relations in Two-and Three-Fluid Systems for several NAPLs in Different Porous Media," *Ground Water*, 33(4): 570-578).

Carman, P. C. (1941) "Capillary Rise and Capillary Movement of Moisture in Fine Sands," Soil Science, 52:1-14.

Carslaw, H. S. And J. C. Jaeger, Conduction of Heat in Solids, Oxford University Press, New York, 1959.

Carter, D. L., Mortland, M. M. and Kemper, W. D. (1986) "Specific Surface," in *Methods of Soil Analysis, Part 1–Physical and Mineralogical Methods*, Second Edition (A. Klute, Editor), Soil Science Society of America, Inc., Madison, WI.

Cary, J. W. (1994) "Estimating the Surface Area of Fluid Phase Interfaces in Porous Media," *Journal of Contaminant Hydrology*, 15: 243-248.

Cary, J. W., Simmons, C. S. And McBride, J. F. (1994) "Infiltration and Redistribution of Organic Liquid in Layered Porous Media," *Soil Science Society of America Journal*, 58: 177-189.

Chan, K. S. And Shah, D. O. (1979) "The Physico-chemical Conditions Necessary to Produce Ultra-low Interfacial Tension at the Oil/Brine Interface," in *Surface Phenomena in Enhanced Oil Recovery* (D. O. Shah, Editor), Plenum Press, New York.

Chatzis, I., Kuntumukkala, M. S. and Morrow, N. R. (1988) "Effect of Capillary Number on the Microstructure of Residual Oil in Strongly Water-wet Sandstones," *SPE Reservoir Engineering*, 3: 902-912.

Chatzis, I., Morrow, N. R. and Lim, H. T. (1983) "Magnitude and Detailed Structure of Residual Oil Saturation," *Society of Petroleum Engineers Journal*, 23: 311-326.

Cockbain, E. G. (1954) "The Adsorption of Sodium Dodecyl Sulfate at the Oil-Water Interface and Application of the Gibbs Equation," *Transactions of the Faraday Society*, pp. 874-881.

Corey, A. T. (1985) *Mechanics of Immiscible Fluids in Porous Media*, (Water Resources Publications, Littleton, CO.

Dane, J. H., Oostrom, M. and Missildine, B. C. (1992) "An Improved Method for the Determination of Capillary Pressure-Saturation Curves involving TCE, Water and Air," Journal of Contaminant Hydrology, 11: 69-81.

Davies, J. T. and Rideal, E. K. (1963) *Interfacial Phenomena*, Academic Press, New York.

Demond, A. H. and Roberts, P. V. (1989) "Effect of Interfacial Force on Two-Phase Capillary Pressure-Saturation Relationships," *Water Resources Research*, 27(3):423-437.

Dullien, F. A. L. (1979) *Porous Media : Fluid Transport and Pore Structure*, Academic Press, New York.

Feenstra, S. and Cherry, J. A. (1995) "Diagnosis and Assessment of DNAPL Sites," in *Dense Chlorinated Solvents and Other DNAPLs in Groundwater: History, Behavior and Remediation*, (J. F. Pankow and J. A. Cherry, Editors) Waterloo Press, Waterloo, Ontario.

Fischer, E. K. and Harkins, W. D. (1931) "Monomolecular Films. The Liquid-Liquid Interface and the Stability of Emulsions," *American Chemical Society*, 67: 99-110.

Geller, J. T. and Hunt, J. R. (1993) "Mass Transfer from Nonaqueous Phase Organic Liquids in Water-Saturated Porous Media," *Water Resources Research*, 29 (4): 833-845.

Gopal, E. S. R. (1967) "Principles of Emulsion Formation," in *Emulsion Science* (P. Sherman, Editor), Academic Press, New York.

Gray, W. G. and Hassanizadeh, S. M. (1991a) "Paradoxes and Realities in Unsaturated Flow Theory," *Water Resources Research*, 27(8): 1847-1854.

Gray, W. G. and Montemagno, C. M. (1995) "Theoretical and Experimental Study of Multiphase Flow in Porous Media," http://wwwnd.edu/departments/ EN/CEGEOS/ faculty/W_gray/summary_wgg.html

Gray, W. G. and Hassanizadeh, S. M. (1991b) "Unsaturated Flow Theory Including Interfacial Phenomena," *Water Resources Research*, 27(8): 1855-1863.

Gregg, S. G. and Sing, K. S. W. (1982) *Adsorption, Surface Area and Porosity*, Academic Press, London.

Guarnaccia, J. F., Imhoff, P. T., Missildine, B. C., Oostrom, M., Celia, M. A., Dane, J. H., Jaffe, P. R. and Pinder, G. F. (1992) "Multiphase Chemical Transport in Porous Media," *Environmental Research Brief*, U. S. EPA/600/S-92/002, March.

Gvirtzman, H and Roberts, P. V. (1991) "Pore Scale Spatial Analysis of Two Immiscible Fluids in Porous Media," *Water Resources Research*, 27(6): 1165-1176.

Harkins, W. D. and Beeman, N. (1929) "Emulsions: Stability, Area Per Molecule in the Interfacial Film, Distribution of Sizes and the Oriented Wedge Theory," *Journal of American Chemical Society*, 51: 1675-1695.

Hassanizadeh, S. M. and Gray, W. G. (1993) "Thermodynamic Basis of Capillary Pressure in Porous Media," *Water Resources Research*, 29(10): 3389-3405.

Haydon, D. A. and Taylor, F. H. (1960) "On Adsorption at the Oil/Water Interface and the Calculation of Electrical Potentials in the Aqueous Surface Phase: I. Neutral Molecules and a Simplified Treatment for Ions," *Philosophical Transactions of the Royal Society of London, Section A*, 252: 225-248.

Haydon, D. A. and Philips, J. N. (1957) The Gibbs Equation and Surface Equation of State for Soluble Ionized Monolayers in Absence of Added Electrolyte at the Oil-Water Interface, *Transactions of the Faraday Society*, 53: 698-704.

Hillel, D (1990) *Introduction to Soil Physics*, Academic press, San Diego, CA.

Hough, D. B. and Rendall, H. M. (1983) in *Adsorption from Solution at the Solid/Liquid Interface*; (G. D. Parkitt and C. H. Rochester, Editors), Academic Press, New York, pp 247-318.

Hunt, J. R., Sitar, N. and Udell, K. S. (1988) "Nonaqueous Phase Liquid Transport and Cleanup: 1. Analysis of Mechanisms," *Water Resources Research*, 24(8): 1247-1258.

Iwata, S., Tabuchi, T. and Warkentin, B. P. (1988) *Soil-Water Interactions: Mechanisms and Applications*, Marcel Dekker, Inc. New York.

Jin, M., Delshad, M., Dwarakanath, V., McKinney, D. C., Pope, G. A., Sepehnoori, K. and Tilburg, C. (1995) Partitioning Tracer Test for Detection, Estimation and Remediation Performance Assessment of Subsurface Nonaqueous Phase Liquids," *Water Resouces Research*, 31: 1201-1216.

Kipling, J. J. (1965) *Adsorption from Solutions of Non-electrolytes*, Academic Press, New York.

Kueper, B. and Frind, E. O. (1991) "Two-Phase Flow in Heterogeneous Porous Media 2. Model Application," *Water Resources Research*, 27(6): 1059-1070.

Larson, R. G., Davis, H. T. And Scriven, L. E. (1977) Percolation Theory of Residual Phases in Porous Media," *Nature*, 268: 409-413.

Leverett, M. C.(1941) "Capillary Behavior in Porous Solids," *Trans. Am. Inst. Min. Metall. Pet. Eng.*, 142: 152-169.

Mayer, A. S. and Miller, C. T. (1992) The Influence of Porous Medium Characteristics and Measurement Scale on Pore-scale Distributions of Residual Nonaqueous-phase Liquids," *Journal of Contaminant Hydrology*, 11: 189-213.

Mercer, J. W. and Cohen, R. M. (1990) "A Review of Immiscible Fluids in the Subsurface: Properties, Models, Characterization and Remediation," *Journal of Contaminant Hydrology*, 6: 107-113.

Miller, C. T., M. M. Poirier-McNeill and Mayer, A. S. (1990) "Dissolution of Trapped Nonaqueous Phase Liquids: Mass Transfer Characteristics," *Water Resources Research*, 26 (11): 2783-2796.

Mohanty, K. K. (1981) "Fluids in Porous Media: Two-Phase Distribution and Flow," Ph.D. Dissertation, University of Minnesota, Minneapolis, MN.

Mohanty, K. K., Davis, H. T. And Scriven, L. E. (1979) "Thin Films and Fluid Distribution in Porous Media," in *Surface Phenomena in Enhanced Oil Recovery* (D. O. Shah, Editor), Plenum Press, New York.

Moore, T. F. and Slobod, R. L. (1956) The Effect of Viscosity and Capillarity on the Displacement of Oil by Water, *Producers Monthly* 20, No. 10, 20-30.

Morgan, J. C., Schechter, R. S. And Wade, W. H. (1977) "Recent Advances in the Study of Low Interfacial Tensions,"in *Improved Oil Recovery by Surfactant and Polymer Flooding* (D. O. Shah and R. S. Schechter, Editors) Academic Press, New York.

Morrow, N (1970) Physics and Thermodynamics of Capillary Action in Porous Media, *Industrial and Engineering Chemistry*, 62 (6): 32-56.

Morrow, N. R., Chatzis, I. and Taber, J. J. (1988) "Entrapment and Mobilization of Residual Oil in Bead Packs,"*SPE Reservoir Engineering*, August: 927-934.

Morrow, N. R. and Heller, J. P. (1985) "Fundamentals of Enhanced Oil recovery," in *Enhanced Oil Recovery, I: Fundamentals and Analyses*, Elsevier Publishing Co. New York.

Morrow, N. R. And Songkran, B. "Effect of Viscous and Buoyancy Forces on Nonwetting Phase Trapping in Porous Media," in *Surface Phenomena in Enhanced Oil Recovery* (D. O. Shah, Editor), Plenum Press, New York.

Nkedi-Kizza, P., Rao, P. S. C. and Hornsby, A. G. (1987) "Influence of Organic Co-solvents on leaching of Hydrophobic Organic Chemicals through Soils," *Environmental Science & Technology,* 21(11): 1107-1111.

Noronha, J. C. (1980) *Partitioning and Interfacial Tension in Surfactant/Oil/Brine/Alcohol Systems*, Ph.D. Dissertation, University of Florida, Gainesville, FL.

Novosad, J. (1979) "Adsorption of Pure Surfactant and Petroleum Sulfonate at the Solid-Liquid Interface," in *Surface Phenomena in Enhanced Oil Recovery* (D. O. Shah, Editor), Plenum Press, New York.

Oh, S. J. and Shah, D. O. (1993) "Effect of Counterions on the Interfacial Tension and Emulsion Droplet Size in the Oil/Water/Dodecyl Sulfate System," *Journal of Physical Chemistry,* 97(2):284-287.

Osipow, L. I. (1962) *Surface Chemistry: Theory and Industrial Applications* Reinhold Publishing Corporation, New York.

Ottewill, R. H. (1983) in *Surfactants* (Th. F. Tadros, Editor), Academic Press, New York.

Payne, D. (1953) "A Method for the Determination of the Approximate Surface Area of Particulate Solids," Nature, 172: 261-265.

Pennell, K. D., Jin, M., Abriola, L. M. and Pope, G. A. (1994) "Surfactant Enhanced Remediation of Soil Columns Contaminated by Residual Tetrachloroetylene," Journal of Contaminant Hydrology, 16(1): 35-53.

Pennell, K. D., Pope, G. A. and Abriola, L. M. (1995) "Influence of Viscous and Buoyancy Forces on the Mobilization of Residual Tetrachloroethylene During Surfactant Flushing," *Envoironmental Science and Technology,* 30(4): 1328-1335.

Pethica, B. A. (1953) "The Adsorption of Surface Active Electrolytes at the Air/Water Interface," *Transactions of the Faraday Society*, 49: 413-421.

Pfannkuch, H. O.(1984) in *Petroleum Hydrocarbons and Organic Chemicals in Groundwater* Natl. Water Well Assoc., Washington, DC, 1984) pp. 444-458.

Powers, S. E., Abriola, L. M. and Weber, W. J. Jr. (1992) "An Experimental Investigation of Nonaqueous Phase Liquid Dissolution in Saturated Subsurface Systems: Steady State Mass Transfer Rates," *Water Resources Research*, 28 (10): 2691-2705.

Powers, S. E., Loureiro, C. O., Abriola, L. M. And Weber, W. J. Jr. (1991) "Theoretical Study of the Significance of Nonequilibrium Dissolution on Nonaqueous Phase Liquids in Subsurface Systems," Water Resources Research, 27(4): 463-477.

Rao, P. S. C. (1995) Class Lecture Notes *Contaminant Sub-surface Hydrology*, University of Florida, Gainesville.

Reeves, P. C. and Celia, M. A. (1996) "A Functional Relationship between Capillary Pressure, Saturation, and Interfacial Area as Revealed by a Pore-scale Network Model," *Water Resources Research*, 32(8): 2345-2358

Roof, J. G. (1970) "Snap-off of Oil Droplets in Water-Wet Porous Media," *Society of Petroleum Engineers Journal*, March: 85-90.

Rose, W. and Witherspoon, P. A. (1956) Trapping Oil in a Pore Doublet, *Producers Monthly* 21, No. 2, 32-38.

Rose, W. (1949) "Theoretical Generalizations Leading to the Evaluation of Relative Permeability," *Transactions of the American Institute of Mining and Metullurgical Engineers, Petroleum Branch*, 186: 111-126.

Rose, W. and Bruce, W. A. (1949) "Evaluation of Capillary Character in Petroleum Reservoir Rock," *Transactions of the American Institute of Mining and Metullurgical Engineers, Petroleum Branch*, 186: 127-142.

Rosen, M. J. (1978) *Surfactants and Interfacial Phenomena*, John Wiley & Sons, New York.

Saripalli, K. P., PSC Rao and M. D. Annable, "Use of Interfacial Tracers to Characterize Immiscible Fluid Interfaces in Porous Media," American Geophysical Union, Spring Meeting, Baltimore, MD. May 1995.

Schwille, F (1988) *Dense chlorinated solvents in porous and fractured media-Model experiments* (J. F. Pankow, Translator) Lewis Publishers Inc., Chelsea, MI, 146pp.

Skopp, J. (1990) "Oxygen Uptake and Transport in Soils: Analysis of the Air-Water Interfacial Area," *Soil Science Society of America Journal*, 49:1327-1331.

Smith, W. O. (1933) "Minimum Capillary Rise in an Ideal Uniform Soil, *Physics*, 4: 184-193.

Sposito, G. (1984) *The Surface Chemistry of Soils* Oxford University Press, New York, pp. 23-28.

Stegemeier, G. L. (1977) "Mechanisms of Entrapment and Mobilization of Oil in Porous Media," in *Improved Oil Recovery by Surfactant and Polymer Flooding* (D. O. Shah and R. S. Schechter, Editors) Academic Press, New York.

Sutheim, G. M. (1947) *Introduction to Emulsions* Chemical Publishing Co., Brooklyn, NY.

Taber, J. J. (1969) "Dynamic and Static Forces Required to Remove a Discontinuous Oil Phase from Porous Media Containing Both Oil and Water," *Society of Petroleum Engineers Journal*, March: 3-12.

Taber, J. J. (1979) "Research on Enhanced Oil Recovery: Past, Present and Future'" in *Surface Phenomena in Enhanced Oil Recovery* (D. O. Shah, Editor), Plenum Press, New York.

Tadros, Th. F. (1995) *Surfactants in Agrochemicals* Marcel Dekker Inc., New York.

Van Genuchten, M. Th. (1980) A Closed-Form Equation for Predicting the Hydraulic Conductivity of Unsaturated Soils, *SSSA Journal*, Vol. 44, pp. 892-898.

Versluys, J. (1917) *Int. Mitt. Bodenk.* 7, 117.

Wade, W. (1995) Invited Lecture in Hydrologic Science at the University of Florida, Gainesville.

Wilson, R. D. And Mackay, D. M. (1995) Direct Detection of Residual Nonaqueous Phase Liquid in the Saturated Zone Using SF6 as a Partitioning Tracer," *Environmental Science & Technology*, 29(5): 1255-1258.

Wilson, J. L., Conrad, S. H., Mason, W. R., W. Peplinski and Hagan, E. (1990) *Laboratory Investigations of Residual Liquid Organics from Spills, Leaks and Disposal of Hazardous Wastes in Groundwater* EPA/600/6-90/004, U.S. EPA: Ada, OK.

BIOGRAPHICAL SKETCH

Kanaka Prasad Saripalli was born in Visakhapatnam, India, on 17th May, 1967. He was raised in the coastal state of Andhra Pradesh, India, where he obtained a diploma and a bachelor's degree in civil engineering from Andhra University. During this education, he established and ran a consultancy as a licensed engineer and builder. Upon graduation, he joined Clemson University, to obtain a master's degree in environmental systems engineering in 1993. While at Clemson, he held a position as an intern engineer in the Technology Development and Demonstration wing of Rust Remedial Services Inc. He transferred in the summer of 1994 into a doctoral program in environmental engineering & hydrologic science at the University of Florida. In 1994, he married Ratna Vedula, an architect and environmental planner. The candidate seeks to continue research and learning upon graduation in the Ph. D. Program.

I certify that I have read this study and that in my opinion it conforms to acceptable standards of scholarly presentation and is fully adequate, in scope and quality, as a dissertation for the degree of Doctor of Philosophy.

Michael D. Annable, Chairman
Assistant Professor of Environmental
Engineering Sciences

I certify that I have read this study and that in my opinion it conforms to acceptable standards of scholarly presentation and is fully adequate, in scope and quality, as a dissertation for the degree of Doctor of Philosophy.

P. S. C. Rao, Cochairman
Graduate Research Professor of
Soil and Water Science

I certify that I have read this study and that in my opinion it conforms to acceptable standards of scholarly presentation and is fully adequate, in scope and quality, as a dissertation for the degree of Doctor of Philosophy.

Joseph J. Delfino
Professor of Environmental
Engineering Sciences

I certify that I have read this study and that in my opinion it conforms to acceptable standards of scholarly presentation and is fully adequate, in scope and quality, as a dissertation for the degree of Doctor of Philosophy.

Wendy D. Graham
Associate Professor of
Agricultural & Biological Engineering

I certify that I have read this study and that in my opinion it conforms to acceptable standards of scholarly presentation and is fully adequate, in scope and quality, as a dissertation for the degree of Doctor of Philosophy.

Kirk Hatfield
Associate Professor of Civil Engineering

This dissertation was submitted to the Graduate Faculty of the College of Engineering and to the Graduate School and was accepted as partial fulfillment of the requirements for the degree of Doctor of Philosophy.

December, 1996

Winfred M. Phillips
Dean, College of Engineering

Karen A. Holbrook
Dean, Graduate School